Investigation of thermogenic mechanisms in adipose tissue during recovery from sepsis

Dr Robert Tidswell

University College London

Supervisors

Professor Mervyn Singer

Professor Michael Duchen

Bloomsbury Institute of Intensive Care Medicine

Department of Experimental and Translational Medicine

Division of Medicine

and

Department of Cell and Developmental Biology

Division of Biosciences

A thesis submitted for the degree of

Doctor of Philosophy

July 2023

Declaration

I, Robert Tidswell confirm that the work presented in this thesis is my own. Where information has been derived from other sources, I confirm that this has been indicated in the thesis.

Abstract

Background – Sepsis is defined as a dysregulated host response to infection resulting in organ dysfunction and, in some cases, death. Temperature impacts outcomes from sepsis – patients with fever are more likely to survive. However, in the recovery phase, thermogenesis may be detrimental. Survivors frequently develop cachexia and sepsis-induced myopathy which impairs recovery and increases long term mortality. In conditions akin to sepsis, including burn injury and cancer-associated cachexia, this has been attributed to catabolism driven by hypermetabolism due to a process called 'browning'. Browning describes the switch of energy-storing white adipose tissue to a thermogenic energy-burning brown adipose tissue-like phenotype. Identification and prevention of browning in sepsis may improve outcomes.

Hypothesis – In survivors of sepsis, browning of white adipose tissue occurs and drives cachexia and myopathy.

Methods – Experimental sepsis was induced in rats using intraperitoneal zymosan. Body mass, muscle mass and myofibre cross sectional area were used to assess cachexia and myopathy. Expression of thermogenic browning mechanisms were studied in epididymal and retroperitoneal adipose tissue (eWAT and rpWAT, respectively) using thermal imaging, respirometry, RNA-sequencing and Western blot. Mitochondrial function and tissue morphology was interrogated by multiphoton imaging in live rpWAT explants.

Results – Rats with zymosan peritonitis developed a sepsis-like illness with a 14-day mortality of 17%. In the recovery phase survivors developed hypermetabolism, cachexia and myopathy with reduced muscle mass and myofiber thickness. Oxygen consumption of eWAT and rpWAT per milligram of tissue was elevated at days 3, 7

and 14 of sepsis recovery. However, when controlled for protein content, lipid droplet size or mitochondrial or cell number, the increase was abolished. RNA sequencing of rpWAT demonstrated up-regulation of inflammatory genes and down-regulation of genes related to oxidative phosphorylation and thermogenesis during recovery. Notably, SERCA2 mRNA and SERCA2 protein were increased. Multiphoton microscopy showed neither increased mitochondrial density nor lipid multiloculation consistent with browning. The NAD(P)H pool was, however, more oxidised in tissue from animals recovering from sepsis, indicating altered metabolism.

Conclusion – Hypermetabolism, cachexia and myopathy in the recovery phase of experimental sepsis are not caused by classical browning. Calcium cycling mechanisms in adipose tissue may be implicated and merit further investigation.

Impact Statement

The thesis presented here provides novel data in the study of the recovery phase of sepsis. Sepsis is the cause of 40,000 admission to intensive care units in the UK per year, of whom approximately 27,000 will survive. The majority of these will suffer 'post-intensive care syndrome' which commonly manifests as weakness and locomotor impairment. This impairs recovery, quality of life, ability to work and is associated with social, psychological and cognitive morbidity. The recovery phase is poorly understood, and under-researched. The findings here contribute three main impacts to the field: First, the process of browning has previously been believed to occur in adipose tissue in animal models of sepsis, and has been associated with post-sepsis weakness. This study is more comprehensive in scope than previous studies and concludes this is not the case, thus, contributing a novel viewpoint to the literature which may inform future studies and prevent unnecessary research, use of animals or incorrect direction of clinical management. Second, the study identifies a phenotype of adipose tissue in the recovery phase of sepsis akin to other cachexia syndromes (e.g. cancer) which is not described in the literature and will hopefully provoke further research and development of the field. Third, the study involves the development and description of novel techniques for the study of adipose tissue in animal models of sepsis, which can be used by myself and others for future studies.

The project has also forged links through collaboration with Yale University and the University of Reading which will enable new lines of research, knowledge sharing and skills development with impact beyond this project. Finally, it has provided myself with a scientific grounding which will hopefully lead to future studies and improvements in the care of patients with sepsis.

Acknowledgements

My thanks to Merv for being a constant source of laughter, gossip, anecdote and dubious-quality jokes since we met in 2016. Witnessing his dedication to both the clinical and academic world of Intensive Care, his boundless energy and imagination and dogged trouncing of dogma, has been a true scientific education. I look forwards to more meandering conversations and Battenburg cake.

Great appreciation and thanks to Michael for his supervision, insight and guidance throughout my PhD, and for the best piece of advice regarding interview panels – "never overestimate their knowledge, but never underestimate their understanding". An adage which has stuck with me. I will remember our discussions on the parlous state of politics and tending allotments and of course the delicious courgette flowers.

Thanks also to Professor Matthew Rodeheffer for hosting me during my brief stint at Yale. A formative time guiding my understanding of basic adipose tissue biology and development of very tricky microscopy techniques.

Thank you to Nish as a constant source of sense-checking both my work and the reality of scientific life, and for the endless supply of cigars and whisky when sense was absent.

Thank you to Anna for teaching and maintaining scientific rigour and for listening to my endless whinging about Western blots, but also the more enjoyable conversations on art and literature.

Thank you to Dr Alex Dyson for a gentle but thorough introduction to the world of animal models and the fabulous world of sulphides and selanides – and of course for the beers and good times.

Thank you to Ali Alqallaf and Professor Ketan Patel for a stimulating and productive collaboration and the exciting opportunity to use novel therapies for the treatment of sepsis-induced weakness in our side-projects.

A special mention to the Dr Scott Shepherd and Dr Omid Sadeghi-Alavijeh of the LRB PhD support group for good laughs, and putting the world into perspective.

Finally a thank you to everyone else in the lab without whom the project wouldn't exist and wouldn't have been so much fun. A special mention to Joe, Johnny and Walter for their time and hard work.

Table of Contents

Table of figures

List of tables

Abbreviations

ANOVA	Analysis of variance
APACHE	Acute physiology and chronic health evaluation score
ARDS	Acute respiratory distress syndrome
AT	Adipose tissue
ATP	Adenosine triphosphate
BAT	Brown adipose tissue
BI	Burn injury
BIOPS	Biopsy preservation medium
BMI	Body mass index
BODIPY	Boron difluoride dipyrromethene
CAC	Cancer associated cachexia
CIM	Critical illness myopathy
CN	Cyanide
CSA	Cross-sectional area
CT	Computer tomography
CT PET	Computer tomography positron emission tomography
DAMPS	Disease-associated molecular patterns
eWAT	Epididymal white adipose tissue
FCCP	Carbonyl cyanide-*p*-trifluoromethoxyphenylhydrazone
FFA	Free fatty acid
FT	Facultative thermogenesis
GO	Gene Ontology
ICU	Intensive Care Unit
IL-x	Interleukin-x
iWAT	Inguinal white adipose tissue
KEGG	Kyoto encyclopaedia of genes and genomes
MCP-1	Macrophage chemoattractant protein-1

mRNA	messenger ribonucleic acid
MyHC	Myosin heavy chain
OMY	Oligomycin
OR	Odds ratio
OT	Obligatory thermogenesis
PAMP	Pathogen associated molecular pattern
PGC1α	Peroxisome proliferator-activated receptor-gamma coactivator α
PMG	Pyruvate, malate, glutamate
PRR	Pattern recognition receptor
RCT	Randomised controlled trial
rpWAT	Retroperitoneal white adipose tissue
SD	Standard deviation
SERCA2	Sarcoplasmic endoreticulum ATPase 2
Succ	Succinate
TBST	Triss buffered saline with Tween
TLR	Toll-like receptor
TMRM	Tetramethylrhodamine methyl ester
TNF	Tumour necrosis factor
UCP1	Uncoupling protein 1
UCP2	Uncoupling protein 2
UCP3	Uncoupling protein 3
VTi	Velocity time integral

Chapter 1. Introduction

Sepsis is defined as a dysregulated host response to infection leading to organ failure and an increased risk of death.[1] Approximately 70% of patients with sepsis survive, however many will suffer long term physical, psychological and/or cognitive dysfunction.[2]

Long term physical morbidity is predominantly due to cachexia and muscle wasting which impairs recovery and reduces quality of life.[3] In diseases akin to sepsis, including burn injury and cancer, a process called 'browning' has been identified as a driver of the tissue wasting.[4,5] Browning describes the switch of energy-storing white adipose tissue into a thermogenic brown adipose tissue-like phenotype, known as beige adipose tissue. The thermogenesis (heat production) caused by browning is potentially maladaptive and may drive muscle and adipose tissue wasting (cachexia) through hypermetabolism.[6] The identification of browning in burn injury and cancer has led to advancements in care; further understanding of the role of browning in sepsis may enable similar progress.

Heat and thermogenesis are already recognised to influence outcome from sepsis. In early sepsis, thermogenesis manifests as fever. This ancient and highly conserved process is controlled, adaptive and beneficial and correlates strongly with survival in patients presenting with sepsis.[7] Whether browning thermogenesis represents an uncontrolled, maladaptive and detrimental process in the recovery phase of sepsis remains to be seen.

This study aims to identify thermogenic processes in adipose tissue as a potential driver of cachexia and muscle loss seen in survivors of sepsis.

1.1 Sepsis

In 400 BCE Hippocrates described sepsis as biological decay leading to 'auto - intoxication'.[8] The re-definition of sepsis in 2016 as '*life-threatening organ dysfunction caused by a dysregulated host response to infection'* re-emphasised the host response in the pathophysiology of sepsis, echoing Hippocrates' focus on the host as the source of intoxication.[1]

Robust epidemiological data are hampered by inaccurate diagnosis, syndrome heterogeneity and reliance on administrative databases.[9] Approximately 40,000 cases of sepsis are admitted to Intensive Care Units (ICU) in England annually, of whom 27,000 leave hospital alive.[10] Beyond management of the infection and organ support, no specific therapies exist. Improvements in care have resulted largely from minimising iatrogenic harm.[11] Most (>75%) sepsis-related deaths in developed countries are in elderly, frail patients aged 75 years or above.[12] Florid sepsis caused by a severe infection in an otherwise young, healthy person does occur, but is relatively rare. In children aged 0-18 years, hospital mortality from sepsis is 0.075%.[12]

The above statistics should not however minimise the problem. Sepsis still carries a high mortality rate and is a common complication of major surgery, chemotherapy and immunosuppressive treatments.[13] Mortality from sepsis is falling, in part due to better understanding and less iatrogenic harm, but also due to increased recognition and earlier intervention.[14,15] Further increases in survivors can be anticipated. However, recovery is not complete on discharge from intensive care – many patients develop '*post-intensive care syndrome'*, in which myopathy and cachexia occur in conjunction with many other pathophysiological processes.

1.1.1 Pathophysiology

The diagnosis of sepsis involves the identification or suspicion of infection plus the development of new-onset organ dysfunction. Infection can, and does, exist without sepsis. Sepsis pathophysiology remains incompletely understood. While the clinical syndrome can present in many ways, common pathways are described. The pathogen (bacterial, viral, fungal, parasitic, atypical) carries pathogen-associated molecular patterns (PAMPs), such as DNA, RNA, exotoxins and endotoxins (the Gram negative cell wall component, lipopolysaccharide). PAMPs are recognised by the host through pattern recognition receptors (PRR). PRRs also recognise host cell contents released by damage to tissues, such as DNA and mitochondria; these are known as damage-associated molecular patterns (DAMPs). Activation of PRRs by PAMPs and DAMPs triggers leukocyte and endothelial activation, with transcription and release of both pro- and anti-inflammatory mediators including cytokines (e.g. tumour necrosis factor (TNF)alpha, interleukins such as IL-1, IL-6, IL-10, and interferons), gaseous mediators (e.g. nitric oxide), thromboxanes and prostaglandins, and complement activation. Release of proteases and oxidative species further contribute to organ dysfunction and cellular injury.[13] Endothelial activation results in capillary leak; while this aids translocation of white blood cells to the site of injury, there is systemic extravasation of fluid and immune cells from the circulation into non-affected tissues, resulting in oedema and distant injury unrelated to the infection itself. The pro-inflammatory stress response initially predominates but is later superseded by an overall anti-inflammatory immunoparetic state characterised by reduced antigen presentation and leukocyte deactivation, and increased susceptibility to secondary infections.[13]

The exaggerated immune response also triggers up- or down-regulation of systemic homeostatic mechanisms including cardiovascular, hormonal, coagulation, nervous and metabolic pathways. While these may be adaptive, they may also become

ultimately maladaptive, leading to organ dysfunction.[16] Precise mechanisms underlying organ dysfunction remain unclear, but mitochondria are increasingly implicated.[17] Mitochondrial biogenesis, protein synthesis, and electron transport chain function are all impaired while generation of reactive oxidative species are increased, resulting in further cellular damage.[18]

Of note, post-mortem studies in sepsis patients demonstrate little or no cell death in organs that had failed pre-mortem.[19,20] Organ function also generally recovers in survivors over days to weeks, even in those organs with little regenerative capacity.[19,20] Given that ATP production is impaired, yet cell death pathways are not triggered, a parallel reduction in ATP demand and metabolism must occur, allowing a transient 'shutdown' of function. This shutdown may explain the reversible organ failure manifested in sepsis.[20] Precise mechanisms remain uncertain but may involve uncoupling proteins which uncouple phosphorylation of ADP from oxidation. While this paradoxically reduces ATP synthesis, it will also reduce excessive reactive oxygen species generation and cellular damage.

Much less is known about the recovery phase of sepsis.[21] Recovery is associated with early activation of mitochondrial biogenesis. Whether these processes can become maladaptive and contribute to long term morbidity is unknown.[21]

1.1.2 Sepsis induced myopathy and cachexia

Survivors of sepsis frequently develop myopathy. This has been traditionally badged under the label of 'critical illness myopathy' (CIM) which encompasses any critical illness requiring intensive care. Most of these critical illnesses not triggered by infection, such as trauma, burn injury, pancreatitis and major surgery, also involve

similar activation of inflammatory and immune pathways and an exaggerated stress response.[22]

CIM is characterised by a generalised, symmetrical weakness of limb and diaphragm skeletal muscle with relative sparing of facial and ocular muscles.[22] The reported prevalence varies from 25-73% of critically ill patients. Suggested risk factors include disease severity, prolonged organ support, hyperglycaemia, early parenteral nutrition and drugs such as corticosteroids and neuromuscular blockers. No specific treatments exist despite considerable efforts. Two randomised controlled trials of the anabolic growth hormone even resulted in a significant increase in mortality.[23] Novel therapies are needed, but this will be predicated on a better understanding of the pathophysiology and better identification of the correct time to intervene and to dose optimally. In the meantime, management relies predominantly on organ support, optimising modifiable risk factors and avoidance of iatrogenic harm.[22]

CIM is associated with increased in-hospital mortality and longer ICU and hospital stays. Long-term mortality is increased further in those with CIM. The weakness itself reduces quality of life and can persist up to 8 years.[22] A recent meta-analysis of 11,693 survivors of the acute respiratory distress syndrome, which describes the severe pulmonary dysfunction manifest in many patients with sepsis, found an ongoing reduced quality of life due to physical impairment at 5 years;[2] muscle strength was reduced in 92% and measurable by a reduced distance achieved in a 6 minute walk test.[2] In tandem, this study also reported ongoing psychological, cognitive and social impairments.

Mechanisms of critical illness myopathy include increased proteolysis with activation of the ubiquitin-proteosome system, a relative reduction in protein synthesis relative

to breakdown, dysregulated autophagy, patchy necrosis and reduced numbers of progenitor cells.[24–26] Disuse atrophy likely contributes, but does not explain the extent and specific myosin/actin fibre loss seen in CIM.[27] In one study sampling vastus lateralis muscle from patients with critical illness, myofibre cross-sectional area (CSA) was reduced by 70% in type I myosin heavy chain fibres and by 75% in type II heavy chain fibres.[28] In contrast, fibre CSA loss was only 13% following 6 weeks of bedrest alone.[27] Other studies demonstrate a predominant myopathy in type II fast twitch fibres in CIM, with a shift from fast-to-slow fibre type - the opposite is reported in disuse atrophy.[26] Other distinctive features include sarcomere disruption, present in every ICU patient at day 7 in one study, preferential loss of myosin-related proteins compared to disuse atrophy, and reduced excitation-contraction coupling.[29] CIM is not explained simply by reduced nutrient intake. Indeed, a randomised controlled trial of early versus late intravenous feeding in critically ill patients found that early feeding exacerbated muscle weakness.[30]

Sepsis-induced myopathy forms part of a cachexia syndrome. Cachexia is a complex syndrome that affects all body organs and is associated with poor outcomes in many conditions.[31] It is characterised by muscle wasting and a negative energy balance despite adequate calorie intake, and is always associated with an inflammatory disorder. In contrast to malnutrition induced sarcopenia, there is marked loss of muscle and fat mass that cannot be reversed by nutritional or lifestyle supports.[32] A study of survivors of ARDS reported patients were severely wasted at ICU discharge having lost 18% of their baseline body weight. Twenty-nine percent of patients had not returned to their baseline weight by one year.[3] Cachexia is intrinsically linked to multi-system illness including endocrine, immune and metabolic disturbances, and is increasingly recognised as a metabolic syndrome in itself.[31]

1.1.3 Management of sepsis

1.1.3.1 General management

The main tenets of sepsis management are to:

1) treat the triggering infection

2) support failing organs

3) reduce harmful effects of supportive measures.

Sepsis is a highly heterogeneous syndrome. One treatment does not fit all, though the general principles are (i) to promptly identify patients with severe infection who are developing signs of organ dysfunction; (ii) to treat the underlying infection with appropriate antibiotics ± source control (e.g. surgical repair, interventional radiological drainage, removal of infected catheters); (iii) support or temporarily replace failing organs using vasoactive medications (classically catecholamines) for cardiovascular failure, mechanical ventilation for respiratory or neurological failure, renal replacement therapy for acute kidney injury, and blood and blood products for haematological and liver dysfunction. All of these therapies are relatively crude and carry significant associated risks of harm. Good care lies in the minimisation of these necessary evils.[13]

1.1.3.2 Temperature management

In health, body temperature is controlled to around 37°C.[33] In sepsis approximately 10-15% of patients present with hypothermia (<36°C), 40-50% with normothermia (36-38°C), and 40-50% with pyrexia (>38°C), acknowledging that reported temperature thresholds vary by study.[34]

Extensive physiological, behavioural and social resources are spent on maintaining body temperature. In cold conditions, metabolic rate is increased by both shivering and non-shivering thermogenesis, peripheral blood vessels constrict to decrease heat loss and warmer places are sought. When hot, on the other hand, there is sweating, peripheral vasodilation and shade is sought. Patients with sepsis are often obtunded and unable to control such reflexes. The Surviving Sepsis Campaign guidelines make no recommendations on the management of temperature in patients with sepsis; management is thus largely dictated locally.[35]

In general, pyrexia continues to be seen as a problem. Patients are given paracetamol or tepid sponging to suppress further fevers, in keeping with often misguided efforts to normalise physiology during critical illness. This may be reasonable in awake patients who are feeling discomfort, however, in sedated patients trials have repeatedly shown no outcome benefit from pharmacological anti-pyretic therapy.[36] This is now reflected in some sepsis guidelines.[37] Similarly, patients who are hypothermic are often warmed to normothermia using external devices such as external warming blankets. The optimal target temperature for warming remains to be established, but a preliminary study published in 2022 indicate febrile temperatures may be beneficial.[38] Cooling patients to hypothermic levels has, however, been repeatedly shown in RCTs to be harmful.[39,40]

During the recovery phase of sepsis patients are normally alert and more mobile. They are assumed to have recovered normal thermostatic control although, to my knowledge, this has not been formally studied. Mice suffering from cancer-induced cachexia seek warmer environmental temperatures and show a gradual decline in body temperature, indicating a loss of thermostatic ability.[41] Cachexia is a disease of whole-body metabolism regardless of cause so, conceivably, the same occurs in humans with sepsis-induced cachexia.[42]

1.2 Thermogenesis in health and sepsis

As mentioned above, thermogenesis in the form of fever is strongly associated with survival from sepsis. However, thermogenesis in the recovery phase may be detrimental by driving cachexia and muscle wasting. Here I discuss thermogenesis in health, in the early phase of sepsis, and during the recovery phase.

1.2.1 Metabolism and thermogenesis in health

Metabolism is defined as the chemical processes occurring within an organism. Whole body metabolism is measured indirectly by oxygen consumption as the majority of processes depend on oxidation. Growth, reproduction and external work include 'work done' with the transfer of chemical energy into matter or kinetic energy. Eating also causes thermogenesis; this is known as 'diet-induced thermogenesis' whereby metabolic rate is increased above basal levels due to digestion, absorption, metabolism, transport and storage of food. This also activates thermogenesis in brown adipose tissue (BAT) through histamine release.[43] Excluding these processes, homeostasis maintains equilibrium such that all energy utilised is lost as heat.[44]

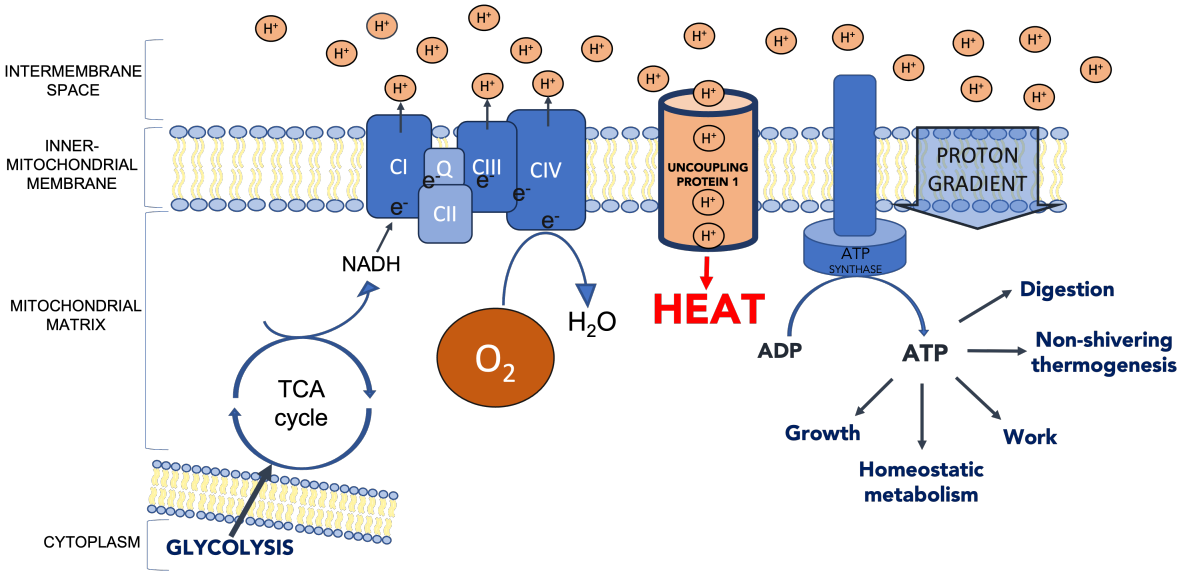

Figure 1. Schematic depiction of oxidative phosphorylation and conversion of chemical energy into heat and generation of ATP.

Oxidative phosphorylation is the process by which chemical energy (food and substrates) are converted into potential energy (in the form of a proton gradient across the mitochondrial membrane) which then drives ATP production by ATP synthase. This drives the ATP/ADP ratio away from equilibrium increasing Gibbs free energy which can then be used for work, growth, digestion of food, homeostasis and thermogenesis. If the organism is not growing, digesting or doing work, then all of the energy will eventually be dissipated as heat.[44] The proton gradient can also be dissipated independently of ATP synthase through uncoupling proteins (UCP1 shown here), which releases the potential energy directly as heat - this is the canonical thermogenic mechanism in brown adipose tissue.[44,45] Over 90% of metabolism is dependent on oxidative phosphorylation, in which oxygen is the final electron acceptor from complex four (CIV) of the electron transport chain. Without oxygen the transport chain is inhibited and oxidative phosphorylation stops. This dependence on oxygen allows us to measure metabolism indirectly as oxygen consumption. And because in the resting state (basal metabolism) all the energy is eventually dissipated as heat, oxygen consumption is therefore equivalent heat production (thermogenesis). This is the basis of indirect calorimetry and the measurement of thermogenesis.

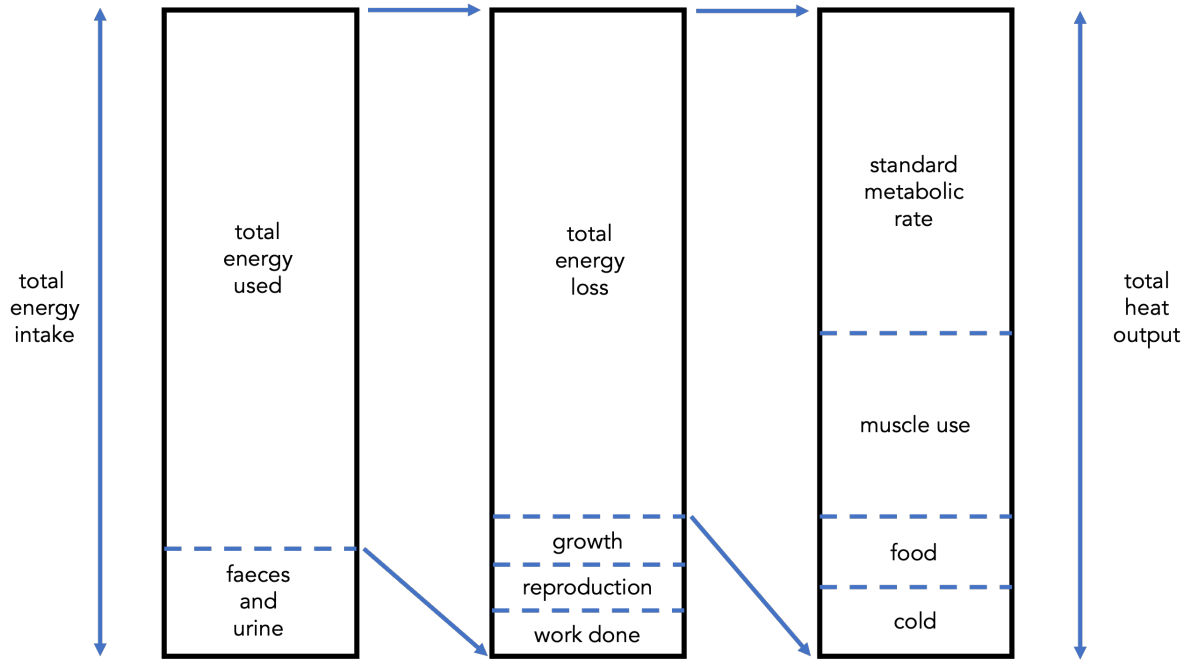

Figure 2. Schematic of metabolism and energy flow through the human body demonstrating the majority of energy consumed is released as heat.
The schematic reads from left to right to demonstrate the dissipation of energy through an organism. Total energy intake (typically measured indirectly as total oxygen consumption) is depicted on the left. Energy is lost as heat through excretia. Remaining energy is then either transferred to matter (growth, reproduction) or through 'work done' e.g. walking. The remaining energy, assuming homeostasis with the organism, is dissipated through bioenergetically imperfect reactions involved in ongoing metabolism, muscle use, food digestion and adaptive thermogenesis (in the presence of cold stress). Scaling is approximate. Adapted from Rolfe and Brown, Physiology Reviews 1993[44]

Heat generated can be split into 'obligatory' and 'facultative' (also known as adaptive) thermogenesis. Obligatory thermogenesis (OT) is heat released by necessary but bioenergetically imperfect chemical processes required for homeostasis, such as gluconeogenesis and maintenance of electrochemical gradients.[46] At thermoneutral ambient temperatures (21-23°C for humans, 26°C for rats, 30°C for mice) obligatory thermogenesis is sufficient to maintain body temperature without expending energy to specifically produce heat.[47]

Below thermoneutral temperatures 'facultative' thermogenesis (FT) is induced to maintain body temperature. FT can be subdivided into shivering and non-shivering thermogenesis. Shivering generates heat by increasing ATP hydrolysis and therefore oxygen consumption by up to 6-fold compared to basal metabolic rate.[44] This conversion of chemical energy into kinetic energy is effective but inefficient; locomotion is impaired and the metabolic rate cannot be maintained. Non-shivering facultative thermogenesis also increases oxygen consumption and heat production but in a more sustainable manner and without the functional impairment of shivering.[48] Non-shivering FT involves both ATP dependent and independent mechanisms (discussed below).

1.2.1.1 ATP-independent facultative thermogenesis – Uncoupling Proteins

ATP-independent thermogenesis occurs through 'proton leak' which dissipates the mitochondrial membrane potential independently of ATP synthase. The potential energy is released as heat and the coupling efficiency is reduced. This results in increased metabolism and oxygen consumption for the same quantity of ATP, generating more heat. Proton leak includes both 'basal' unregulated leak and 'inducible' regulated leak catalysed by specific inner mitochondrial membrane proteins, including uncoupling proteins. Basal proton leak correlates with mitochondrial anion carrier proteins levels such as the Adenine Nucleotide Translocase (ANT). Relative contributions to leak depend on the animal and tissue.[49]

Basal proton leak is physiologically significant. It accounts for 20-30% of resting metabolic rate in hepatocytes and 50% in rat skeletal muscle. Basal proton leak is 4-5 times higher in warm-blooded compared to cold-blooded animals. It thus contributes to obligatory thermogenesis to maintain body temperature and to

reduce reactive oxygen species (ROS) generation linked to higher oxidative phosphorylation rates.[49]

Inducible proton leak is mediated by adenine nucleotide translocase (ANT) and uncoupling proteins (UCP).[49] Five uncoupling protein homologs exist. UCP1, also known as 'thermogenin', is the main thermogenic unit in brown (and beige) adipose tissue. UCP2 is expressed in most viscera while UCP3 is only expressed in skeletal muscle and BAT. UCP1 shares 59% homology with UCP2 and 3, while UCP2 and 3 share 72% homology.[50] UCP4 and UCP5 are less well characterised but have roles within the central nervous system.

UCP1 is intrinsic to rodent thermoregulation – UCP1 knockout mice are intolerant of cold.[51] UCP1's role in adult human thermoregulation is less clear. Humans have proportionally smaller BAT deposits and can exert behavioural control over ambient temperature. UCP2 and 3 are not thought to be vital to thermoregulation although UCP3 is implicated in pathological hyperthermic states – UCP3 knockout mice are protected from fatal hyperthermia induced by a lethal dose of Ecstasy.[52]

UCP1 proton leak is constitutively active but is also inducible by $ß_3$-adrenergic stimulated lipolysis and the presence of fatty acids. UCP2 and UCP3 proton leak is only active in the presence of fatty acids and/or reactive oxygen species.[53]

UCP1 accounts for 5-8% of BAT mitochondrial protein and constitutes the main thermogenic mechanism in this specialised heat-producing organ containing dense mitochondrial networks, abundant lipid substrate and liberal perfusion.[54] Rodents have multiple thoracic BAT deposits of which the interscapular deposit is the largest. Functional BAT in adult humans is a fairly recent discovery as it was previously thought to be lost after infancy.[55] Although small (approx. 70-200g in humans), BAT

is thought to influence whole body metabolism – lean men display larger and more active BAT deposits than obese individuals.[56] BAT and other facultative thermogenic mechanisms are now a focus of research in tackling the obesity pandemic.

1.2.1.2 ATP-dependent thermogenesis – Futile Substrate Cycles

ATP-dependent facultative thermogenesis uses futile substrate cycles to release heat. Futile substrate cycles involve two or more opposing chemical processes occurring in tandem with no net loss or gain of a product. Reactions can be seemingly futile, for example have no purpose other than to generate heat, or can make otherwise necessary processes, such as calcium homeostasis, more inefficient. Both processes require ATP, the generation and hydrolysis of which releases heat. Multiple substrate cycles have been identified including, but not limited to, calcium, fatty acids, Na^+/K^+ pumps, creatine and ADP/ATP.[57]

Sarcoplasmic reticulum ATPase (SERCA)-mediated calcium cycling is perhaps the best understood futile substrate cycle involved in thermogenesis. Under adrenergic control, calcium is released from the sarcoplasmic or endoplasmic reticulum through the ryanodine receptor down a concentration gradient. The calcium is then either 1) pumped back into the sarcoplasm, with a stoichiometry of 2:1 with ATP hydrolysis, or 2) under the influence of 'regulins', the dominant form of which in skeletal muscle is called sarcolipin, SERCA undergoes a conformational change reducing calcium-binding affinity, but not ATP hydrolysis capacity. Calcium transport efficiency is thus reduced with SERCA acting as an ATP sink resulting in thermogenesis.[58]

Substrate cycles are highly conserved - the same calcium cycle is found in the ocular heater organ of billfish which use it to warm their eyeballs and maintain a constant refractive index when diving into cooler waters to catch prey.[59] Like UCPs, substrate cycles can alter cellular environments. For example, SERCA calcium cycling can increase cytosolic and mitochondrial calcium levels, stimulating oxidative phosphorylation.[60]

Both UCP1 and futile cycle thermogenic mechanism are found in brown and beige adipose tissue in diseases akin to sepsis. This will be discussed in detail later.

1.2.2 Metabolism, oxygen consumption and heat production in sepsis

Metabolism is altered during sepsis. Comparison between studies is complicated by stage of disease, methodology, comparator and the heterogeneity of septic patients, but most indicate an increased metabolic rate at the onset. Few studies correlate metabolic state with sepsis severity. Wu *et al* found a higher metabolic rate was an independent predictor of sepsis mortality.[61] Conversely, Kreyman *et al* found patients with uncomplicated infection were hypermetabolic which then decreased towards baseline with ensuing organ failure, culminating in an 'abnormally normal' metabolic rate in those with septic shock.[62] Zauner *et al* found a similar correlation with metabolic rate decreasing with increasing sepsis severity (as assessed by the APACHE-II physiological severity score).[63] Studies performed during the recovery phase show hypermetabolism. Coss-Bu *et al* reported an average increase in metabolic rate of 48% in 19 paediatric patients with sepsis at day 8 after septic insult.[64] Kreyman *et al* found an average rise of 60% above baseline in nine patients at day 22 after admission to the intensive care unit (ICU).[62] Uehara *et al* reported that hypermetabolism in septic patients peaked at 38% above basal metabolic rate at day 8 of hospital admission and remained elevated by 25%

at day 23.[65] To my knowledge, no studies have formally studied the increase in metabolism seen in the recovery phase but it is likely related to anabolic processes, healing and repair processes.

As facultative thermogenic mechanisms are inducible and contribute a substantial amount to metabolism in health, it is plausible that they contribute to the altered metabolism seen in sepsis. These mechanisms may be beneficial and protective, or may be maladaptive and harmful. Identifying their presence and effects on metabolism may improve the understanding of sepsis and could aid identification of novel therapeutic strategies.

1.2.2.1 Thermogenesis in early sepsis is adaptive and beneficial - fever

Fever is perhaps the best-known manifestation of thermogenesis. In human sepsis fever displays a strong association with survival. Henning *et al* reported on 378 patients with septic shock, of whom 207 were febrile. Multivariate logistic regression revealed an odds ratio of death of 10.82 (2.45-47.46) in patients who were hypothermic (<36°C) compared to those with fever (>38.3°C). Even those with a normal temperature (36-38.3°C) had an odds ratio of death of 2.33 (1.12-4.86) compared to febrile patients.[66] This relationship has been confirmed across multiple studies,[7,67] and suggests it is an adaptive mechanism.

Mechanisms underlying improved survival are unclear. Heat itself may be beneficial as increased temperature impairs pathogen replication, modulates the immune system through activation of heat shock proteins, increases the efficacy of some antibiotics, and is known to improve mitochondrial function during exercise.[33,68–70] A pilot randomised controlled trial of therapeutic hyperthermia in normothermic septic patients supports the notion of heat as a vital factor. In this study, afebrile

patients were randomised to be warmed by 1.5ºC from their baseline temperature or to 37.5ºC, whichever was higher, for 48 hours, and compared to normal care. Mortality was 18% in the treatment arm compared to 41% in the control arm. No immunological differences were seen between groups, suggesting another mechanism of benefit.[38] Larger RCTs are necessary to confirm these findings, but the data support the benefits of heat, whether endogenous or exogenous.

Conversely, two trials of active cooling in sepsis were stopped early, one due to harm and the other due to futility with a trend towards harm.[39,40] Of note, cold-blooded animals that are unable to generate fever endogenously will generate a fever using their environment and will perish if prevented from doing so, again supporting the importance of heat.[71]

Despite its universality, how fever is generated in humans has not been described. In febrile non-septic humans, each 1°C rise in temperature leads to an 8-12% increase in oxygen consumption.[72] Heat is therefore generated as well as conserved by peripheral vasoconstriction in the early 'heat up' phase. Whether the rise in oxygen consumption represents increased obligatory thermogenesis or induced facultative mechanisms is not known. UCP1 in BAT is unlikely to be responsible due to the low BAT mass in humans, the presence of fever in UCP1 null mice, and in pigs that inherently lack functional UCP1.[72–74]

Uncoupling protein 2 is activated during sepsis but is unlikely to generate fever as it is not intrinsically involved in thermogenesis.[75–78] UCP3 may play a role in febrigenesis; fever is abolished in UCP3 knockout ($UCP3^{-/-}$) mice and is recoverable by skeletal muscle specific re-expression of UCP3.[79] Our group studied a murine model of sepsis using $UCP3^{-/-}$ mice and found no difference in temperature or outcomes compared to wildtype mice.[80] Mice do however generate a hypothermic,

hypometabolic response to sepsis, making the study of fever problematic in this species.[81]

To my knowledge, no studies exist that have investigated ATP-dependent non-shivering thermogenic pathways in fever.

1.2.2.2 Thermogenesis in the recovery phase may be detrimental – browning of white adipose tissue

Conversely, in the recovery phase of sepsis heat production may be maladaptive and harmful. In the recovery phase of diseases akin to sepsis, including burn injury and cancer-associated cachexia, heat production causes hypermetabolism and contributes to cachexia and loss of lean tissue. The hypermetabolism is caused by induction of a thermogenic process known as *browning* of white adipose tissue. Browning describes the switch in phenotype of white adipose tissue from energy storing to a thermogenic brown adipose tissue-like phenotype (hence the name '*browning*'). This form of adipose tissue is aptly known as *beige adipose tissue*.[82,83]

1.2.3 Browning of white adipose tissue

1.2.3.1 Types of adipose tissue - white, brown and beige

Functionally, adipose tissue can be divided into three main types – white, brown and beige. White adipose tissue was traditionally considered inert and limited to the storage of triglycerides to protect against episodes of resource stress. Over the last three decades, adipose tissue has been identified as possessing considerable complexity with myriad endocrine, inflammatory, metabolic and cardiovascular functions.[84,85] Its importance should perhaps not be surprising as it physically apposes almost every tissue in the body.

Adipose tissue is formed of adipocytes containing a single large lipid droplet (accounting for >90% of the cytosol) and few mitochondria. The lipid droplet is a store of triglycerides that are hydrolysed into free fatty acids and glycerol, the balance of which is tightly controlled by insulin and catecholamines. Adipocytes comprise approximately 60% of WAT. Adipose tissue also contains preadipocytes, adipose stem cells, macrophages, fibroblasts, endothelial cells, dendritic cells, natural killer cells and T and B cells.[86] WAT is far from homogenous, is highly specialised, and often supports its immediate physical surroundings. For example, perivascular adipose tissue is implicated in vessel tonicity while mammary adipose tissue functions to support lactation. Other deposits may have more impact on whole body metabolism, for example visceral WAT and insulin resistance.[84]

Brown adipose tissue was previously thought to exist only in infant humans until its recognition in older children and adults on CT PET scanning.[55] BAT's primary function is thermogenesis and this is reflected in its ultrastructure. In humans it is predominantly located in the thoracic and cervical regions, and in the intrascapular region in rodents, with an abundant sympathetic innervation (by $ß_3$ adrenergic receptors) and blood supply. Brown adipocytes contain smaller but more numerous lipid droplets than white adipose tissue, as well as more abundant mitochondria, and more constitutively expressed thermogenic mechanisms including UCP1 and futile substrate cycles. BAT shares a mesodermal origin with skeletal muscle, a connection that is continues throughout life via batokines – endocrine and paracrine hormones which influence whole body metabolism.[87,88] Functioning BAT protects against metabolic disorders – UCP1 null mice are prone to obesity, type 2 diabetes and fatty liver disease. Beige adipose tissue straddles between white and brown types and will be discussed in more detail below.

1.2.3.2 Beige adipose tissue results from browning of white adipose tissue

Beige adipocytes result from the phenotypic switch of energy-storing tissue WAT to a thermogenic BAT-like tissue. Browning can be induced by systemic stress including cold exposure, burn injury, cancer-associated cachexia and exogenous catecholamines.[4,82,89] It is believed to be formed in two ways: *de novo* from beige adipocyte precursors dormant within white adipose tissue, and by a phenotypic switch from classical white adipose tissue.[90,91] Induction of beige adipose tissue in disease likely represents recruitment of an evolutionary process designed to protect mammals from hypothermia during prolonged cold stress. Beige adipose tissue recruitment is driven by systemic catecholamine release from the adrenal medulla and locally by sympathetic neurons that drive lipolysis and thermogenic programmes including expression of UCP1 and PGC1α.[92] One group found browning is then perpetuated by positive feedback loops; M2 macrophages are believed to generate further catecholamines under stimulation of IL-4 to further induce a thermogenic program, although this has not been reproduced in the literature.[92] Free fatty acids, such as palmitate, that are released during lipolysis, polarise macrophages to the M2 phenotype, causing further lipolysis and FFA release.[93–95]

Beige adipocytes manifest morphological and molecular changes to enable thermogenesis, including multiloculation of lipid droplets that increases surface area and substrate availability, increased mitochondrial density and expression of thermogenic mechanisms including UCP1 (considered the canonical marker of browning) and futile substrate cycles.[96] Beige adipose tissue returns to WAT on cessation of the driving stimuli by a process of autophagy.[97]

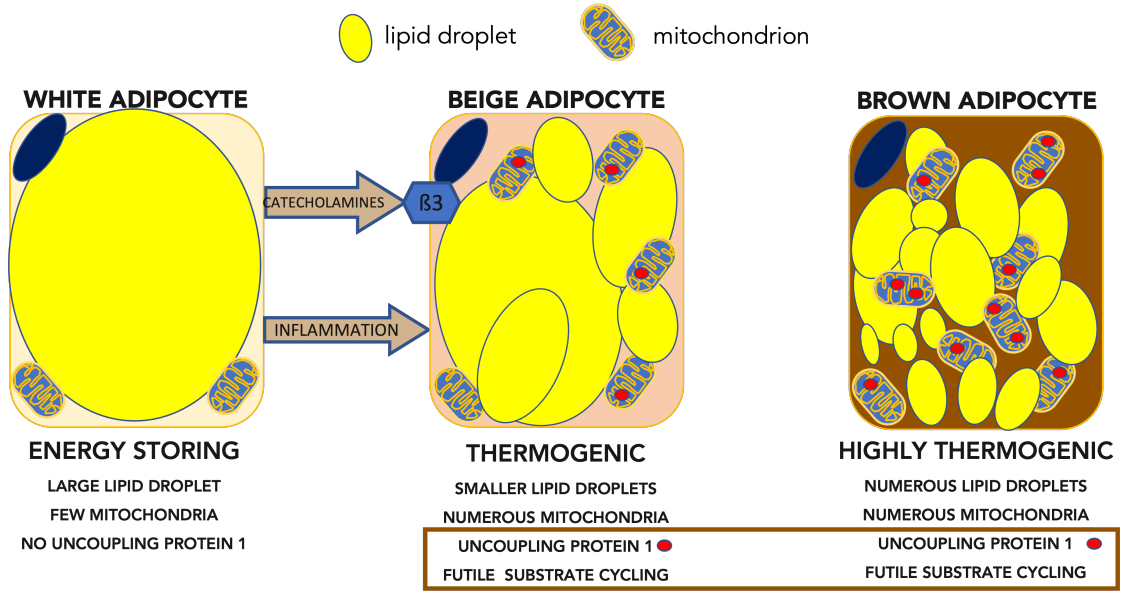

Figure 3. Schematic depiction of white, beige and brown adipocyte morphology.

Browning-induced hypermetabolism has been intensively studied as a potential therapeutic target in obesity and type 2 diabetes because of its effects on weight loss, increased insulin sensitivity and improved metabolic health.[94] Nonetheless, the detrimental effects of browning, including muscle wasting, hepatic steatosis and immunosuppression, are increasingly recognised in diseases akin to sepsis such as burn injury and cancer-associated cachexia.[94] In light of potential therapeutic benefits of browning in some diseases, but detrimental effects in others, it has been referred to as a 'double-edged sword'.[94] In the context of burn injury and cancer-associated cachexia, where it is believed to inappropriately increase metabolic rate and contribute to heat loss catabolism when anabolism would be preferred, it is regarded as maladaptive.[94] The improved recovery of lean tissue mass seen when hypermetabolism is reduced by adrenergic blockade with propranolol in patients recovering from burn injury, supports the hypothesis of a maladaptive role in these conditions.[98] The same could be presumed if it was present in sepsis.

1.2.3.3 Browning mediated thermogenesis may drive cachexia and muscle wasting in diseases akin to sepsis

The hypermetabolic recovery phase of sepsis is under-studied, though more extensive investigations exist in patients with burn injury and cancer-associated cachexia.

1.2.3.3.1 Browning of WAT in burn injury and CAC

Burn injury shares many pathophysiological features with sepsis including marked inflammation, elevated catecholamines and a hypermetabolic recovery phase. Like sepsis, burn injury survivors develop marked cachexia and myopathy that impair recovery and reduces their quality of life.[6] During the hypermetabolic recovery phase of burn injury, both obligatory and facultative thermogenesis increase, however facultative thermogenesis increases to a greater extent. Increased facultative thermogenesis may drive inappropriate hypermetabolism; this induces further tissue breakdown to release substrates but results in cachexia. Hypermetabolism has been attributed to browning of adipose tissue and persists for up to 2 years following burn injury.[6]

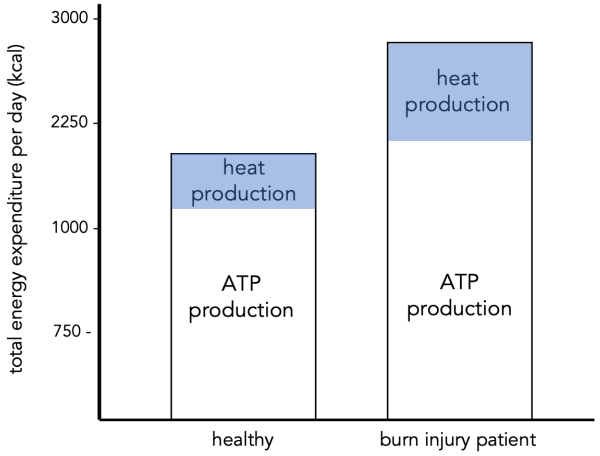

Figure 4. Absolute values of energy expenditure measured by oxygen consumption in the recovery phase of burn injury compared to health.
Total energy expenditure is increased with a greater proportion attributed to thermogenesis. Adapted from Porter et al.[6]

During the hypermetabolic response to critical illness, intake of exogenous substrate (food) may be reduced, poorly absorbed, or less well utilised by tissues. As a consequence, the body auto-cannibalises itself to release substrates.[94] Thermogenesis by beige adipose tissue increases oxygen and substrate consumption further and may drive unnecessary tissue breakdown and cachexia.[94] Indeed, browning is strongly implicated in the development of cachexia in burn injury and cancer. In a study of advanced malignancy, browning was found in most adipose tissue samples taken from cachectic patients with advanced malignancy but was not seen in non-cachectic patients.[82] Browning is thought to develop over days to weeks, but may be present before detection of the causative tumour. Patsouris *et al* demonstrated browning of subcutaneous white adipose tissue in 20 patients recovering from burn injury, as shown by reduced adipocyte size, increased mitochondrial density and increased expression of UCP1 and PGC1alpha at 10-21 days post-injury.[4]

Catecholamines and IL-6 are key mediators. IL-6 knockout mice were protected from burn-induced browning, but this returned on replacement of IL-6 expression

by bone marrow transplantation from wild-type mice.[99] Catecholamine blockade using the non-selective beta-blocker propranolol reduced hypermetabolism, ameliorated cachexia and reversed muscle-protein cachexia in burn injury and cancer-associated cachexia.[82,98]

1.2.3.3.2 Browning as a driver of cachexia and muscle wasting

Hypermetabolism is characterised by free fatty acid release, gluconeogenesis in the liver and release of amino acids from muscle, which contribute to an increased metabolic rate.[94] Further elevation of the metabolic rate through thermogenesis may exacerbate catabolism and drive tissue wasting in order to liberate fuel. Multiple mechanisms are implicated. Lipolysis likely plays a role as mice without adipose triglyceride lipase are protected from cancer-induced cachexia, although the opposite was found in mice with sepsis.[100,101] Lipid toxicity as a result of lipolysis leads to endoplasmic reticulum stress, mitochondrial dysfunction and deranged autophagy in both adipose tissue and muscle; these processes are both associated with cachexia and myopathy.[94]

Elevated circulating free fatty acids, particularly palmitate, provide another link. Palmitate drives adipose tissue wasting and muscle breakdown through palmitoylation. This mechanism is intrinsic to post-translational protein modification and regulation of apoptosis and autophagy, both of which are dysregulated in critical illness-induced myopathy (CIM).[94] Saturated fatty acids, including palmitic acid, also activate the NLRP3 inflammasome in adipose tissue and hepatocytes causing release of IL-1, insulin resistance and hyperglycaemia, which is a recognised risk factor for CIM.[76,94]

1.2.3.4 Browning of white adipose tissue in sepsis

Since the conception of this project molecular and morphological evidence of browning has been demonstrated in animal models of sepsis. Crowell *et al* investigated the inability of mice to replete white adipose tissue deposits following sepsis and identified UCP1 protein in epididymal WAT (eWAT) at 10 days after the septic insult.[102] No other browning-related changes were sought or reported. Ayalon *et al* later showed morphological evidence of browning in epididymal and inguinal WAT in a murine CLP model of sepsis.[103] White adipose tissue displayed breakdown of lipid droplets, increased mitochondrial density and expression of UCP1 at 18 hours, consistent with browning.[102] Of note, this timepoint is significantly earlier than is seen in burn injury, which is held to be the most severe form of adrenergic stress. More recently, Li *et al* also found increased UCP1 expression in eWAT sampled from septic mice at 18 hours. This was accentuated by infusion of noradrenaline, supporting catecholamines as a primary driver of browning in stress states. UCP1 expression was also increased in eWAT in non-septic mice receiving noradrenaline.[89]

To my knowledge, no studies of browning in humans with sepsis have been performed. Browning of adipose tissue in sepsis requires further characterisation and may be a therapeutic target for reducing cachexia and muscle wasting in survivors of sepsis.

1.2.4 Adipose tissue in sepsis

Adipose tissue is an important mediator in sepsis, with both active and reactive roles. Studies of adipose tissue in humans with sepsis are scarce, difficult to perform and necessitate close consideration as most rely on heterogeneous patient populations

of 'critical illness' undergoing confounding treatments (propofol infusion, parenteral nutrition, corticosteroids, insulin therapy).

Preservation of adipose tissue is frequently noted as occurring in critically ill patients.[104] One often cited study found no change in abdominal and femoral adipose deposits on serial CT scans, but was a small study of neurosurgical patients with trauma and intracranial haemorrhage, making extrapolation to other forms of critical illness problematic.[105] Mouse models of sepsis, on the other hand, showed marked reduction in the amount of adipose tissue, largely related to a reduction in adipocyte volume.[86,101,106,107] The loss of fat mass appears to persist and is perpetuated by ongoing inflammation, apoptosis and autophagy.[102]

Biopsies from patients with all-cause critical illness have found increased numbers of small adipocytes, an increase in the pre-adipocyte marker, Pref-1 and the adipogenesis marker, PPARγ.[107–109] These findings have been taken to represent critical-illness induced adipogenesis, but could be interpreted differently. PPARγ is also involved in polarisation of M2 macrophages, by which marked infiltration is seen (expression analysis was performed on bulk adipose tissue). Similarly, smaller adipocytes may result from lipolysis-induced shrinkage of pre-existing adipocytes. Both these processes would be consistent with the presence of beige adipose tissue.

Adipose tissue is increasingly recognised as an inflammatory mediator in sepsis. Macrophage infiltration is extensive, as it is across other body organs including lungs, liver and kidneys.[107,110] A recent study using single-cell RNA sequencing of eWAT from mice at one day and one month after induction of sepsis found that the cell sub-populations were the same but had changed in relative proportion and phenotype. On day 1 neutrophils were the dominant cell type followed by increases in macrophages, natural killer and T cells at one month. Differential gene expression

analysis showed persistence of changes at one month consistent with a syndrome of persistent catabolism - eWAT mass had reduced by 85% at this point. Of note, similar analysis performed in skeletal muscle of the same animals showed resolution of differential gene expression at 1 month, indicating adipose tissue as a likely source of long-term morbidity in patients recovering from sepsis. Macrophages were predominantly polarised to the M2/alternative phenotype characterised by anti-inflammatory cytokine production (IL-4), in keeping with browning.[111]

WAT also produces myriad local and circulating factors which bridge its inflammatory and metabolic functions – more than 50 have now been described.[112] In early critical illness and in response to experimental lipopolysaccharide, WAT produces predominantly pro-inflammatory cytokines including IL-6, IL-1ß, MCP-1 and TNFalpha.[113–115] In tandem with the inflammatory infiltrate, these adipocytokines increase insulin resistance leading to hyperglycaemia. Free fatty acids released during lipolysis also act as pro-inflammatory signalling molecules causing further insulin resistance and inflammation through TLR2 and 4 agonism.[113,116]

These studies show an initially predominantly pro-inflammatory phenotype which later switches to the amelioration of inflammation. These changes may be adaptive, but may also become dysregulated as seen in other organs and systems in sepsis. This dysregulation may lead to maladaptive changes, including browning.

1.2.4.1 The impact of obesity on sepsis

The potential importance of adipose tissue in sepsis has been highlighted following several observational studies reporting reduced mortality in patients classified as overweight or obese. This is known as the 'obesity paradox'. While obesity is more

commonly associated with ill health, with development of cardiac disease, diabetes and the metabolic syndrome, some data suggest it is protective in sepsis.

A meta-analysis of 7165 patients with sepsis found patients classified as overweight (body mass index (BMI) of 25-30) or obese (BMI 30-35) found odds ratios of death of 0.83 (0.73-0.91)) and OR 0.82 (0.67-0.99), respectively.[117] Another meta-analysis of 9696 patients found overweight patients but not obese patients were protected.[118] Strikingly, a large retrospective cohort of 55,038 patients found BMI to be inversely proportional to survival, even at BMIs over 40. Such studies are limited in their accuracy of weight and height measurement and the variability of body habitus reflected by simple BMI measurements. However, the paradox is seen in other wasting conditions including advanced malignancy, heart failure, end stage renal failure and HIV-related diseases, suggesting it is a topic worthy of study.[117] Obesity has also been shown to impact on long-term outcomes from sepsis. In humans dichotomised as lean (BMI <25) or obese or (BMI >25), lean patients were found to have significant wasting of vastus lateralis on day 8 of critical illness, while this was not seen in obese patients.[119]

As discussed, adipose tissue is a heterogeneous tissue with variable roles dependent on type and location, so the reality is likely more complex than a simple correlation between total fat mass and survival. Patients with higher ratios of visceral to subcutaneous adipose tissue show greater mortality from sepsis regardless of BMI, whilst perivascular WAT influences vasoplegia in septic rats.[120–122]

Many hypotheses have been proffered to explain the obesity paradox. Adipose tissue is intricately linked to whole body metabolism and communicates with many other tissues. Adipokines, such as irisin and adiponectin from adipose tissue and

resistin from adipose tissue macrophages, impact upon whole body metabolism and insulin resistance, both of which correlate with survival in patients with sepsis.[112,123]

Nutrient availability has also been suggested, although the evidence is conflicting. Obese mice with sepsis have higher circulating triglycerides, non-esterified fatty acids and ketones indicating enhanced lipolysis.[101] Blockade of lipolysis by knock-out of adipose tissue-specific lipase worsened muscle weakness while a parenteral ketone infusion was protective.[100] Compared to lean humans, obese humans are less lipolytic per unit of subcutaneous adipose tissue but show an increased overall systemic lipolysis response to beta-agonism.[124]

Obesity also appears to protect from browning and may explain why obese patients suffer less critical illness-induced myopathy. In studies of sepsis-induced browning discussed above, eWAT from mice with diet-induced obesity showed blunted UCP1 expression and lipid droplet budding and decreased mitochondrial density.[89,106] Underlying mechanisms remain unclear but reduced cellular infiltration and reduced $ß_3$-adrenergic receptor expression in adipose tissue in obese subjects have been proposed.[89,106]

1.3 Summary of introduction

- Survivors of sepsis frequently suffer from cachexia and muscle wasting which impairs recovery, reduces quality of life and is associated with increased long-term morbidity and mortality.

- Thermogenesis impacts upon sepsis outcomes. In the early phase of sepsis thermogenesis (in the form of fever) is associated with increased survival. In the

recovery phase however, it may be detrimental by driving hypermetabolism and thus lead to further cachexia and muscle wasting.

- In diseases akin to sepsis, such as burn injury and cancer-associated cachexia, browning of white adipose tissue contributes to hypermetabolism, cachexia and muscle wasting. Browning describes the switch of energy storing in white adipose tissue to a brown adipose tissue-like phenotype, known as beige adipose tissue.

- Browning has been demonstrated in animal models of sepsis but requires further characterisation. It may represent a target for the treatment of cachexia and muscle wasting in sepsis survivors.

1.4 Hypotheses

- Adipose tissue becomes thermogenic in the recovery phase of sepsis
- The thermogenesis is caused by browning of white adipose tissue
- Browning causes hypermetabolism in the recovery phase of sepsis and contributes to cachexia and muscle wasting

Chapter 2. Characterisation of a zymosan peritonitis model of sepsis recovery

2.1 Background

2.1.1 Zymosan peritonitis causes a sepsis-like syndrome, myopathy and cachexia

My host lab has an established long-term model for study of the recovery phase of sepsis, which has been characterised both by the lab and other groups.[125–127] The model utilises zymosan, a glucopolysaccharide fungal cell wall component from *Saccharomyces cerevisae*, which is injected into the peritoneal cavity.

Zymosan induces inflammation via pathways common to bacterial sepsis. The acute phase is characterised by peritonitis and is driven by activation of Pathogen Recognition Receptors, predominantly toll-like receptor 2, and macrophage activation following phagocytosis.[128] This leads to complement activation, increased generation of reactive oxygen species, prostaglandins and leukotrienes, and a cytokine cascade characterised by high levels of circulating TNFα and IL-6 in the acute phase and elevated inflammatory cytokine mRNA in tissues.[129–132]

Zymosan is non-degradable and thus provides a prolonged inflammatory stimulus, which is further protracted by suspension in a mineral oil such as liquid paraffin. Two- and three-phase illnesses have been described.[125,127] Both begin with an acute phase with a clinical nadir at 24-48 hours and variable mortality, followed by recovery from days 3 to 7. Volman *et al* described a third phase from days 7 to 14 characterised by further deterioration and multi-organ dysfunction. Mortality is reported at 20-30% in this phase and is attributed to ongoing systemic inflammation and bacterial translocation from the gastro-intestinal tract, although mortality is still seen in sterile animals.[133] In our experience, and that of Rooyackers *et al*,[126] the

third phase is absent and animals continue to recover to day 14 without further mortality.

Illness severity and mortality vary by dose, but the sustained inflammatory response caused by zymosan allows for a prolonged clinical syndrome with lower lethality, reflecting the timelines of human sepsis and enabling study of the recovery phase.[126]

Zymosan peritonitis has predominantly been utilised as a model of critical illness myopathy and cachexia. Previous work from my host lab demonstrated a patchy necrotising myopathy phenotype persisting to at least 14 days in soleus muscle but not in gastrocnemius.[24] Reductions in soleus and gastrocnemius mass were both seen at day 14, reflected functionally by increased treadmill fatiguability and decreased tetanic force and grip strength.[126]

Multiple myopathic pathways have been identified in sepsis including protein wasting, impaired muscle protein synthesis and proteosome dysfunction.[24,125,126] In my host lab's model, negative regulators of muscle mass MuRF1, MAFBx and myostatin were elevated at days 2-4 but normalised by day 7.[126] Necrotising histological findings in soleus muscle at day 14 were associated with activation of caspases 3 and 9 and polyubiquitin proteins, and elevation of proteosome substrates (myofibrillar actin).[24]

The associated cytokine response also mimics human sepsis. Pro-inflammatory cytokine IL-6 peaks around 6 hours and normalises by day 2, while 'anti-inflammatory' IL-10 remains elevated to day 14.[126] In contrast to human sepsis, however, oxygen consumption and CO_2 production both fell acutely. In humans, oxygen consumption initially increases with severe infection and early sepsis then falls to 'abnormally normal' levels with increasing illness severity.[62] The model also

shows a reduction in respiratory quotient, indicating a switch to lipid metabolism, and this is reflected by reduced total body fat mass at day 12.[126]

The severity of the model is an important consideration. Ideal models reflect human mortality rates and illness severity while minimising animal suffering but enabling study of the recovery phase. Rooyackers *et al* reported 16% mortality using a zymosan dose of 50mg/100g body mass.[125] Previous work from my host lab, using 30mg zymosan/100g body mass resulted in a mortality rate of 1.4%. Importantly, this dose failed to generate the sepsis phenotype in 10% of animals, which then could not be used for downstream experiments.[126] Both models achieved a post-sepsis cachectic myopathic phenotype. Of note, zymosan doses are not directly comparable due to batch-to-batch variation.

Taken together, zymosan peritonitis causes a sepsis-like syndrome leading to myopathy. This reasonably mimics human sepsis and may therefore be appropriate for the study of browning of adipose tissue during the recovery phase.

2.1.2 The importance of thermoneutrality in animal models

Thermoneutral temperature is the environmental temperature at which the animal does not expend energy on facultative thermogenesis to maintain body temperature. Facultative thermogenesis is energetically costly, hence feeling cold is unpleasant to encourage the person to find warmth and to reduce unnecessary energy expenditure.[44] Thermoneutral temperature in lightly clothed humans is 21°C, 26°C for rats and 30°C for mice.[47] Housing below thermoneutral temperatures induces 'cold stress' and profound metabolic alterations that may confound or obfuscate the study of metabolic processes, yielding unreliable data.[47,134,135]

Mice housed at 22°C rather than at thermoneutrality (30°C) experience a 50% increase in metabolic rate, food intake and heart rate and significant alterations in body mass and leukocyte count.[47] Extreme cold stress (4°C) induces browning of WAT to protect from hypothermia.[136] The febrile response is also dependent on ambient temperature – mice and rats at thermoneutrality develop pyrexia and raised metabolic rates whereas sub-thermoneutral temperatures induce a hypometabolic, hypothermic response. A recent study in humans reported similar findings, with increased rates of hypothermic sepsis associated with colder environmental conditions.[135,137,138] Studies of tolerant and resistant responses to inflammation found that cold stress of 22°C induced mice to enter into an immunologically 'tolerant' state, rather than mounting 'resistance', and thus profoundly altered their sepsis phenotype.[139] These findings signal the importance of conducting future studies at thermoneutrality, including both the acute and recovery phases of critical illnesses.

Other differences between rodent and human thermoregulation should also be considered, including the role of fur and the tail in temperature control, and the proportionally much larger BAT deposits present in rodents.[134]

2.2 Methods

2.2.1 Zymosan peritonitis model of sepsis

Zymosan peritonitis was chosen as an appropriate model of sepsis recovery because it induces a prolonged inflammatory sepsis-like syndrome followed by marked cachexia, despite a lower mortality, allowing for study of the recovery period. All experiments were performed under Home Office approved Project Licence (PPL 6856925) under the Animals (Scientific Procedures) Act 1986. The model had been used extensively by the lab previously, but not in recent years. I therefore re-established and optimised the model for the project. All the following work was performed by myself except where specifically acknowledged.

2.2.2 Animals and acclimatisation

Male adult albino Wistar rats weighing 300-411g were used for all experiments (Charles River, Harlow, UK). Animals were acclimatised to thermoneutrality at 26°C for a minimum of 48 hours before experiments commenced. Thermoneutrality was achieved in a closed room heated with a Dyson 'Hot and Cool' jet heater which contains an internal thermostat to accurately control room temperature. Ambient room temperature was also monitored by a thermocouple and mercury thermometer to ensure accuracy.

2.2.3 Zymosan preparation

Zymosan A (Sigma Z4250) was suspended in liquid paraffin (Sigma 232-384-2) at a concentration of 40 mg/ml. All experiments were performed using a single batch of zymosan to reduce batch-to-batch variation and the need for dose adjustment.

Zymosan suspension was stored at 4°C and sonicated at 37°C in an ultrasonic water bath to create a homogenous suspension at body temperature before use.

2.2.4 Sepsis induction

Animals were randomised to sham controls or to receive a zymosan septic insult. All animals were then anaesthetised under 2% isoflurane anaesthesia and received buprenorphine analgesia (0.06 mg/kg body weight, subcutaneously). Animals randomised to undergo sepsis had a 14 gauge cannula introduced into the peritoneum through which zymosan suspension was injected at a dose of 400 mg/kg body weight (e.g. a 300g animal received 3 ml). This dose was established during pilot studies to achieve a sufficiently severe insult with a low mortality. Animals were then recovered under direct observation until independently mobile. Animals randomised to the sham arm did not receive an intraperitoneal injection because of the risk of visceral trauma, but received all other interventions identically to animals in the sepsis arm.

The zymosan-peritonitis sepsis model was continued to multiple time points of interest: 6 hours (sham=5, sepsis=5), 1 day (sham=5, sepsis=5), 3 days (sham=9, sepsis=9), 7 days (sepsis=6) and 14 days (sham=9, sepsis=9). In addition, seven septic animals either died or were culled due to illness severity before the experiment end-point.

2.2.5 Housing, feed and illness severity assessment

All animals were individually housed at thermoneutrality (26°C) with standard chow (18.4% protein, fat 6%, carbohydrate 44.2%, fibre 18.5%, ash 5.5%. Teklad, Envigo, Bicester, UK) and water provided *ad libitum*.

Clinical scoring was performed a minimum of four times daily using an in-house validated scoring system. The system comprises of three categories - Appearance, Behaviour, Clinical with each category scoring between 0 and 3. 0 corresponds to normal, 1 to mild, 2 to moderate and 3 to severe. The highest score in any category was documented as the score for the animal at that time. A score of 3 mandated increased monitoring, and termination if the score persisted. A fourth category identifies diarrhoea for > 48 hours, bleeding, ataxia, focal weakness or convulsions, vocalisation and untreatable skin wounds, all of which result in immediate termination. The scoring system predicts non-survival, allowing for timely and humane termination if necessary.

2.2.6 Physiological measurements

Body mass was measured at the same time (mid-morning) each day. Food consumption was measured daily by weighing the remaining food available to the animals, including large pieces collected from the cage floor. Measurement of water consumption was not possible due to repeated leakage from bottles.

Core temperature was measured in a subset of animals (sham 6, sepsis 10) at baseline, 6 hours and at 1, 3, 7 and 14 days. Temperature was measured by insertion of a thermocouple into the rectum/colon while under 2% isoflurane anaesthesia. Echocardiography was performed on the same subset of animals at baseline, 6 hours and at 1, 3 and 7 days during recovery from sepsis. In this subset a small patch of fur was shaved from the left aspect of the chest, followed by removal of stubble with hair removal cream (Veet, Boots, Nottingham, UK). The velocity time integral (VTi) was measured by visualisation of the aortic outflow tract, Doppler spectral analysis of aortic blood flow, and calculation of the area-under-the-curve per ejection from the heart. Five measurements were taken and the mean

calculated to account for variation across the respiratory cycle. Stroke volume was then calculated by multiplying the VTi with the cross-sectional area of the ascending aorta, calculated from a fixed diameter established in the literature.[140]

Animals undergoing temperature measurement and echocardiography were anaesthetised on 5 occasions. Other animals were only anaesthetised on induction at the experiment end.

Grip strength was measured in a subset of animals at baseline, 10 and 14 days. Grip strength has been used by our lab and others previously, with attempts by myself to develop it further to improve accuracy. Animals were trained to grip a grid attached to an isometric force transducer (Linton Instruments, Diss, UK) with both forelimbs. Once firmly attached they were then gently but firmly pulled backwards until their grip was overcome. Five measurements were taken per animal, with 20 seconds of rest between efforts. The three highest readings were used for analysis. This technique yielded highly variable results with significant inconsistency due to animal stress, compliance and effort and was therefore not extended to all animals. Repeated attempts to improve consistency through animal training, alterations in timing between measurements, and reduction of stress proved unsuccessful.

2.2.7 Experiment end and sample collection

The experimental end point at day 14 was used following optimisation experiments for the following reasons: animals demonstrated a cachectic phenotype including visible frailty, myopathy and marked weight loss which was not recovered despite resolution of clinical illness scores and food consumption; demonstration of browning in mouse models of sepsis in the literature at days 1 and 10[102,106]; and

reflection of timescales of human sepsis where the initial insult has dissipated and weakness and cachexia has developed.

At the end of the experiment the animal was anaesthetised with 2% isoflurane until the temperature had been measured. Isoflurane was then increased to 4% to induce deep anaesthesia and a midline laparotomy performed. In a subset of animals a thermal image of the abdominal cavity was taken encompassing the liver and eWAT. The diaphragm was then incised and a 21 gauge needle introduced into the left ventricle. Blood was withdrawn until exsanguination or absent flow. The heart was then removed to ensure cessation of circulation.

Epididymal and retroperitoneal adipose tissue were removed, washed in phosphate-buffered saline (PBS) and placed into either ice-cold biopsy preservation medium (BIOPS, for respirometry or multiphoton imaging, see table for contents) or snap frozen in liquid nitrogen. Soleus, gastrocnemius, plantaris, extensor digitorum longus and tibialis anterior were dissected from the hindlimb and either placed in ice-cold BIOPS (for respirometry or microscopy) or snap frozen in liquid nitrogen and immediately weighed. Muscle mass was normalised to baseline body mass to control for variation in starting weight of the animals.

Table 1. Biopsy preservation medium constituents.

Constituent	Final concentration (mM)
CaK_2EGTA	2.77
K_2EGTA	7.23
Na_2ATP	5.77
$MgCl_2 \cdot 6H_2O$	6.56
Taurine	20
Na_2Phosphocreatinine	15

Imidazole	20
Dithiothreitol	0.5
MES hydrate	50
Final pH adjusted to 7.1	

2.2.8 Collection of plasma and serum

Blood collected from cardiac puncture was placed into a serum tube containing a silica serum activator (BD Vacutainer, Becton Dickinson, Plymouth, UK). These were then centrifuged at 1300g at room temperature for 10 minutes. The supernatant of serum was then aliquoted and stored at -80°C.

2.2.9 Circulating markers of organ function

Serum samples taken from day 14 sham animals (n=5) and animals at day 1 (n=5) and 14 (n=5) of sepsis recovery were sent for analysis at the Pathology Lab, Royal Veterinary College, Potters Bar, Herts, UK. Creatinine, urea, bilirubin, albumin, alanine transaminase and creatine kinase were measured by photoelectric colorimetry on a AU680 analyser (Beckman Coulter, High Wycombe, UK). Haemolysis, lipaemia and icteric indices were checked for each sample.

2.2.10 Cytokine Multiplex Assay

Serum cytokines were measured using a bead-based multiplex assay panel (LegendPlex Rat Inflammation Panel, Cat 740401, BioLegend, London, UK) with the kind assistance of Dr Pelin Golforoush, Hatter Institute, UCL (samples were collected and prepared by myself and the assay run by Dr Golforoush). The panel allows simultaneous quantification of 13 cytokines per well on a 96 well plate. Sample was

added to beads conjugated to an analyte-specific antibody. The beads of each analyte have a unique size and internal fluorescence. The sample was washed and a detection antibody added which binds to the analyte, forming a sandwich-ELISA-type configuration. A fluorescent signal (Streptavidin-phycoerythrin) was then added which binds to the detection antibody. Flow cytometry was then performed to ascertain the beads of each analyte and the quantity of bound fluorescent analyte, yielding serum concentrations of cytokines. Cytokines were measured in serum from 8 day 14 sham animals and 5 at day 3, 7 at day 7 and 7 at day 14 of recovery from sepsis.

2.2.11 Immunohistochemistry of myosin heavy chain composition of skeletal muscle

Immunohistochemistry and analysis of myofibre type and cross-sectional area was kindly performed by Dr Ali Alqallaf, Dept of Biomedical Sciences, University of Reading. As discussed above, critical illness myopathy is characterised by reduction in muscle mass and cross sectional area and was used to quantify myopathy in this study. Extensive mechanistic studies of myopathy have been performed using this model by my lab and others and were not repeated here.[24,126] Myosin heavy chain typing was performed in soleus and tibialis anterior (superficial and deep) from sham animals and at days 3 and 14 of recovery from sepsis to look for signs of sepsis-induced myopathy. Muscles were mounted in OCT LT Embedding Compound (TAAB Lab Equipment Ltd, Berkshire, UK) and snap frozen in liquid nitrogen cooled isopentane. Blocks were then cryo-sectioned to a thickness of 15 µm using a cryostat (Bright Instruments, Huntingdon, UK), collected onto slides and stored at -80°C for later use.

For analysis, sections were incubated at room temperature for 15 minutes. A PAP pen (Agar scientific L4197S, Stansted, UK) was then used to make a hydrophobic

barrier after which the sections were left to dry for 15 minutes. Slides were then washed three times in PBS, in permeabilization buffer for 15 minutes, washed again in PBS and incubated in blocking buffer for 30 minutes. Slides were incubated with the primary antibody overnight at 4°C followed by three 10 minute washes in blocking buffer to remove excess primary antibodies. Secondary antibodies diluted in blocking buffer were incubated with the slides for 1 hour at room temperature, again followed by three 10 minutes washes with blocking buffer. The next primary antibody of interest was added and the steps repeated.

Once addition of the primary antibodies was complete, slides were mounted with a drop of nuclear stain DAPI (4',6-diamidino-2-phenylindole, 1:2000 (Fisher Scientific D1306)) and Dako fluorescence mounting medium (Agilent, REF S3023, Didcot, UK) Slides were imaged with a AxioImager epifluorescence microscope with AxioVision SE64 software (Zeiss, Cambourne, UK). Myosin heavy chain fibre type and cross-sectional area were measured using ImageJ (NIH, Bethesda, USA). Different myofibres were identified by staining and 2 dimensional areas measured by circumscribing individual myofibres using the 'region of interest' tool followed by 'measurement' which yields the cross sectional area. Potential selection bias was mitigated by measurement of myofibres in each field.

Table 2. Primary antibodies for immunohistochemistry.

Antigen	Type	Dilution ratio	Supplier
MyHC I - A4.840	Monoclonal	1:1	DSHB
MyHC IIA - A4.74	Monoclonal	1:1	DSHB
MyHC IIB - BF-F3	Monoclonal	1:1	DSHB

Table 3. Secondary antibodies for immunohistochemistry.

Antibody	Host species	Dilution	Supplier
Alexa flour 488 anti-mouse	Goat	1:200	Invitrogen Cat # A-11029

Alexa flour 594 anti-mouse	Goat	1:200	Invitrogen Cat # A-21044
Alexa flour 594 anti-rabbit	Goat	1:200	Invitrogen Cat # A-11037

2.2.12 Statistical analysis

Normality was judged using frequency plots and normality testing using D'Agostino-Pearson normality test. Parametric tests (t tests, ANOVA) were used for normally distributed data and non-parametric tests (Mann-Whitney, Kruskal-Wallis) for non-normally distributed data. Parametric data are displayed as means with error bars representing standard deviation (SD). Non-parametric data are displayed as medians and inter-quartile range (IQR). Where small sample sizes preclude assessment of distribution, larger data sets of directly related data were used to guide testing. Where no reference data set exists non-parametric tests are used.

2.3 Results – Zymosan peritonitis causes a sepsis-like inflammatory syndrome leading to myopathy and cachexia in the recovery phase

2.3.1 Sepsis phenotype caused by zymosan peritonitis

A total of 69 adult male Wistar rats weighing 300-411g were used, of which 28 underwent sham experimentation and 41 received intraperitoneal zymosan. Seven of the 41 animals receiving a septic insult died or were culled prematurely due to illness severity in keeping with our clinical scoring system, indicating a mortality of 17%. Mortality was 0% in the sham arm.

In keeping with the 3Rs framework of humane animal research, tissues and samples were collected from those requiring premature termination, but were not used for ex-vivo studies (respirometry, microscopy) for logistical reasons. The nature of studying recovery means that only survivors were used for downstream experiments. The majority of premature deaths and terminations occurred at 18-36 hours; it is thus plausible that animals in studies that were terminated at 6 and 24 hours were non-survivors, however signs of illness were not severe enough to indicate this.

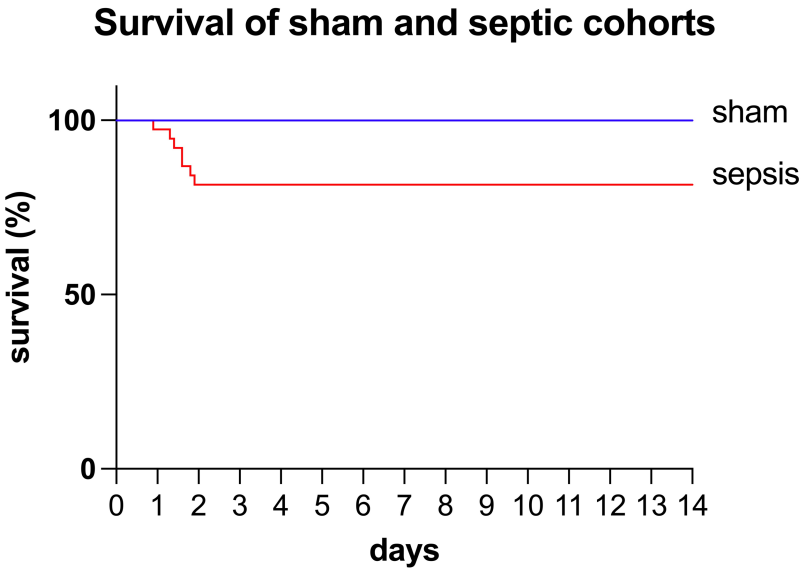

Figure 5. Survival of sham and septic animals.

Kaplan-Meier curve demonstrating survival in sham and septic animals over 14 days of study. Mortality was 0% (0/28) in sham animals, and 17% (7/41) in animals receiving a septic insult, all of which occurred 24-48 hours after the septic insult. Of note, ten animals were culled before the 24-48 hour timepoint (5 at 6 hours, 5 at 24 hours).

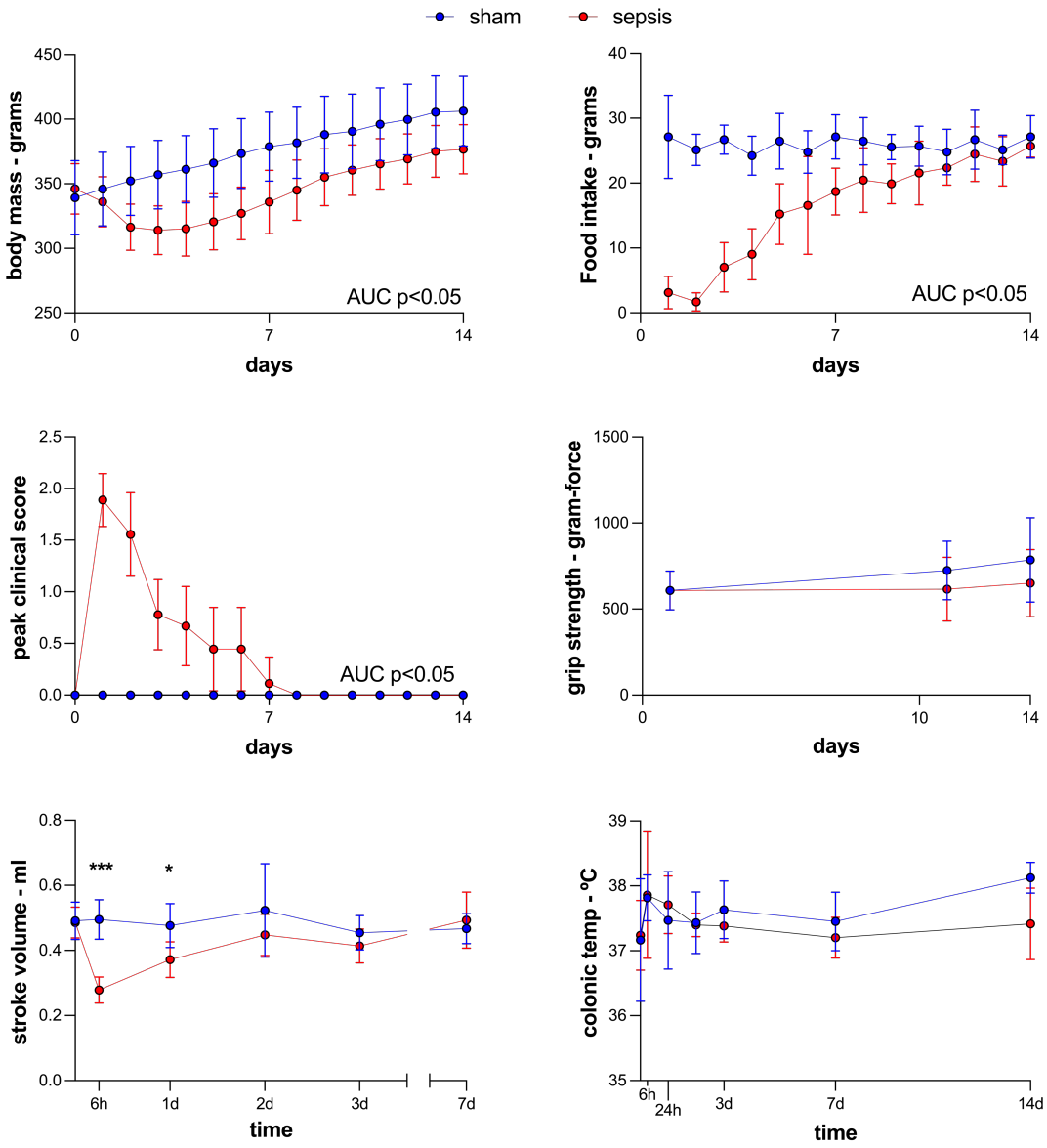

Figure 6. Physiological parameters of 14-day zymosan peritonitis model of sepsis recovery

a) Body mass in sham vs septic rats measured over 14 days. Septic animals (AUC 4797g (CI 5126-5421)) lost more weight compared to sham animals (AUC 5269g sham (CI 4691-4904). Data shown as mean ± SD.

b) Daily intake of standard chow available ad libitum to sham and septic animals. Animals with sepsis had a reduced food intake until day 9 (AUC 214.5g (95% CI 193.7-253.3) compared to sham animals (AUC 335.7g (95% CI 318-352). Data shown as mean ± SD.

c) Peak daily clinical score assessed across three scored parameters. Septic animals developed acute illness reaching its peak at 24-48 hours, followed by recovery by days 3-5. Data shown as mean ± SD.

d) Grip strength measured at baseline, 10 and 14 days in sham and septic animals. No significant difference was seen in grip strength between sham and septic animals. Data shown as mean and SD. Mixed effects analysis.
e) Stroke volume measured by echocardiography in sham (n=6) and septic (n=9) animals at baseline, 6 and 24 hours, 3 and 7 days. Stroke volume was significantly reduced in septic animals at 6 and 24 hours compared to sham. Data shown as mean and SD. Mixed effects analysis.
f) Colonic temperature in sham (n=6) and septic (n=9) animals at baseline, 6 and 24 hours, and at 1 3, 7 and 14 days. Temperature was equivalent between groups throughout the experiment. Data shown as mean ± SD.

2.3.2 Illness severity score and clinical trajectory

Animals underwent assessment to monitor severity of illness and to identify their clinical phenotype. Following recovery from anaesthesia, animals in the sham arm appeared and behaved normally and showed no signs of illness, scoring 0 across illness severity scores. Animals receiving a septic insult initially appeared and behaved normally, typically scoring 0-1 in the first 2 hours after recovery. After 2 hours septic animals appeared unwell, displaying pilo-erection, a hunched posture and facial grimacing. Behaviour change was also displayed with reduced spontaneous movement, lack of interest in their surroundings and reduced or absent food foraging. Clinical assessment revealed panting and increased respiratory rate. The peak of the acute illness occurred at 18-36 hours when the modal clinical score was 2 and food intake at its nadir. Overall, clinical scores were significantly higher in septic animals compared to sham (AUC 5.9 (4.2-7.6) vs. 0 (95% CI 0-0).

In survivors, septic animals began to recover from day 3 onwards, as signalled by normalisation of appearance, behaviour, clinical signs and resumption of food intake. By day 3 behaviour was typically normal with no clinical signs of illness present (e.g. panting). Some animals continued to score 1 for appearance due to pilo-erection, but this was absent by day 9. Clinical score did not differ significantly between sham and septic animals from days 8-14 (AUC 0 (95% CI 0-0) vs 0.17 (CI 0-3.9)).

The sepsis phenotype was also apparent on subjective assessment. Sham animals felt and looked normal while septic animals appeared frail, felt physically weak and developed a notable cachectic appearance continuing to day 14.

2.3.3 Body mass and daily food intake

Sham and septic groups had equivalent body mass at baseline. Sham animals ate a mean of 24 ± 3.5g of chow per day. Septic animals displayed a nadir of food intake at day 2 with a mean intake of 1.7 ± 1.4g. Thereafter food intake increased in septic animals, reaching equivalence with sham animals by day 10.

Body mass increased uniformly in sham animals by 4.7 ± 1.8g per day. Of note, rats of 3-4 months are still in a growth phase. Septic animals lost weight, displaying a nadir of body mass at day 3 with a mean loss of 32 ± 11g body mass or 9.2 ±3%. Thereafter septic animals gained weight uniformly at a mean of 6.3 ± 1.5g per day. Septic animals remained significantly lighter than sham animals at day 14 (406g vs 376g, p=0.017), indicating a state of cachexia.

2.3.4 Core temperature

Core temperature measured by insertion of a rectal/colonic thermocouple under anaesthesia at 6 hours, 24 hours and 3, 7 and 14 days was equivalent between groups. Sham animals displayed a mean temperature of 38.1°C compared to 37.4°C in septic animals at day 14.

2.3.5 Stroke Volume

The reduction in stroke volume may be caused in part by myocardial depression related to a sepsis-induced cardiomyopathy. Our lab has established this in a tethered faecal peritonitis model of sepsis involving fluid resuscitation from 2 hours after insult. The equivalent is not possible in the zymosan peritonitis model as it does not use fluid resuscitation. The drop may also reflect fluid loss into the 'third space' e.g. peritoneal cavity and tissue oedema, and reduced fluid intake. However, the latter is less likely as rats can conserve water very efficiently.

2.3.6 Grip strength

Attempts were made to assess functional indicators of myopathy. Grip strength measurement was problematic due to variable animal compliance, effort and the importance of avoiding unnecessary stress (both for animal welfare and the reliability of results). Multiple efforts to train animals in the week preceding experiments were unsuccessful. Sham animals showed a significant rise in mean grip strength at 14 days compared to baseline, which was not seen in septic animals ($p=0.049$). Treadmill testing using electrical stimulation, as previously performed in the lab, is no longer permissible under the terms of the Project Licence. Efforts to use encourage treadmill use to fatigue including dried banana and peanut butter were entirely unsuccessful.

2.3.7 Circulating markers of organ function

Markers of organ function were measured to identify sepsis-related organ dysfunction, gauge illness severity and understand the biochemistry of the recovery phase. Serum levels of creatinine, bilirubin and creatine kinase were not significantly different between sham animals and those at day 1 and 14 septic insult. Urea was

significantly lower at day 14 of sepsis recovery compared to day 1 ($p=0.0189$), but neither septic group differed compared to sham animals.

Alanine transaminase was significantly lower in animals at day 1 and 14 after their septic insult compared to sham animals ($p=0.0001$ and $p=0.0066$, respectively), in keeping with previous experience with the model.

Albumin was significantly lower at day 1 of sepsis compared to both sham animals and at day 14 of sepsis recovery ($p<0.0001$ and $p=0.005$, respectively). By day 14 of recovery albumin levels were equivalent to those seen in sham animals.

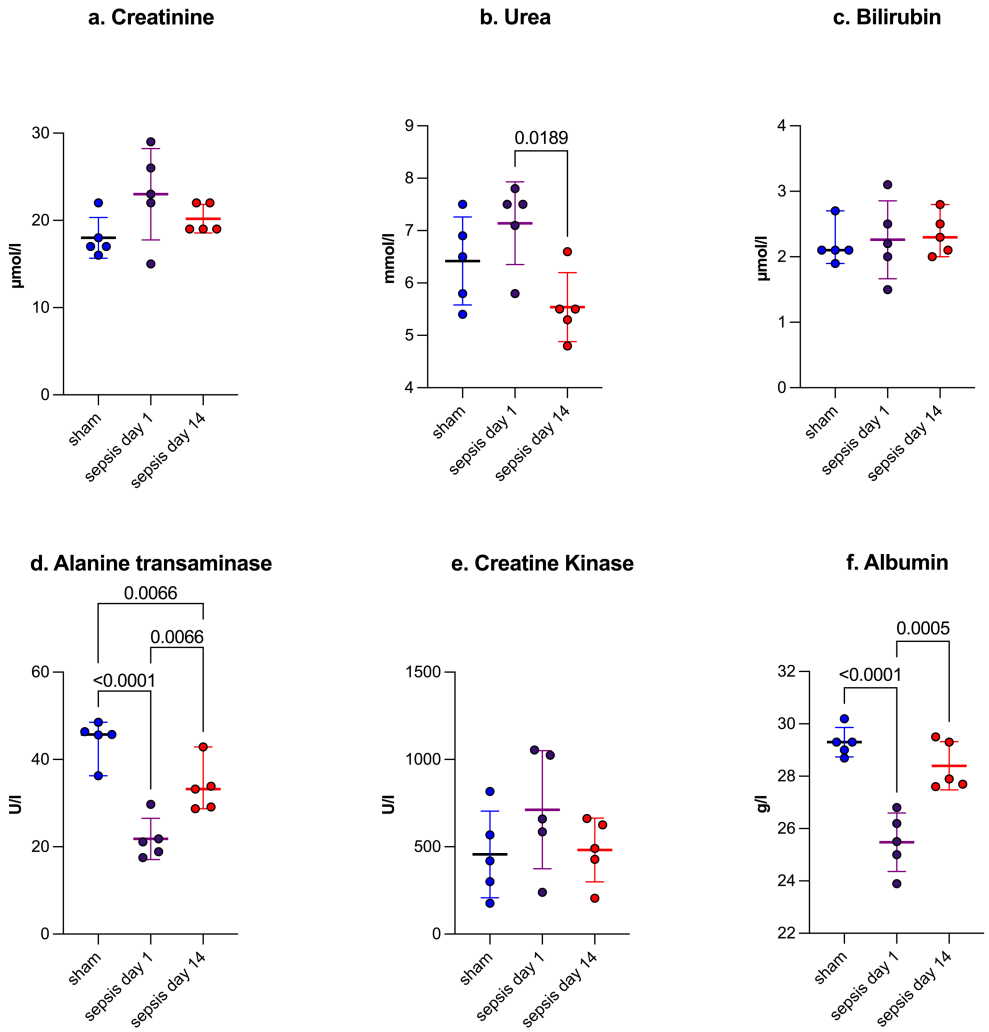

Figure 7. Circulating markers of organ function in sham control animals and at days 1 and 14 of sepsis

a. Creatinine did not differ significantly between sham and septic animals, but showed a trend towards elevation at day 1 of sepsis.

b. Urea showed a trend towards elevation at day 1 but did not reach statistical significance. Urea was significantly lower at day 14 of sepsis recovery compared to day 1.

c. Bilirubin did not differ between sham and septic groups.

d. Alanine transaminase was reduced at day 1 compared to sham and at day 14.

e. Creatine kinase did not differ between sham and septic groups.

f. Albumin was significantly reduced at day 1 compared to sham, and at day 14.

Data shown as mean and SD. Statistics: one-way ANOVA.

2.3.8 Inflammatory cytokine panel

Serum cytokines were measured to understand the inflammatory phenotype and trajectory of illness, and as driving factors in adipose tissue physiology and browning.

Serum levels of IL-1α, IL-1β, TNF-α, INF-γ, IL-18, GM-CSF, CXCL1, IL-17A, IL-33, IL12p70 and IL-10 did not significantly differ between sham animals and animals at days 3, 7 or 14 of sepsis recovery.

Compared to sham, IL-6 was raised at day 3 ($p=0.005$), day 7 ($p=0.0024$) and day 14 ($p=0.0021$) of sepsis recovery.

MCP-1 was raised at day 7 and day 14 of sepsis recovery compared to sham ($p=0.01$).

These findings were not consistent with previous experience of the model.[126] For example, IL-6 fell to normal levels before day 3 while IL-10 remained elevated at later time points, neither of which were seen here. Internal quality control of the cytokine multiplex did however indicate a successful assay.

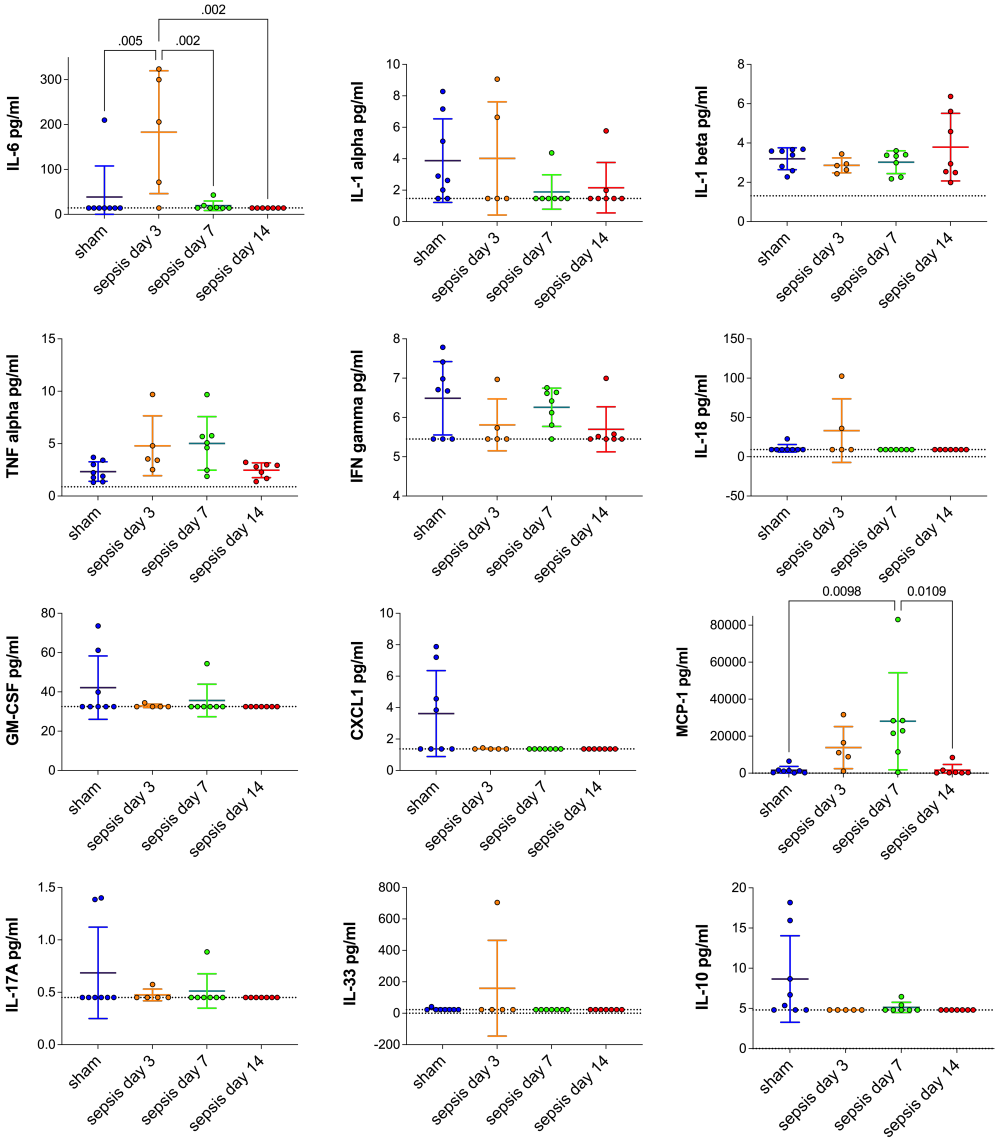

Figure 8. Serum cytokines from sham animals and day 3, 7 and 14 of recovery from sepsis.

Serum analysed by flow cytometry immunoassay panel from sham (n=8), day 3 (n=5), day 7 (n=6) and day 14 (n=7) sepsis recovery animals. IL-6 was significantly raised at day 3 compared to sham and day 7 and 14 sepsis recovery. MCP-1 was significantly raised at day 7 compared to sham and day 14 sepsis recovery. All data shown as mean and SD. Statistics: one-way ANOVA. Dotted horizontal line is the lower limit of detection of the assay.

2.3.9 Zymosan peritonitis causes a myopathy in the recovery phase of sepsis

Evidence of myopathy was present in the hindlimbs by day 3 after the septic insult and persisted to day 14. Later timepoints were not investigated. Tibialis anterior and gastrocnemius mass was significantly reduced at days 3 and 14 after the septic insult compared to sham controls. Mass was significantly reduced at day 3 in soleus, extensor digitorum longus and plantaris compared to sham controls, but had returned to levels equivalent to sham muscle mass by day 14.

The proportion of myofibres comprising each muscle (classified by myosin heavy chain expression) did not differ in soleus or tibialis anterior from septic animals compared to controls. In tibialis anterior, the percentage of type IIX fibres was reduced at day 14 of sepsis recovery compared to sham controls ($p=0.0095$).

The cross-sectional area (CSA) of different myofibre types indicated the presence of a myopathy. In soleus muscle, type I fibres taken at days 3 and 14 after the septic insult showed significantly reduced CSA compared to sham controls (both $p<0.0001$). Type IIA fibre CSA was significantly reduced at day 3 ($p<0.0001$) compared to sham controls, but was unchanged compared to sham controls by day 14. Type IIX fibre CSA was equivalent across sham and septic groups.

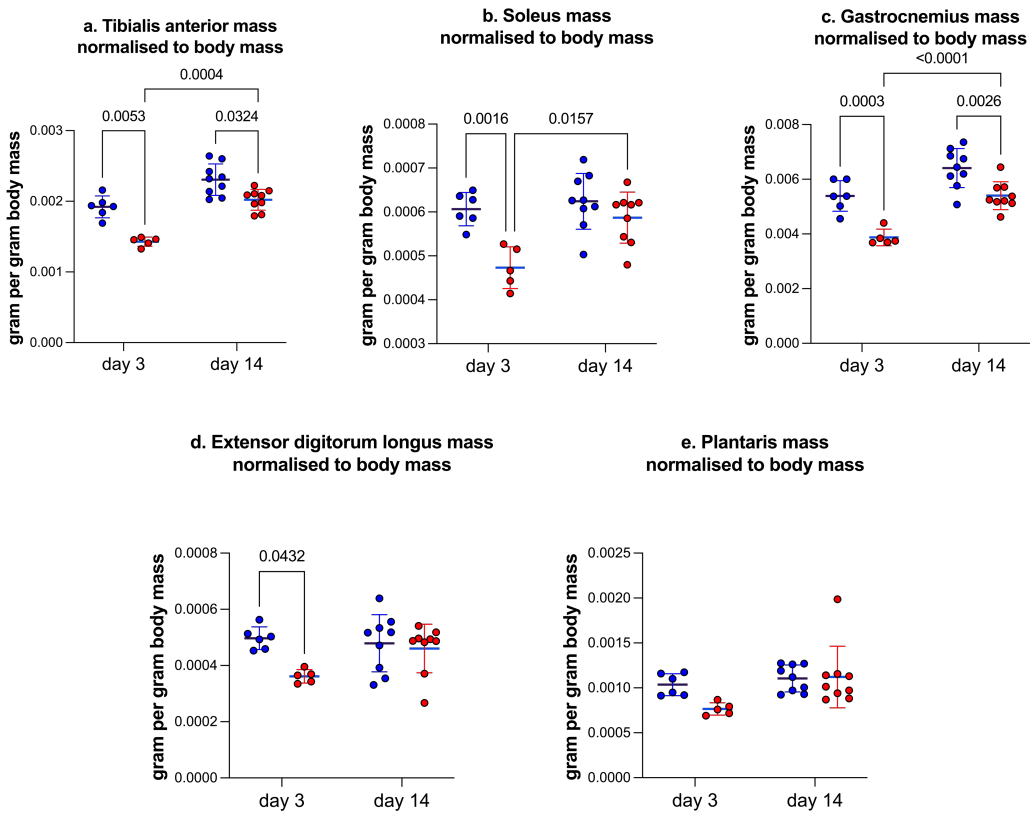

Figure 9. Mass normalised to body mass of muscles isolated from the hindlimb of sham animals (blue circles) and at day 3 and 14 of recovery from sepsis (red circles).

a. Tibialis anterior mass was reduced at days 3 and 14 compared to sham, but by day 14 had recovered to a significant degree compared to day 3 of sepsis recovery.

b. Soleus mass was significantly reduced at days 3 and 14 of sepsis recovery compared to sham.

c. Gastrocnemius mass was reduced at both days 3 and 14 of sepsis recovery compared to sham.

d. Extensor digitorum longus mass was significantly reduced at days 3 and 14 of sepsis recovery compared to sham.

e. Plantaris mass was not significantly different between sham and sepsis recovery animals at days 3 or 14.

Data shown as mean and SD. Statistics: mixed effect model.

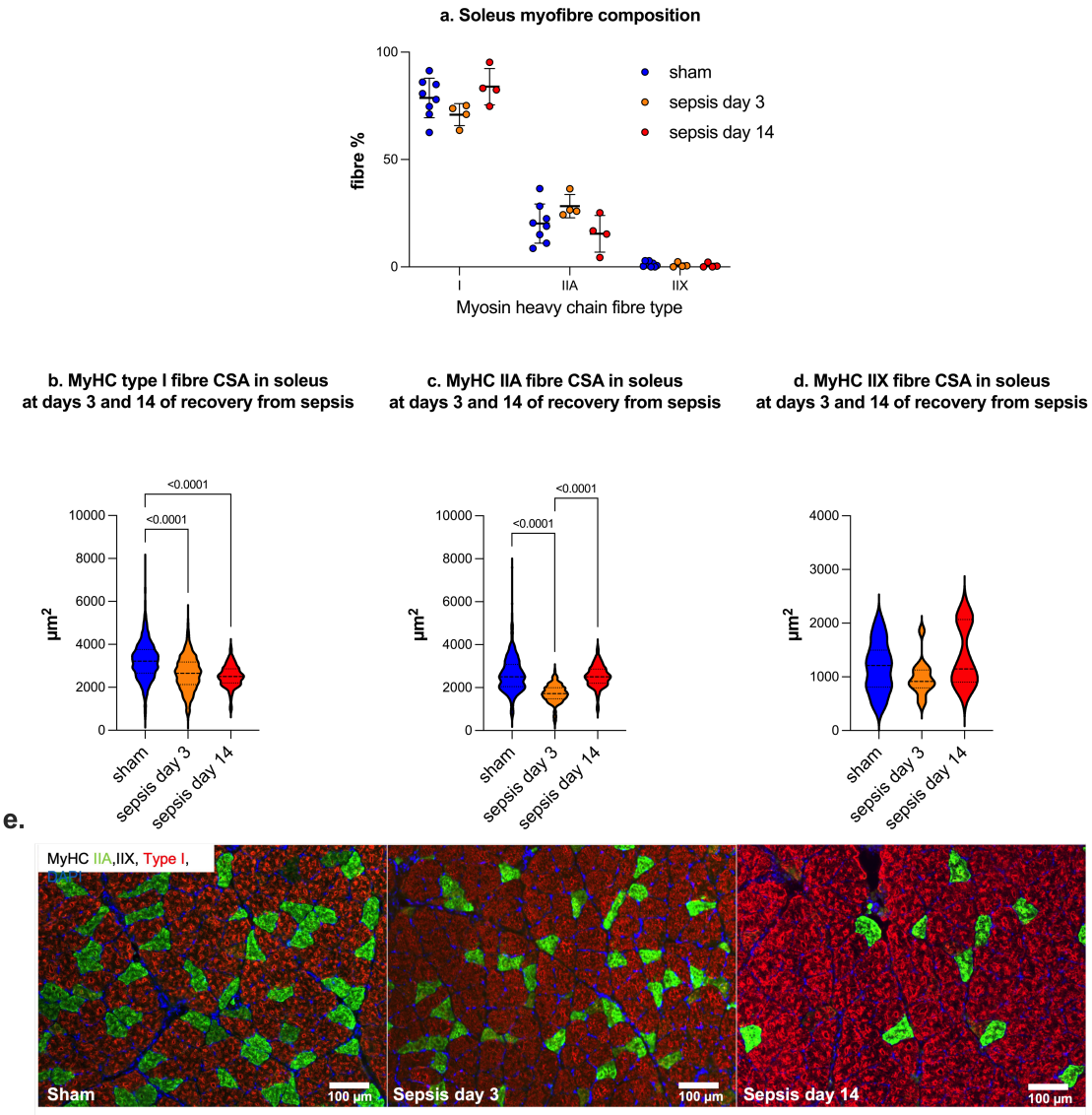

Figure 10. Cross sectional area (CSA) of muscle fibres identified by myosin heavy chain isoform expression in soleus muscle of sham animals and at days 3 and 14 of sepsis recovery.

a. Myofibre composition determined by myosin heavy chain expression did not differ between sham and septic animals.

b. CSA of type I myofibres was reduced at both days 3 and 14 of recovery from sepsis.

c. CSA of type IIA myofibres was reduced at day 3 but recovered by day 14 compared to sham animals.

d. CSA of type IIX myofibres showed no change between groups.

e. Representative immunofluorescent images of soleus muscle from sham animals and at days 3 and 14 of sepsis recovery.

Sham (n=8, pooled sham day 3 and 14 animals) and animals at day 3 (n=4) and day 14 (n=4) of sepsis recovery. Statistics: one-way ANOVA.

In deep tibialis anterior muscle type IIA, IIX and IIB fibre CSA was significantly reduced at days 3 and 14 after the septic insult compared to sham controls (all $p<0.0001$). However, by day 14 the fibre CSA had partially recovered and was significantly higher than at day 3 (all $p<0.0001$).

In superficial tibialis anterior type IIX fibre CSA was unchanged between sham and septic groups. Type IIB fibre CSA was significantly reduced at days 3 and 14 compared to sham controls (both $p<0.0001$) but, again, significantly higher at day 14 compared to day 3 ($p<0.0001$).

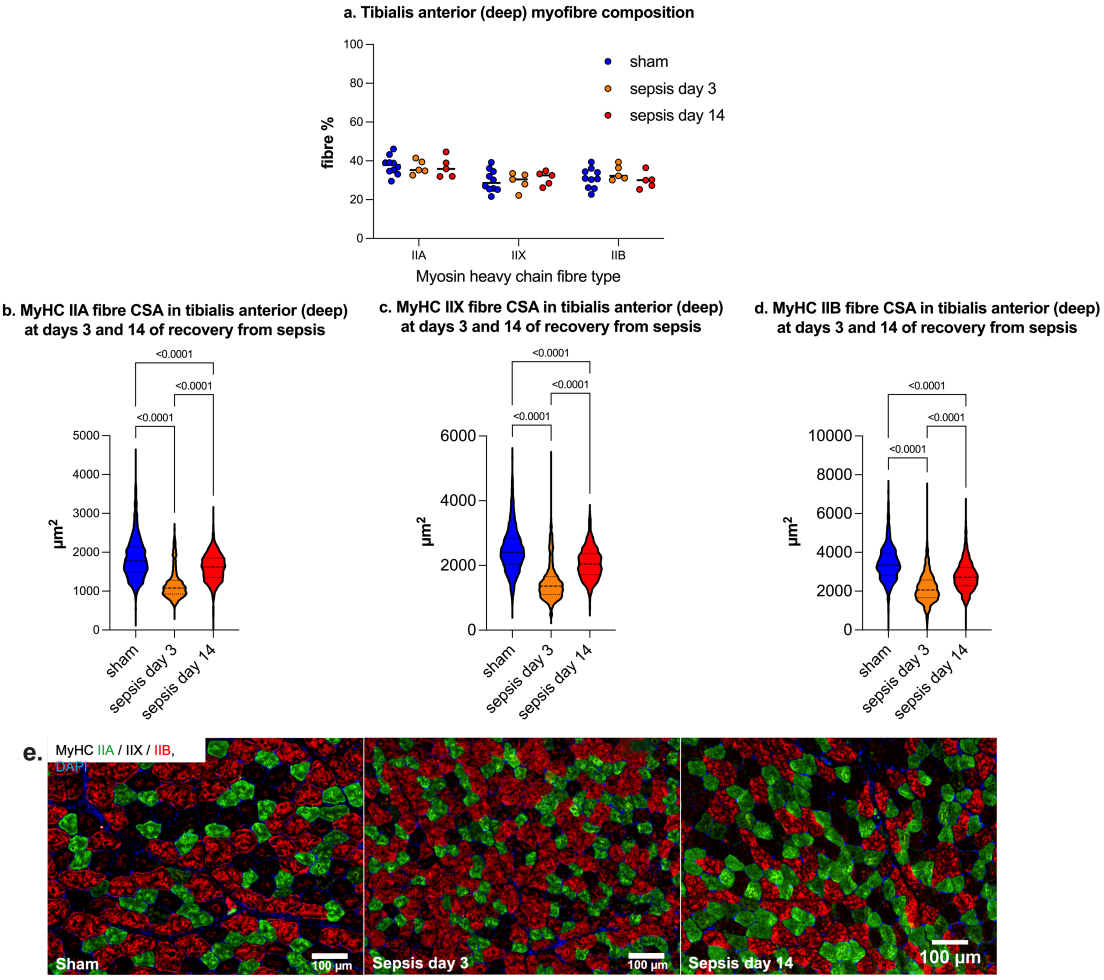

Figure 11. Cross sectional area of muscle fibres identified by myosin heavy chain isoform expression in deep tibialis anterior muscle of sham animals and at days 3 and 14 of sepsis recovery.

a. Myofibre composition determined by myosin heavy chain expression did not differ between sham and septic animals.

b-d. CSA of type IIA, IIB and IIX myofibres in deep tibialis anterior was reduced at days 3 and 14 of recovery from sepsis, compared to sham controls. CSA recovered to some degree by day 14 when it was significantly greater than at day 3 of recovery from sepsis.

e. Representative immunofluorescent images of deep tibialis anterior muscle from sham animals and at days 3 and 14 of sepsis recovery.

Sham (n=8, pooled sham day 3 and 14 animals) and animals at day 3 (n=4) and day 14 (n=4) of sepsis recovery. Statistics: one-way ANOVA

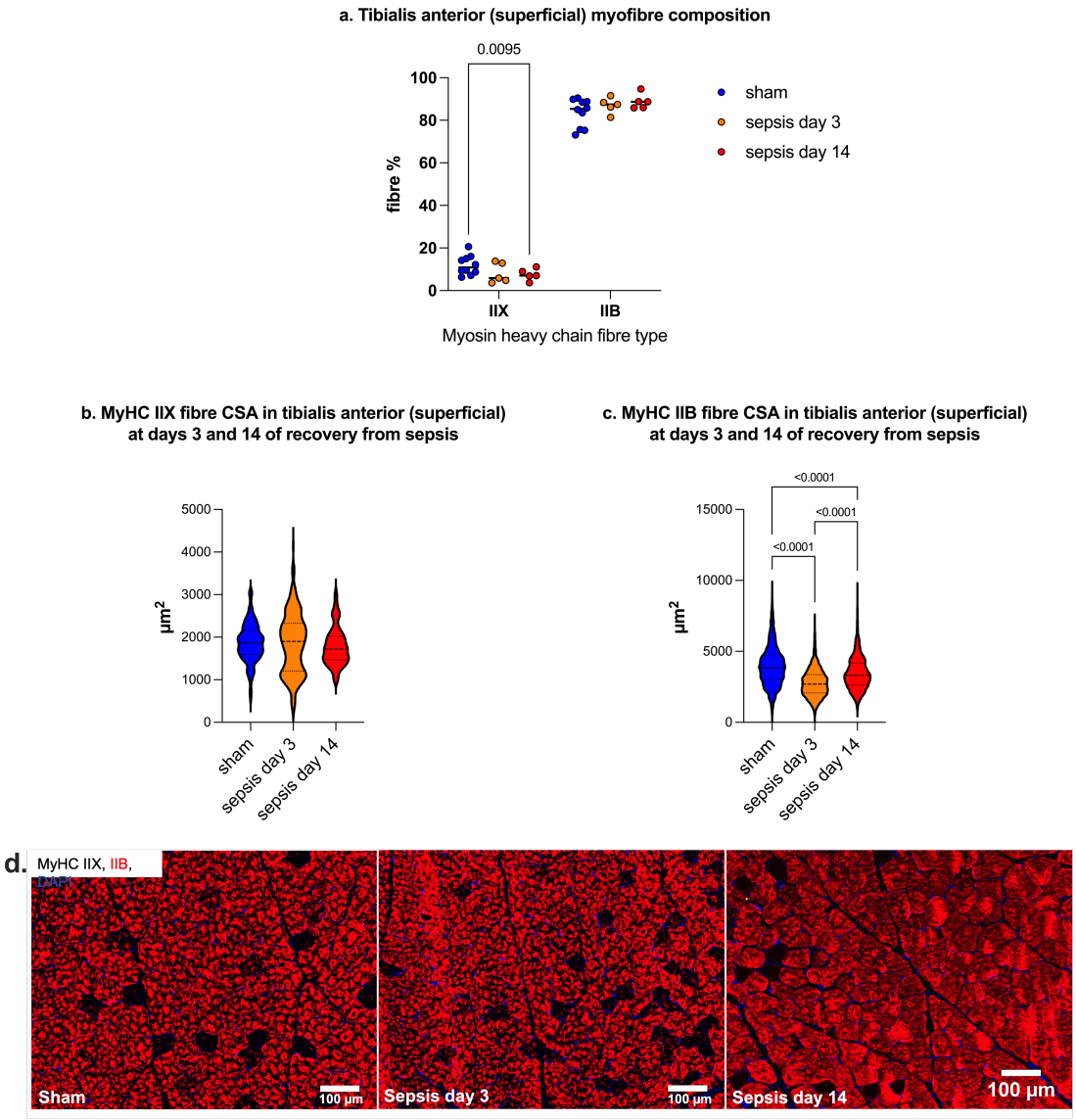

Figure 12. Cross sectional area of muscle fibres identified by myosin heavy chain isoform expression in superficial tibialis anterior muscle of sham animals and at days 3 and 14 of sepsis recovery.

a. At day 14 of recovery from sepsis, superficial tibialis anterior myofibres contained proportionally less type IIX fibres than sham controls. Proportions of type IIB fibre were unchanged between sepsis and control.

b. CSA of type IIX fibres did not differ between sham and sepsis groups.

c. CSA of type IIB myofibres was reduced at days 3 and 14 of recovery from sepsis compared to sham controls. CSA was significantly lower at day 3 compared to day 14.

d. Representative immunofluorescent images of deep tibialis anterior muscle from sham animals and at days 3 and 14 of sepsis recovery.

Sham (n=8, pooled sham day 3 and 14 animals) and animals at day 3 (n=4) and day 14 (n=4) of sepsis recovery. Statistics: one-way ANOVA.

2.3.10 Summary of results

- Zymosan peritonitis causes systemic inflammation, organ failure and, in some cases, death.
- Zymosan peritonitis causes a cachectic phenotype during 14 days of recovery and is associated with myopathy.
- The myopathy was present at day 3 and persisted to day 14. At day 14 it was characterised by reduced CSA of type I myofibres in soleus; type IIA, IIX and IIB in deep tibialis anterior; and type IIB myofibres in superficial tibialis anterior.
- These findings are consistent with the previous lab experience and those reported in the literature with this longer-term sepsis insult.

2.4 Discussion

Sepsis is defined as a dysregulated host response to infection leading to organ dysfunction and death.[1] Zymosan is a fungal cell wall component rather than a live pathogen and therefore does not cause an infection *per se* but, by activating many pathways shared with pathogen-stimulated sepsis, it generates a reasonable approximation that can be used as a laboratory model. Future studies could examine long-term recovery from different pathogen insults.

Organ dysfunction is an intrinsic aspect of sepsis and must be demonstrated in relevant models. In the above study a mortality rate of 17% was observed, including those which were culled pre-emptively to reduce suffering, which indicates organ dysfunction is present, as this is required for death. Reduction in stroke volume at 24 and 48 hours suggests sepsis-induced cardiac dysfunction may also be present. This is well characterised at the early phase of the host lab's 3-day faecal peritonitis model of sepsis, though normalisation is seen thereafter.[141] However, the reduction in stroke volume may also be due to intravascular hypovolaemia caused by decreased fluid intake and vascular leak. Reduced fluid intake is unlikely to lead to such a marked drop at 6 hours as the rats have free access to fluids and are excellent at preservation of water when needed. Vascular leakage and subsequent 'third spacing' likely contributes, but in itself indicates dysfunction of the vascular system.

Renal impairment was not conclusively present at the timepoints tested. Circulating markers of renal function (creatinine and urea) were raised at day 1 after the septic insult, indicating a level of renal impairment, but did not reach statistical significance. Albumin, a negative phase protein which falls in acute illness was significantly lower at day 1, indicating acute illness, but is not specific to liver failure.

The degree of weight loss (>9%) was in keeping with the literature. Published work by our group using a zymosan dose of 30mg/100g caused an initial 10-15% reduction in weight, consistent with that seen by Minnaard *et al* using the same dose.[142] Studies by Minnaard *et al* and Rooyackers *et al* demonstrated weight loss was at least as severe in sham animals pair-fed with septic animals, indicating an important role for calorific intake in the drop in body mass and consistent with a reduced metabolic rate (demonstrated in the next chapter) in septic animals.[125,142] However, increased protein catabolism and a more marked myopathy were seen in animals receiving zymosan than those pair-fed but without sepsis, indicative of the additional impact of a critical illness myopathy.[125] Pair feeding was not performed in my study as this is not included within our Project Licence.

Cytokine levels tested by multiplex assay were remarkably low compared to previous experience with the model.[126] Timepoints of 3, 7 and 14 days were chosen to demonstrate the recovery phase and are likely too late to capture peaks in early inflammatory cytokines such as IL-6. IL-6 was significantly raised at day 3 but with a mean serum concentration of 190 pg/ml, which is an order lower than that seen in early stages of sepsis. The reason for the remarkably low cytokine levels is unclear, but has been a persistent problem in our lab for this model and others. Extensive efforts to identify the cause, including alteration of rat strain, collection method (plasma vs serum, direct cardiac puncture vs arterial line) and measurement techniques (different ELISAs), have been performed but no cause was found. Further studies indicate rat serum may effect standard curve measurements leading to inappropriately low results. Work is ongoing to clarify this.

Monocyte chemoattractant protein 1 (MCP1, also known as CCL2) was elevated at day 7 compared to sham and day 14. MCP1 is important in macrophage recruitment and is raised in both infectious and non-infectious inflammatory conditions. MCP1

is implicated in macrophage recruitment to adipose tissue during inflammation, a process key to the initiation and perpetuation of browning.[143] MCP-1 is also an adipokine, i.e. a cytokine secreted by adipocytes to influence other tissues. Skeletal muscle is highly sensitive to MCP-1. At physiological levels of 200 pg/ml (one tenth of the levels measured here) it impairs insulin signalling and glucose uptake in skeletal muscle. This results in using hyperglycaemia, a known risk factor for critical illness myopathy, and indicates a potential role in the adipocyte-muscle axis of sepsis-induced cachexia.[115]

Of note, IL-10 was absent at all time points. This is in contrast to what was previously described in this model where levels were elevated early and remained high until day 14, consistent with the prolonged anti-inflammatory phase of human sepsis.[126] This, and the absence of other cytokines, suggests a methodological error however all positive controls did work correctly. While the apparent absence of many circulating cytokines indicates systemic resolution of inflammation, ongoing tissue inflammation was visibly evident in the peritoneal cavity as erythema and ascites at day 14 so does call into question the accuracy of the multiplex assay. Previous studies have demonstrated elevated tissue cytokine mRNA levels, suggesting local inflammation may be present even if absent in the blood.[127] Local perpetuation of inflammation and immune cell-tissue cross talk are intrinsic to browning of adipose tissue and adipokine/myokine cachexia pathways and may serve to drive the myopathy seen above.

As discussed, critical illness myopathy (CIM) is defined as a myopathy in critically ill patients where the only plausible cause is the underlying critical illness. Work from our group in rats showed a necrotising phenotype in soleus at day 14 (mainly type I), but near-normal histology in gastrocnemius (mainly type II).[24] A study of biopsies from the vastus lateralis of humans showed decreased CSA across all fibre types but

more marked loss in type II fibres.[29] Biopsies from humans with critical illness have shown CIM affects both limbs and respiratory muscles. In my study only hindlimb muscles were investigated, and these did show decreased CSA in both type I and type II fibres, and across different muscles, recapitulating findings made in humans.

Previous studies by the lab using the same model have described the intra-muscular myopathic processes. My study does not seek to duplicate this, but rather established the presence of myopathy through detailed phenotyping of myofibre cross sectional area. Loss of total body fat mass despite resolution of normal food intake has also been seen in this model, in keeping with a cachectic phenotype.[126]

The limitations of using animal models to mimic human sepsis are discussed in detail in Chapter 5. A limitation specific to this model is the use of a sterile insult (zymosan is a fungal cell wall extract, not a live pathogen). However it is known to stimulate pathogen- and damage- associated molecular patterns also triggered by live pathogens, and cause an inflammatory insult similar in magnitude and timeframe to that seen in human sepsis, making it a useful model, despite the inherent limitations of not studying humans directly. Importantly, it recapitulates the recovery phase, where pathogen clearance has normally been achieved in humans (through antibiotics or source control), which is the period of interest for this project.

In summary, zymosan peritonitis causes a sepsis-like syndrome resulting in either death or a recovery characterised by cachexia and a myopathy caused by the initial illness. The model demonstrates a cachectic phenotype and decreased CSA of myofibres in keeping with the well described myopathy, and is therefore appropriate for the investigation of browning as a driver of these processes.

Chapter 3. Investigation of thermogenesis and thermogenic mechanisms in white adipose tissue during recovery from sepsis

3.1 Methods background

3.1.1 High Resolution Respirometry

This is an established method for measuring oxygen consumption in isolated mitochondria, cells and tissues in an environment that can be manipulated by introduction of substrates and inhibitors. Respirometry was performed in a modular system (O2k, Oroboros Instruments, Innsbruck, Austria) that comprises two identical closed chambers (A and B) attached to an oxygen-sensing electrode. The chamber is continuously stirred by a magnetic stirrer ensuring an homogenous oxygen tension measured at two-second intervals. Changes in oxygen concentration are derived as a function of time, generating a rate of oxygen consumption (*Oxygen Flux)*. The chamber stopper contains a port through which solutions can be added to manipulate mitochondrial processes. The change in oxygen flux is attributed to changes in conditions with conclusions then drawn about mitochondrial function. Oxygen flux is displayed in real-time on DatLab software (Oroboros, Innsbruck, Austria) allowing for continuous assessment of specimen behaviour and optimisation of protocols.

Oroboros has advantages compared to other respirometers. Samples are suspended and do not rely upon adherent cell populations, allowing for analysis of intact tissues and non-adherent cells. Realtime feedback indicates the success of the assay and allows accurate interpretation of results. The number and combination of substrates and inhibitors are large, and limited largely only by ongoing viability of the sample. Disadvantages include the availability of only two chambers per

machine and the relatively large amount of sample required, especially if using rare or precious samples.

3.2 Methods

3.2.1 Thermal Imaging

Thermal imaging of epididymal (e)WAT was performed on animals at day 14 of recovery from sepsis. Imaging of retroperitoneal (rp)WAT was not possible because of overlying viscera. Immediately after laparotomy the abdominal cavity was exposed to allow a static image of the liver and eWAT to be taken using an A35 thermal imaging camera and Research Studio Software (FLIR, Oregon, USA). A needle was used to indicate the location of eWAT in relation to viscera. Colonic core temperature was measured simultaneously. eWAT temperature was normalised to both core and liver temperature to identify differences between sham animals and those recovering from sepsis. The camera was calibrated to a thermocouple before use and is reportedly accurate to 0.001°C.[144]

3.2.2 Whole organism respirometry

A subgroup of 4 sham and 4 septic animals underwent indirect calorimetry in metabolic carts (OxyMax CLAMS, Columbus Instruments, Columbus, OH, USA). Animals were individually housed in a sealed ventilated cage and acclimatised for 48 hours before administration of the septic insult. All other experimental conditions were identical to normal housing except the metabolic carts were cleaned daily. The model was run for 14 days after insult. The metabolic carts measure oxygen consumption (VO_2) and carbon dioxide production (VCO_2) every 8 minutes. From these measurements, the respiratory exchange ratio (equivalent to respiratory quotient) and heat production can be calculated.

3.2.3 High Resolution Respirometry of Adipose Tissue

High resolution respirometry was performed using an Oroboros O2k respirometer and DatLab 8 software to measure tissue oxygen consumption as a proxy of metabolic rate and heat production. Both chambers underwent air calibration on each day of use. All studies were performed in Mir05 respiration buffer (see Table 4 for contents) at 37°C.

Constituent	Final concentration (mM)
EGTA	0.5
$MgCl_2$	3
Lactobionic acid	60
Taurine	20
KH_2PO_4	10
HEPES	20
D-sucrose	110
Adjusted to final pH 7.1	

Table 4. Constituents of Mir05 respiratory media.[144]

White adipose tissue was identified by visual inspection, resected and placed immediately in ice-cold BIOPS. The tissue was then extracted from BIOPS and dissected to remove visible vessels and connective tissue. It was then dissected further into small (approx. $0.5mm^3$) sections and weighed. No chemical permeabilization was performed. 30-50 mg of WAT was used per chamber. Tissue mass and protocols were optimised to ensure a concentration of 100-200 nmol/ml oxygen throughout each experiment. All experiments were run in duplicate simultaneously with identical conditions in chambers A and B.

After addition of tissue to the chambers, stoppers were placed to ensure an air-tight seal. The samples were allowed to equilibrate as indicated by a stable rate of oxygen consumption; this took approximately 15 mins. Complex I substrates - pyruvate

(final concentration 5mM), malate (2mM) and glutamate (10mM) - were added by a Hamilton syringe to saturating levels and the chamber allowed to re-equilibrate for a further 5 minutes. Complex II substrate (succinate (10mM)) was then added and again allowed to equilibrate. Finally, the chemical uncoupler carbonyl cyanide p-trifluoro-methoxyphenyl hydrazone (FCCP) was added at a pre-optimised saturating final concentration of 2μM to assess maximal electron transport chain function.

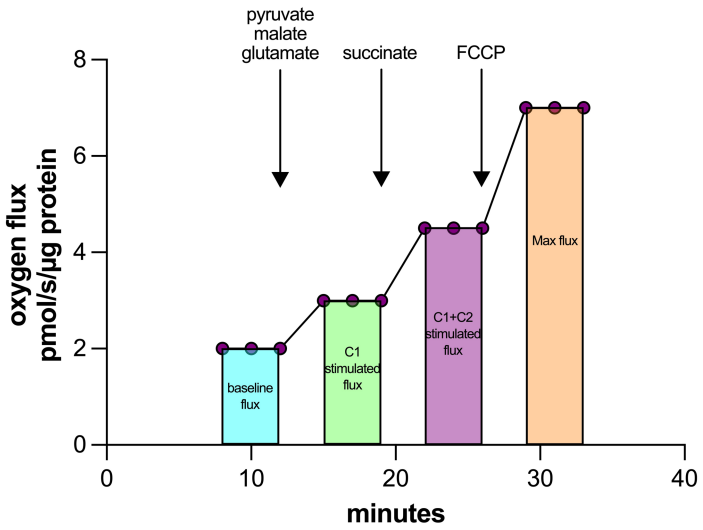

Figure 13. Schematic of respirometry protocol and oxygen flux measurement.
Respirometry was performed in duplicate simultaneously across chambers A and B. Tissue was added and the chamber was allowed to equilibrate before baseline flux was measured. Complex I substrates (pyruvate, malate, glutamate) were then added and flux re-measured. Succinate was then added as a complex II substrate and flux re-measured. The chemical uncoupler, FCCP, was added to measure oxygen flux at maximal electron transport capacity. The signal was allowed to stabilise between substrate additions and measurement.

Multiple other respirometry protocols were attempted, including use of GDP for inhibition of uncoupling protein 1, thapsigargin for inhibition of SERCA2 and oligomycin for inhibition of ATP synthase. These protocols were trialled in BAT activated by adrenaline but resulted in inconsistent and implausible findings and were therefore not adequate for the study of browning in WAT.

Data collection of oxygen flux was performed by Dr Joseph Harris who was blinded to the treatment condition of each sample. Three readings were taken in each state after stabilisation of the signal. A mean of these readings was used for statistical comparison between groups.

3.2.4 Tissue permeabilisation optimisation experiments

Some substrates of oxidative phosphorylation, such as succinate and ADP, are impermeable to intact cell membranes. If these substrates are to be used, cells and tissues must be permeabilised. This classically involves a detergent that targets cholesterol in the cell membrane to form pores. Mitochondrial membranes do not contain cholesterol and therefore do not become permeabilized. Substrates are instead transported into mitochondria.

To assess the need for permeabilization, tissue from naive animals (n=3) was prepared as described above and placed in Oroboros chambers A and B (technical duplicates) without permeabilization agents. Saturating levels of succinate and ADP were then added. Any increase in oxygen flux indicates some degree of permeability. Rotenone was then added to block electron transport through complex I, ensuring all respiration occurs through complex II. The permeabilisation agent, digitonin, was then titrated against increases in oxygen flux, resulting in increased substrate availability. If no further increase was seen, cells were considered optimally permeabilized. In the absence of a permeabilization agent, any permeability can be attributed to mechanical permeabilization resulting from tissue handling and manipulation.[145]

A further experiment was conceived to ensure WAT was optimally permeabilized to succinate which is considered unable to cross intact cell membranes. WAT from

three sham animals was prepared as above and added to the chambers in duplicate. Saturating levels of succinate were then added. Methyl-succinate, which is freely permeable through cell membranes, was then added to assess if further stimulation of complex II occurred, indicating incomplete permeabilization.

3.2.5 RNA-sequencing

RNA sequencing was performed to quantify differential gene expression between rpWAT from sham animals and those at day 14 of recovery from sepsis. RNA sequencing and subsequent bioinformatic analysis were performed as a paid service by NovoGene Ltd (Cambridge, UK).

3.2.5.1 RNA isolation

RNA was isolated using a RNeasy lipid tissue mini kit (Qiagen, Hilden, Germany) from rpWAT taken from five sham animals and five at day 14 of sepsis recovery. In brief, 80 mg of rpWAT was homogenised in Qiazol lysis buffer by bead-milling three times for 20 seconds, with 60 second intervals on ice between rounds. Chloroform was then added before centrifugation to isolate the aqueous phase containing the RNA. The RNA was then isolated using RNeasy columns and eluted into RNase free water for downstream processing. The optional DNase digestion step was not performed.

3.2.5.2 RNA quantification and quality control

Initial RNA quality control and quantification was performed using a Nano-Drop spectrophotometer (Thermofisher, Massacheusetts, USA). In brief, 1 µl of RNA-containing solution was added to the Nanodrop which measures absorption at both 260 nm and 280 nm. An absorption ratio of 2 indicates 'pure' RNA. Lower figures indicate protein and/or phenol contamination.

Further quality control was performed with an Agilent 2100 Bioanalyser (Agilent, Town, State, USA). RNA integrity was assessed by automated gel electrophoresis with subsequent analysis of the ratio of 18S and 28S ribosomal bands to generate an 'RNA Integrity Number' (RIN). RIN ranges from 1-10; values above 7 are considered 'good'.

Both quality control methods were repeated by NovoGene.

3.2.5.3 RNA sequencing

The following steps of RNA sequencing were performed as a paid service by NovoGene Ltd (Cambridge, UK). Detailed methods are provided in the appendix but, in brief: total RNA was used as the input material from which messenger RNA (mRNA) was purified. mRNA was then fragmented and reverse transcribed to cDNA. cDNA underwent end-repair, A-tailing, adapter ligation, size selection, amplification and purification. Index coded samples were clustered using a cBot Cluster Generation System using TruSeq PE Cluster Kit v3 cBot HS and sequenced on an Illumina Novaseq platform.

Post-sequencing quality control was performed to remove low quality reads from the data. The transcriptome was mapped to the species specific (rattus norvegicus) reference genome using HiSat2 v2.0.5. Mapped reads were assembled using StringTie v1.3.3b to quantitate full length transcripts for each gene locus.

Gene expression estimates were calculated as reads mapped to each gene and expressed as Fragments Per Kilobase of transcript sequence per Million base pairs sequenced (FPKM), which accounts for gene length and sequencing depth. Differential gene expression between sham and sepsis recovery rpWAT was performed using SESeq2 R package 1.20.0. P-values were adjusted (padj) using the Benjamini and Hochberg correction which controls for the False Discovery Rate using sequential

modified Bonferroni correction for multiple hypothesis testing. Adjusted p-values ≤0.05 are considered significant.

Gene Ontology (GO) and Kyoto Encyclopaedia of Genes and Genomes (KEGG) enrichment analysis were performed to cluster biologically related genes and identify differentially expressed pathways.

Paired-end sequencing to a length of 150 base pairs was performed to generate high-quality alignable sequence data. Read length of 150 base pairs was chosen as sufficient for accurate expression profiling.

3.2.6 Mitochondrial number, lipid droplet number and volume and nuclei count in rpWAT

Mitochondrial number, lipid droplet number and volume and nuclei count in rpWAT were measured using multiphoton microscopy of live explanted tissue. Detailed methods of microscopy techniques can be found in Chapter 5. In brief, z-stacks of 100 μm depth in 5 μm slices were taken of rpWAT from sham and sepsis recovery animals after staining with TMRM, Hoechst and BODIPY. Counts were then performed using Imaris software (Oxford Instruments, Abingdon, UK) or Fiji (Image J, NIH, Bethesda, MD, USA). To calculate mitochondrial density, stacks were converted into SumSlices 2D images and thresholded using the Otsu algorithm. Individual adipocytes were identified by their morphology and the number of positive pixels were taken to represent mitochondria. The number of positive pixels per adipocyte represents mitochondrial number and density. Nuclei were defined as structures in the blue channel that could accommodate a sphere of 5 μm^3. Surfaces were then generated and the threshold altered until surfaces which only represented nuclei were included. A total count was then taken. To count lipid droplets, the same process was performed in the green channel for objects that

could accommodate 35 μm^3 spheres. Surfaces were made and visually inspected and falsely adjoined structures 'cut' to separate lipid droplets.

3.2.7 Western Blot

Western blot was performed to compare protein expression between sham control tissues and tissues from animals recovering from sepsis.

3.2.7.1 Western blot sample preparation

50-100mg white adipose tissue was immersed in ice-cold radio-immunoprecipitation assay buffer containing protease and phosphatase inhibitors (Pierce, Thermo Scientific, Massacheusetts, USA). Tissue was homogenised by bead milling in a Minilys Homogenizer (Bertin Technologies, Ile-de-France, France) for 20 seconds and repeated twice, with intervals of at least 60 seconds on ice between rounds. Samples were then left on ice for 30 minutes before centrifugation at x12000 rpm at 4°C for 10 minutes. This produces a three-layered product: the bottom layer of cell debris combined with beads, the middle liquid supernatant containing proteins of interest, and a dense fatty 'cake' at the surface. To avoid contamination of the liquid supernatant with fat, a 21-gauge needle was introduced through the side of the bead-milling tube below the fat cake and the liquid supernatant aspirated into a fresh 1.5 ml Eppendorf tube. The process was repeated twice to minimise fatty contamination of the sample.

Lysate protein concentration was calculated by a bicinchoninic (BCA) protein assay (Pierce, Thermofisher Scientific, Massacheusetts, USA) with samples diluted in 5x loading buffer and RIPA to ensure 40 µg of protein per 14 µl.

3.2.7.2 Electrophoreisis, transfer and development

Electrophoresis was performed using hand-cast 10% SDS-Page gels with 15 wells per gel using a Bio-Rad mini-Protean chamber. 14 µl of sample were added per well. Gels were run at 120V until loading buffer reached the end of the gel. Gel contents were then transferred onto PVDF membrane (Immobilon-P, Merck New Jersey, USA) using a Bio-rad Trans-Blot semi-dry transfer cell.

Membranes were washed in TBST and stained with ink to check for uniform protein transfer before blocking with 5% BSA in TBST for 1 hour at room temperature. Membranes were incubated with the primary antibody overnight at 4°C (see Tables 5 and 6 for primary and secondary antibodies). Membranes were incubated with appropriate secondary antibodies for an hour at room temperature. Blots were then developed by chemiluminescence onto film or using a Biorad ChemiDoc system (Bio-Rad, UK).

Table 5. Table of primary antibodies used for Western blots.
All diluted in 5% BSA in TBST with 0.02% sodium azide.

Target protein	Primary Antibody	Dilution	Blocking
UCP1	Santa Cruz 293418	1/1000	5% BSA
UCP1	Santa Cruz 518024	1/1000	5% BSA
SERCA2	Santa Cruz 376235	1/500	5% BSA
PGC1α	CalBiochem ST1202-1SET	1/2000	5% BSA
Complex 1 NDUF9	Invitrogen	1/1500	5% BSA
UCP2	ProteinTech 11081-I-AP	1/1000	5% BSA
TFAM	Santa Cruz 23588	1/1000	5% BSA

Table 6. Table of secondary antibodies used for Western blot.
All diluted in 5% BSA in TBST without sodium azide.

Target species	Secondary Antibody	Dilution
Rabbit	Polyclonal goat P0448	1/3000
Mouse	Polyclonal rabbit P0260	1/3000
Goat	Polyclonal rabbit P0449	1/3000

3.3 Results

3.3.1 Thermal imaging

Thermal imaging of epididymal adipose tissues was used as a novel way to detect localised heat production compared to other organs and structures. Thermal imaging allows high resolution, high accuracy measurements to be taken without interfering with the tissue (e.g. inserting a temperature probe). Marked reductions in temperature were seen over a matter of minutes following laparotomy likely due to evaporation of ascitic fluid and vasodilatation due to isoflurane. For this reason, thermal images were taken immediately after the laparotomy and adipose tissue temperatures were normalised to either core or liver temperatures to account for changes in total body temperature.

There was no significant difference in core, liver or crude eWAT temperatures between sham (n=9) and sepsis (n=8) recovery animals.

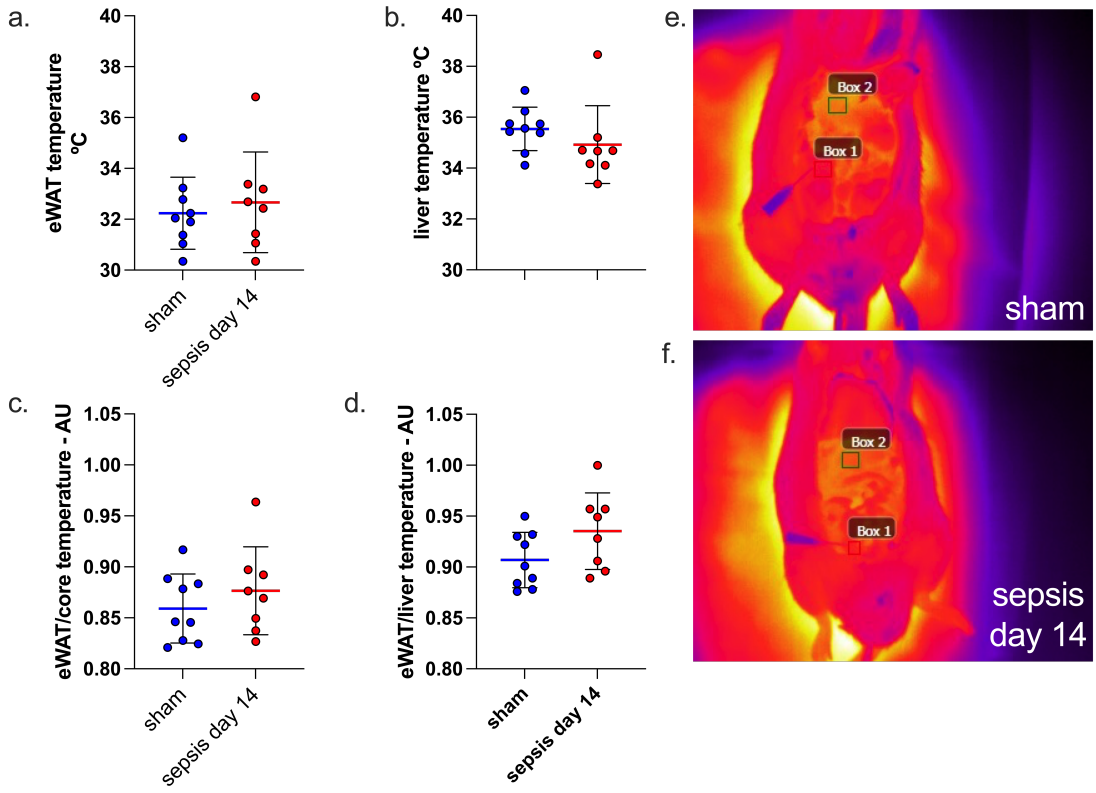

Figure 14. Tissue temperature measured by thermal imaging in sham animals and at day 14 of recovery from sepsis.

a-b. Crude eWAT and liver temperature measured by direct visualisation under anaesthesia after laparotomy. No difference between groups.

c-d. eWAT temperature normalised to liver or core temperature. Normalisation performed to account for variability in body temperature between subjects. No difference between groups.

e-f. Representative images taken with the thermal imaging camera. Box 1 localises eWAT and Box 2 the liver. A needle is placed to aide accurate eWAT localisation and avoid conflation with surrounding viscera.

All data shown as mean ± SD. Statistics: t test.

Liver temperature, used for normalisation because of good perfusion and ease of imaging, was higher than eWAT from both sham (35.4°C vs 32.2°C , $p<0.001$) and sepsis recovery animals (34.9°C vs 32.7°C, $p=0.023$). Core temperature measured by colonic thermocouple was higher than eWAT temperature in both groups, indicating the losses induced by exposure of the viscera by the laparotomy and relatively lower perfusion.

The gradient between eWAT and both core and liver temperatures did not differ significantly between sham animals and those recovering from sepsis. Normalisation of eWAT temperature to core and liver temperatures also revealed no significant difference between sham and sepsis recovery animals.

3.3.2 Whole organism respirometry

The zymosan peritonitis model of sepsis recovery was performed in metabolic carts for a subgroup of animals (4 sham, 4 sepsis) for 14 days. Animals with sepsis showed an initial hypometabolic phase followed by a later hypermetabolic recovery phase. At days 0-10, oxygen consumption was significantly less in septic animals (sham AUC 567000 ml/animal (95% CI 562000-572000) vs septic 523000 ml/animal (517000-530000). At days 11-14, animals undergoing recovery from sepsis became hypermetabolic compared to sham controls (AUC septic 246000ml/animal (240000-250000) vs sham 229000ml/animal (95% CI 226000-233000).

VCO_2 production was reduced in animals with sepsis from days 0-8 (AUC 470000ml/animal (95% CI 465000-476000) compared to sham animals (392000 ml/animal (384000-400000). From days 8-14, CO_2 production was equivalent between groups (281000ml/animal (95% CI 278000-284000) sham vs sepsis recovery 283000 ml/animal (280000-286000).

The respiratory exchange ratio (calculated as VCO_2/VO_2) was reduced in animals with sepsis from days 0-8 (AUC 1080 (1080-1100)) compared to sham animals (AUC 1190 (95% CI 1180-1200), indicating a switch to lipid metabolism. From days 9-12 the RER was equivalent between groups (AUC 504 (95% CI 499-510) vs 505 (492-514)). The RER then dropped again in septic animals at days 13-14, indicating another switch to lipid metabolism (AUC 240 (95% CI 238-244) vs 228 (218-238)).

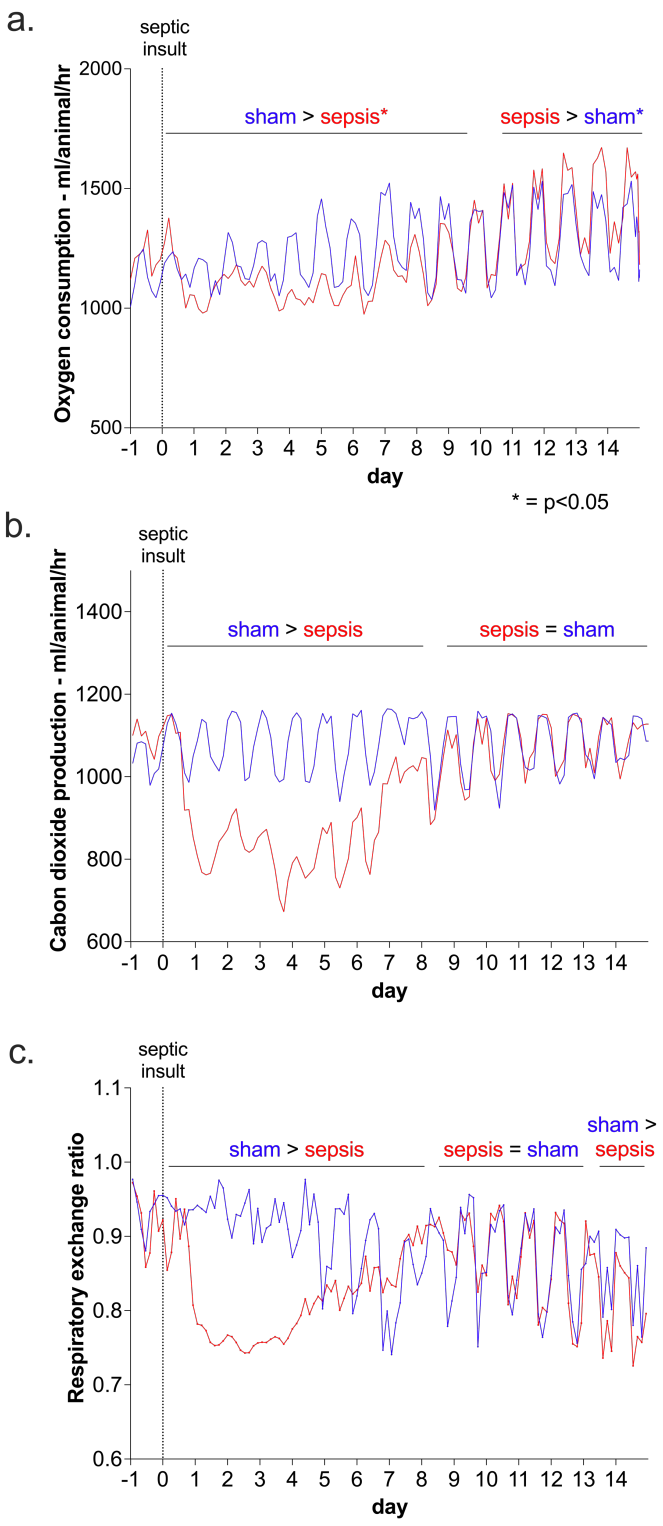

Figure 15. Whole organism respirometry of sham animals and in the acute and recovery phases of sepsis.

The zymosan peritonitis model was performed in metabolic carts in 4 sham and 4 septic animals over 14 days. Oxygen consumption and carbon dioxide production were measured

every 8 minutes. The respiratory exchange ratio (RER, calculated as VCO_2/VO_2) is derived from VO_2 and VCO_2.
a. Animals with sepsis showed an initial hypometabolic phase followed by a later hypermetabolic recovery phase. Between days 0-10, oxygen consumption was significantly lower in septic animals. At days 11-14, animals recovering from sepsis became hypermetabolic demonstrated by an increase oxygen consumption compared to sham controls.
b. VCO_2 production was reduced in animals with sepsis from days 0-8 compared to sham animals. From days 8-14, CO_2 production was equivalent between groups.
c. The respiratory exchange ratio (calculated as VCO_2/VO_2) was reduced in animals with sepsis from days 0-8 compared to sham animals, indicating a switch to lipid metabolism. From days 9-12 the RER was equivalent between groups. The RER then dropped again in septic animals at days 13-14.
Sham n= 4, sepsis n= 4. Statistics: area under the curve (AUC) with 95% confidence intervals. Numerical data in text (3.3.2)

3.3.3 High resolution respirometry of adipose tissue from sham animals and at days 3, 7 and 14 of recovery from sepsis.

3.3.3.1 Permeabilisation optimisation

Permeabilization optimisation experiments demonstrated that white adipose tissue was adequately permeabilisated to allow use of succinate and ADP without chemical permeabilization. Titration of digitonin had no additional effect, indicating no further permeabilization was necessary.

Addition of freely permeable methyl-succinate to ascertain if levels of non-methylated succinate were saturating without chemical permeabilization also showed no increase in oxygen flux. Thus, succinate levels were already saturating due to permeability in the absence of digitonin.

The permeability of the tissue was likely due to mechanical forces secondary to handling and chopping, which is a recognised and documented phenomenon. In light of these findings, chemical permeabilization was not performed.

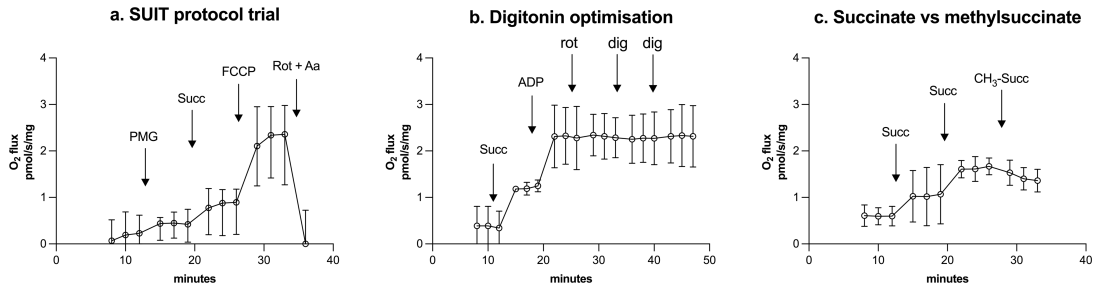

Figure 16. Optimisation experiments to establish white adipocyte permeability during high resolution respirometry.

a. Standard substrate-uncoupler-inhibitor trial (SUIT) was used to interrogate adipocyte respiration. Baseline respiration was measured before addition of electron donors to complex I (PMG – pyruvate, malate, glutamate) followed by addition of succinate (Succ) as an electron donor to complex II. FCCP was then added as a chemical uncoupler to establish maximal electron transport chain function. Rotenone and Antimycin A were then added to establish non-mitochondrial oxygen consumption (not done in later experiments).

b. Digitonin optimisation protocol demonstrated adipocytes were adequately permeabilized without the addition of the permeabilizing agent, digitonin.

c. Addition of freely permeable methylsuccinate (CH_3-Succ) did not increase oxygen consumption, indicating that the adipocytes are fully permeabilized.

3.3.3.2 Oxygen consumption in eWAT taken from animals at days 3, 7 and 14 of recovery from sepsis

Respirometry was performed on eWAT taken from sham animals and at days 3, 7 and 14 of recovery from sepsis. Oxygen consumption was normalised to tissue mass (per mg) and tissue protein content (per µg). Efforts to normalise eWAT oxygen consumption to adipocyte size were stymied by methodological issues with the immunohistochemistry.

When normalised to tissue mass:

- baseline oxygen consumption of eWAT was significantly higher at days 3, 7 and 14 of recovery from sepsis, compared to sham.
- oxygen consumption of eWAT following complex I stimulation was significantly higher at days 3, 7 and 14 of recovery from sepsis, compared to sham.
- oxygen consumption of eWAT following complex II stimulation was significantly higher at days 3, 7 and 14 of recovery from sepsis, compared to sham.

Following addition of the chemical uncoupler, FCCP, oxygen consumption representing maximum electron transport chain function was significantly higher at day 14 of sepsis recovery compared to sham and days 3 and 7 of sepsis recovery. Oxygen consumption at days 3 and 7 of sepsis recovery were not significantly higher than sham eWAT, but did trend towards higher rates.

Protein concentration varied by group. Mean protein content in eWAT from sham animals was 4.27 μg/mg, 16.1 μg/mg at day 3 and 22.1 μg/mg at day 14. Protein concentration was not measured at day 7 due to insufficient sample. When eWAT oxygen consumption was normalised to protein content, no difference in VO_2 was seen between sham and sepsis groups at baseline respiration or following stimulation of complexes I and II. Following addition of FCCP to generate maximum oxygen consumption, rates were significantly lower in eWAT taken at days 3 and 14 of recovery from sepsis compared to sham. Taken together, the results indicate increased oxygen consumption per milligram of adipose tissue with increasing duration of recovery.

The increase in protein content per milligram of tissue with increasing length of sepsis recovery indicates increased protein expression and/or reduction of other cellular elements, most likely lipids.

When controlled for protein concentration, the abolition of increased VO_2 in tissue from sepsis recovery animals, and the reduction in maximum VO_2 compared to sham, indicate that the increased oxygen consumption is due to the presence of more respiratory protein rather than an increased activation state. The reduced oxygen flux per µg of protein in eWAT taken at days 3 and 14 of sepsis recovery may be due to a relative increased expression of non-oxidative phoshorylation proteins or mitochondrial dysfunction. The findings do not however support induction of thermogenic processes in eWAT.

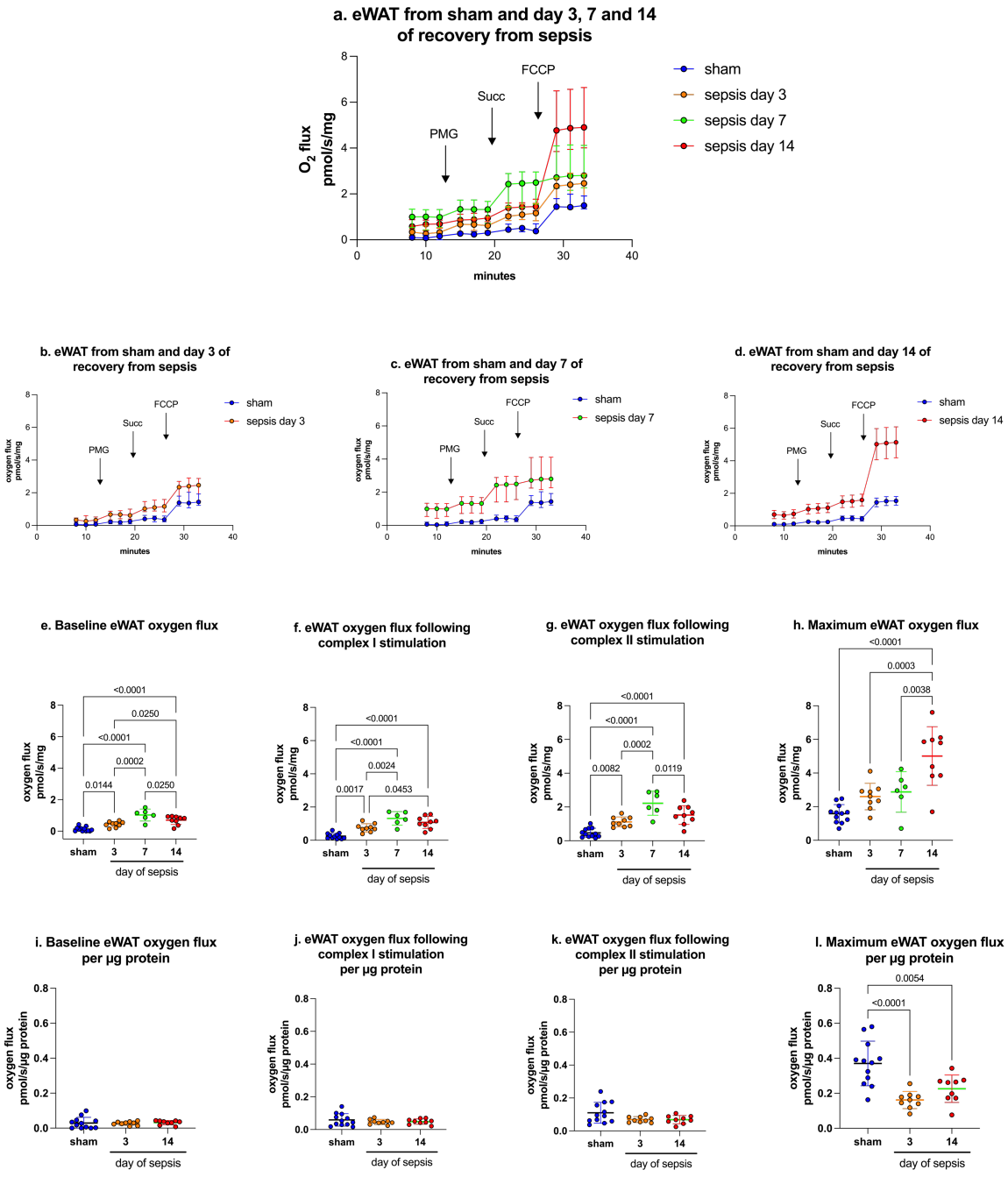

Figure 17. Oxygen consumption rate in epididymal white adipose tissue taken from sham animals and at days 3, 7 and 14 of recovery from sepsis, normalised to tissue mass and protein content.

a-d. Oxygen consumption at baseline, following stimulation of complex I (PMG – pyruvate, malate, glutamate) and complex II (Succ – succinate), and at maximal respiration induced by the chemical uncoupler FCCP. Data shown normalised to mg tissue mass.

e. Baseline oxygen consumption in eWAT was significantly higher at days 3, 7 and 14 of recovery from sepsis compared to sham, and days 7 and 14 compared to day 3 of sepsis recovery.

f. Following stimulation of complex I, oxygen consumption was significantly higher at days 3, 7 and 14 of recovery from sepsis compared to eWAT from sham animals, and at days 7 and 14 compared to day 3.
g. Following stimulation of complex II, oxygen consumption was significantly higher at days 3, 7 and 14 of recovery from sepsis compared to eWAT from sham animals, and at day 7 compared to day 3.
h. Maximal oxygen consumption induced by addition of FCCP was significantly higher in eWAT from animals at day 14 of sepsis recovery, compared to sham and at days 3 and 7.
i-l. Oxygen consumption in eWAT normalised to protein content at baseline, following complex I and II stimulation, and at maximal stimulation in sham animals and at days 3 and 14 of sepsis recovery. There was no significant difference between sham and septic tissue at baseline or following complex I or I stimulation. Maximal oxygen consumption following addition of the chemical uncoupler FCCP was significantly higher in sham eWAT compared to eWAT taken from animals at days 3 and 14 of sepsis recovery.
Data shown as mean ± SD. Statistics: one-way ANOVA. Pooled sham n=12, sepsis day 3 n=9, sepsis day 7 n=6, sepsis day 9 n=8.

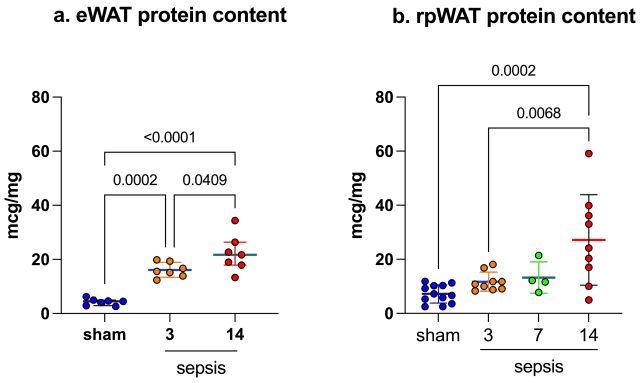

Figure 18. Protein content in eWAT and rpWAT from sham animals and those recovering from sepsis.
Total protein content was measured by BCA assay in duplicate and normalised to tissue mass.
a. Total protein content in eWAT increased with duration of recovery from sepsis. Pooled sham n=7, sepsis day 3 n=7, sepsis day 14 n=7 (no day 7 data due to insufficient sample).
b. Total protein content in rpWAT was significantly greater at day 14 of sepsis recovery than at day 3 or in sham animals. Pooled sham n=12, sepsis day 3 n=9, sepsis day 7 n=4, sepsis day 14 n=9. Data shown as mean ± SD. Statistics one-way ANOVA.

3.3.3.3 Oxygen consumption in retroperitoneal rpWAT taken from sham animals and at day 14 of recovery from sepsis

Identical experiments to those performed with eWAT were performed with rpWAT to assess other WAT deposits. The rpWAT deposit was chosen for two reasons: 1) it not known to contain brown adipocytes, and 2) rpWAT is a dorsal extra-peritoneal deposit which does not abut the inflammatory milieu caused by peritonitis, thus reducing the likelihood of immune cell infiltration due to local inflammation, rather than a part of the browning process.

When normalised to tissue mass, oxygen consumption in rpWAT from sepsis recovery animals was higher at baseline, following complex I and II stimulation, and at maximal flux after addition of FCCP. As with eWAT, the increase at baseline and following complex I and II stimulation was abolished when normalised to protein content. As with eWAT, following addition of FCCP, the maximal oxygen flux per microgram of protein was significantly less at day 14 of sepsis compared to sham tissue.

Importantly, it should be noted that gross protein content was measured; oxygen flux was not normalised to a specific mitochondrial protein. Efforts to do this with citrate synthase and mitochondrial DNA copy number were unsuccessful due to methodological failures.

Sepsis-induced cachexia results in reduced fat mass. This may be due to adipocyte shrinkage, in which case normalisation to mass alone would result in comparison of unequal numbers of mitochondria and cells. Therefore respirometry data were normalised to cell volume (measured by lipid droplet volume, an accepted proxy[146]), mitochondrial density and total cell number.

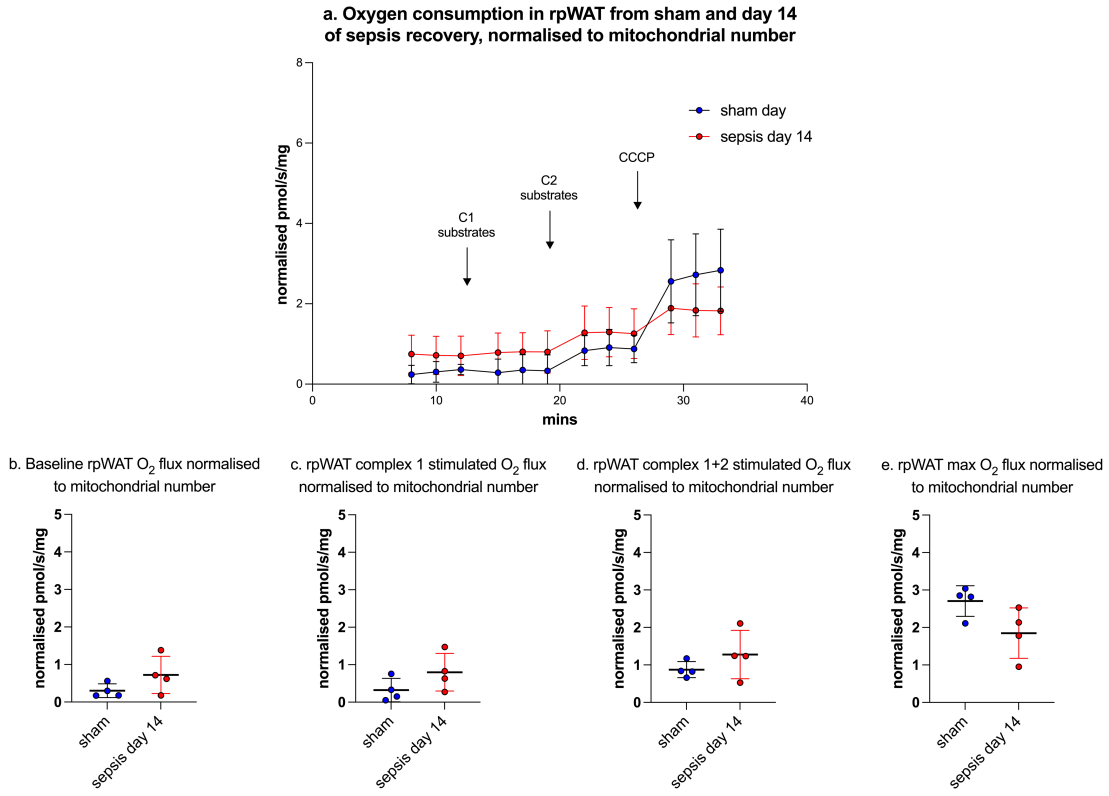

Figure 19. Oxygen consumption rate in retroperitoneal white adipose tissue taken from sham animals and at day 14 of recovery from sepsis, normalised to number of mitochondria.

a. Time series of oxygen consumption rates of rpWAT from sham animals and animals at day 14 of recovery from sepsis showing that separation of the groups was abolished by normalisation to mitochondrial number.

b. When normalised to mitochondrial number, baseline oxygen consumption did not differ between sham and septic tissue.

c. When normalised to mitochondrial number, oxygen consumption following complex I stimulation did not differ between sham and septic tissue.

d. When normalised to mitochondrial number, oxygen consumption after complex I and II stimulation did not differ between sham and septic tissue.

e. Maximal oxygen consumption normalised to mitochondrial number trended towards a significantly higher flux in tissue taken from sham animals ($p=0.07$).

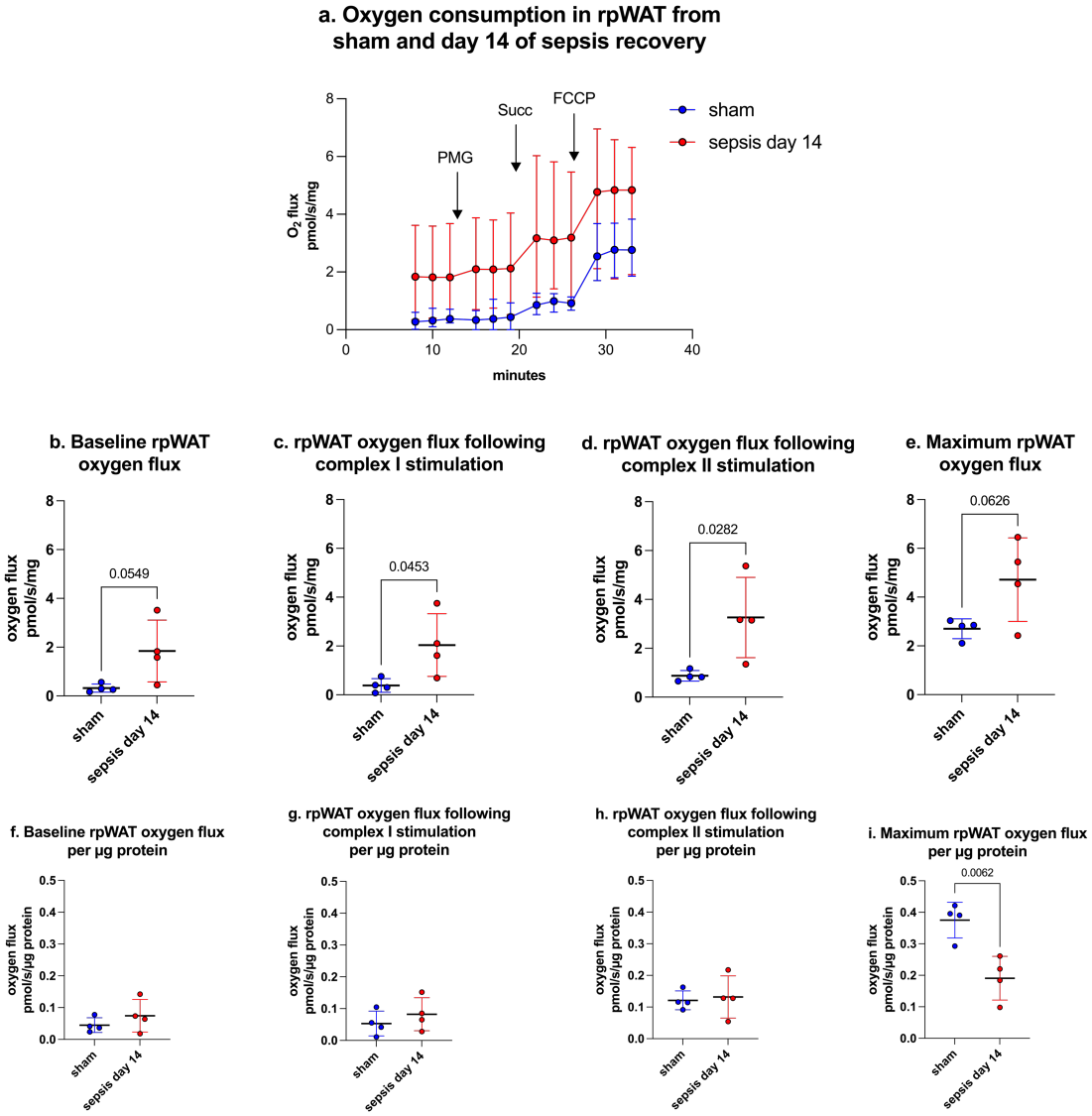

Figure 20. Oxygen consumption rate in retroperitoneal WAT taken from sham animals and at day 14 of recovery from sepsis, normalised to tissue mass and protein content.

a. Oxygen consumption at baseline and following stimulation of complex I (PMG – pyruvate, malate, glutamate), complex II (Succ – succinate), and at maximal electron transport chain respiration induced by FCCP. Data are normalised to milligram of tissue mass.

b. Baseline oxygen consumption in rpWAT trended towards a higher flux at day 14 of recovery from sepsis compared to sham (p=0.055).

c. Following stimulation of complex I, oxygen consumption was significantly higher at day 14 of recovery from sepsis compared to rpWAT from sham animals.

d. Following stimulation of complex II, oxygen consumption was significantly higher at day 14 of recovery from sepsis compared to rpWAT from sham animals.

e. Maximal oxygen consumption induced by addition of FCCP trended towards a significantly higher flux in rpWAT from animals at day 14 of sepsis recovery, compared to sham (p=0.063).

f-h. Oxygen consumption at baseline, following complex I and II stimulation, and at maximal stimulation normalised to protein content in rpWAT from sham animals and at day 14 of sepsis recovery. There was no significant difference between sham and septic tissue at baseline or following complex 1 or 2 stimulation.
i. Maximal oxygen consumption following addition of the chemical uncoupler FCCP showed significantly higher rates in sham rpWAT compared to rpWAT taken from animals at day 14 of sepsis recovery. Statistics: one-way ANOVA.

An increase in mitochondrial number could result from mitochondrial biogenesis (indicating browning) or due to adipocyte shrinkage resulting in more mitochondria per milligram of tissue. When oxygen flux was normalised to mitochondrial density per adipocyte, the increase in flux in septic rpWAT was abolished. Maximal oxygen flux in septic tissue trended towards lower rates.

When normalised to lipid droplet volume, oxygen consumption in rpWAT from animals at day 14 of sepsis recovery remained higher than in sham animals, but to a lesser degree. Oxygen consumption at baseline and following complex I stimulation was higher in sepsis recovery tissue but failed to reach statistical significance. Following complex II stimulation oxygen consumption remained significantly higher in tissue taken from animals recovering from sepsis. Maximum oxygen flux was similar in sham and sepsis recovery tissue.

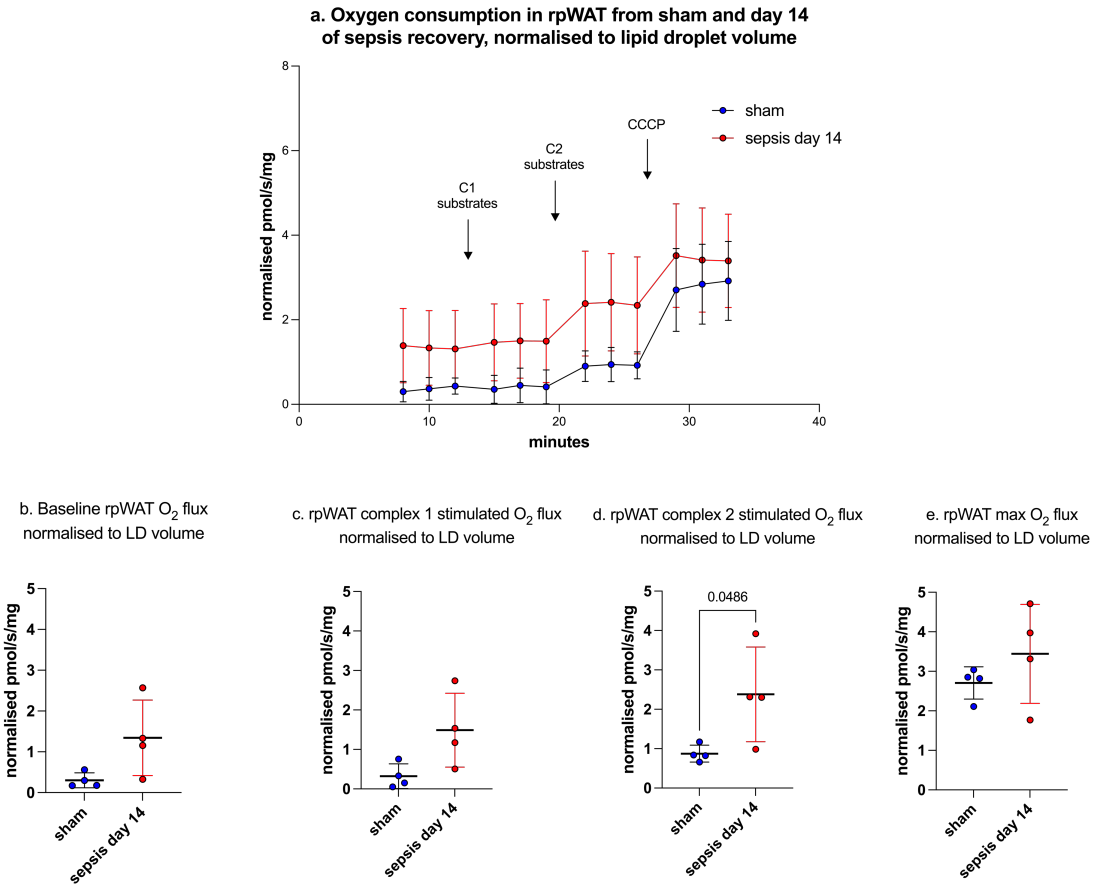

Figure 21. Oxygen consumption of rpWAT taken from sham and animals at day 14 of recovery from sepsis, normalised to lipid droplet volume (as a proxy of adipocyte size).

a. Time series of oxygen consumption rates of rpWAT taken from sham animals and animals at day 14 of recovery from sepsis showing that separation of the groups is diminished but not abolished by normalisation to lipid droplet volume.

b. When normalised to lipid droplet volume, baseline oxygen consumption of day 14 sepsis recovery tissue non-significantly trended towards higher flux compared to sham (p=0.069).

c. When normalised to lipid droplet volume, complex II-stimulated day 14 sepsis recovery tissue trended non-significantly towards higher flux compared to sham (p=0.056).

d. When normalised to lipid droplet volume, complex II-stimulated day 14 sepsis recovery tissue remained significantly higher compared to sham. ($p<0.05$).

e. When normalised to lipid droplet volume, maximum oxygen flux of sepsis recovery tissue was not raised compared to sham. (p=0.3)

Data shown as mean ± SD. Statistics: unpaired t test.

As microscopy was used to measure adipocyte size, cell number and mitochondrial density, this normalisation could only be performed for rpWAT as eWAT was not imaged.

During sepsis, immune cell infiltration of tissues distant from the site of infection is also reported.[110] In order to assess the impact of adipocyte shrinkage and potential immune cell infiltration on oxygen consumption rates, rpWAT respirometry data was also normalised to number of nuclei in order to encapsulate both adipocyte and immune cell numbers. Nuclei/cell number was measured by counting nuclei seen on multiphoton microscopy of explanted rpWAT tissue.

When normalised to cell number, oxygen consumption in rpWAT from animals at day 14 of sepsis recovery appeared higher than in sham animals, but to a lesser degree. Oxygen consumption at baseline, following complex 1 and 2 stimulation was no longer significantly raised compared to tissue from sham animals, but did trend towards higher rates. Maximal oxygen flux was equivocal between groups.

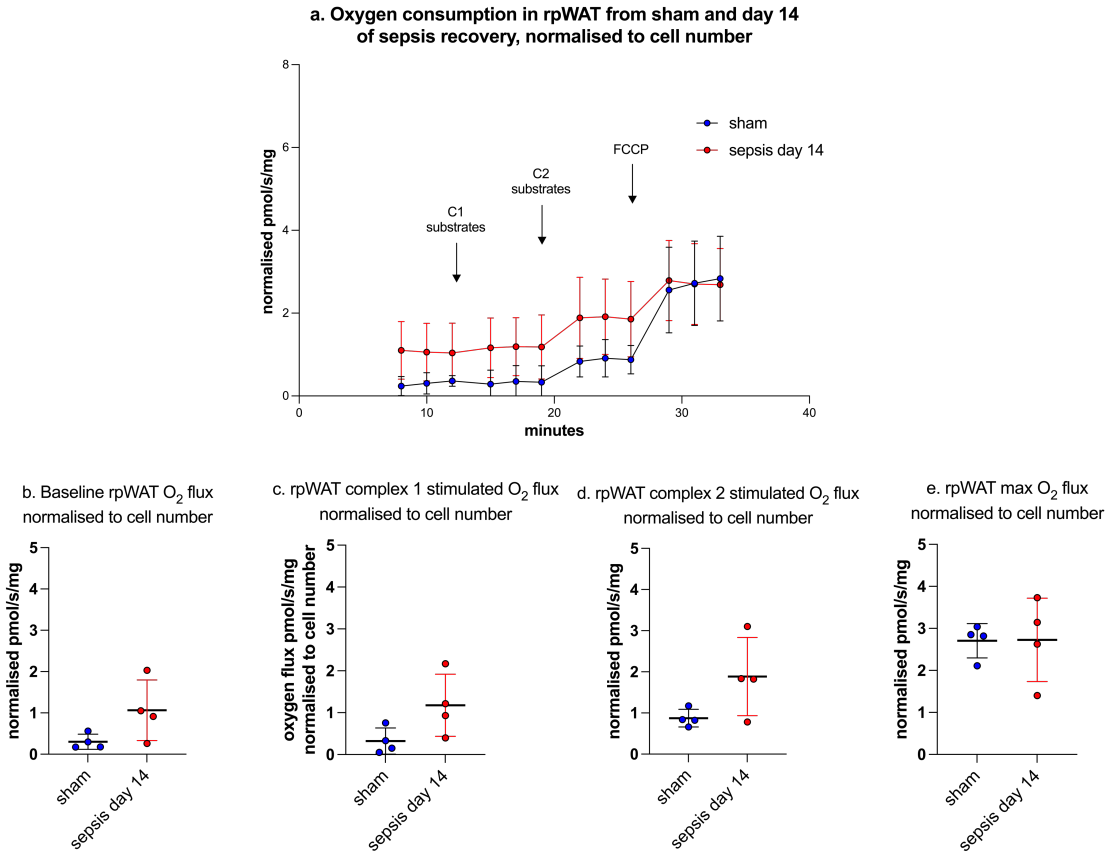

Figure 22. Oxygen consumption of rpWAT from sham and animals at day 14 of recovery from sepsis, normalised to cell number (measured by multiphoton microscopy).

a. Time series of oxygen consumption rates of rpWAT from sham and animals at day 14 of recovery from sepsis showing the separation of the groups is diminished but not abolished by normalisation to cell number.

b. When normalised to cell number, baseline oxygen consumption of day 14 sepsis recovery tissue failed to reach significance compared to sham. (p=0.0895).

c. When normalised to cell number, complex 1 stimulated day 14 sepsis recovery tissue failed to reach significance compared to sham. (p=0.0773).

d. When normalised to cell number, complex 2 stimulated day 14 sepsis recovery tissue failed to reach significance compared to sham. (p=0.0835).

e. When normalised to lipid droplet volume, maximum oxygen flux pf sepsis recovery tissue was not significantly raised compared to sham. (p=0.97)

Data shown as mean and SD. Statistics: unpaired t test.

3.3.4 Circulating markers of lipolysis

Lipolysis is an integral part of browning of white adipose tissue therefore circulating lipolysis markers were measured at various timepoints of recovery from sepsis. Serum lipase was significantly higher at day 1 of sepsis recovery compared to day 14 and sham animals. Triglycerides and glycerol, however, were unchanged between sham and sepsis recovery groups at all time points.

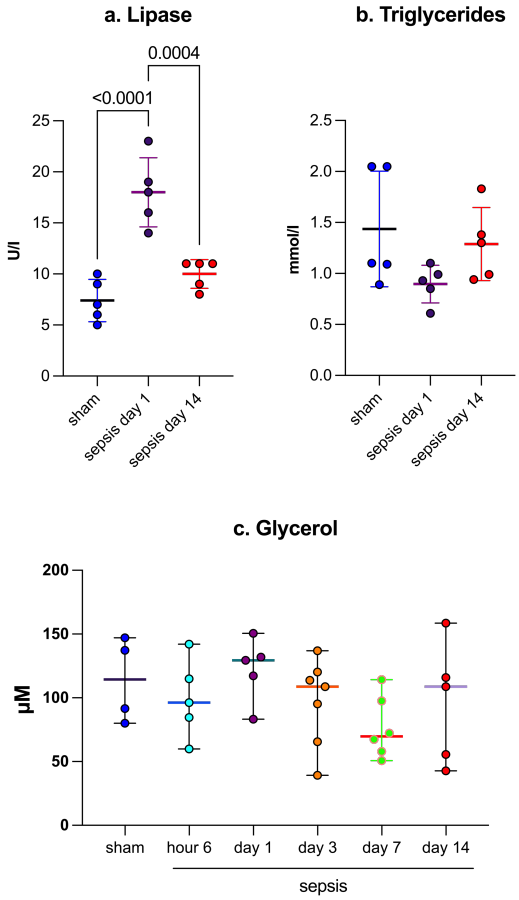

Figure 23. Circulating markers of lipolysis.

a. Lipase was elevated at day 1 of sepsis compared to both sham animals and at day 14 of sepsis recovery. n=5 per group.

b. Triglyceride levels were unchanged between sham and septic animals at days 1 and 14 of recovery. N=5 per group.

c. Glycerol levels were equivalent between sham animals and all sepsis timepoints. Pooled sham (4); Sepsis 6 hours (5), day 1 (5), day 3 (7), day 7 (6), day 14 (5). One way-ANOVA

Pooled sham=4. Sepsis 6 hours=5, sepsis day 1 =5, sepsis day 3=7, sepsis day 7=6, sepsis day 14=5. Statistics: one way-ANOVA.

3.3.5 Transcriptomics of bulk retroperitoneal adipose tissue during the recovery phase of sepsis

Differential gene expression in adipose tissue from sham and septic animals was performed using RNA-sequencing. Day 14 was chosen as the sepsis time point as the animals had clinically recovered from the acute illness, had a marked cachectic phenotype and altered adipose tissue metabolism. RNA-seq was performed on rpWAT instead of eWAT because of concerns that the inflammatory milieu of peritonitis and ensuing adhesions could lead to inflammatory signatures not related to browning and thermogenic activation, and may thus reduce tissue purity.

RNA was isolated from rpWAT from 5 sham animals and 5 animals at day 14 of recovery from sepsis. RNA quantification and quality control were adequate for downstream processing. 9 of 10 samples had RNA integrity numbers (RIN) above 7, indicating adequate quality. One sample (sham_2) demonstrated degraded RNA with a RIN of 4.5. Subsequent downstream quality control checks performed by NovoGene demonstrated the data was of reliable quality, and had a sequencing read error rate of 0.03% which was equivalent to all other samples.

Clear separation was demonstrated between sham and sepsis groups when plotted onto a Pearson correlation heat map, principal component analysis and the cluster analysis heatmap. These broad methods of data depiction demonstrate that within groups (e.g. sham_1-5 or sepsis_1-5) gene expression was similar between biological replicates but different between treatment groups. Pearson's correlates were typically >0.9. Inter-group comparison (e.g. sham 1-5 vs sepsis 1-5) showed

lower correlation coefficients, typically 0.6-0.8, indicating marked differences in gene expression between the two groups.

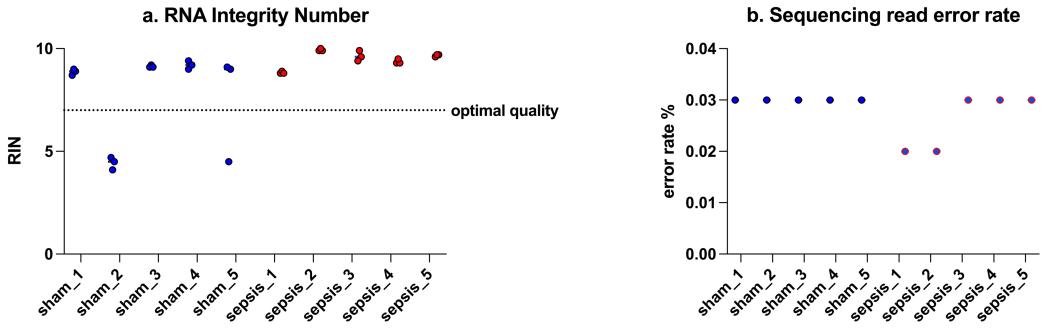

Figure 24. Quality control of RNA and RNA-sequencing performed on rpWAT from sham animals and at day 14 of sepsis recovery.

rpWAT from 5 sham animals was compared to rpWAT from 5 animals at day 14 of sepsis recovery.

a. RNA integrity number was greater than 7 in 9 of 10 samples, indicating adequate quality, One sample had RINs around 5 but subsequent read quality analysis was adequate.

b. RNA sequencing error rate was low in all samples, indicating adequate quality.

Principal component analysis was used to summarise and demonstrate intergroup differences and intragroup duplication. Principal component analysis shows all five sepsis samples clustered together, indicating similar expression profiles. In the sham group, sham 1-5 are clustered along PCA1 (x-axis) but sham_2 and sham_5 are separated along PCA2, indicating a difference in the secondary component found on analysis. However, the clustering is still supportive of acceptable intragroup concordance, and reflects biological heterogeneity.

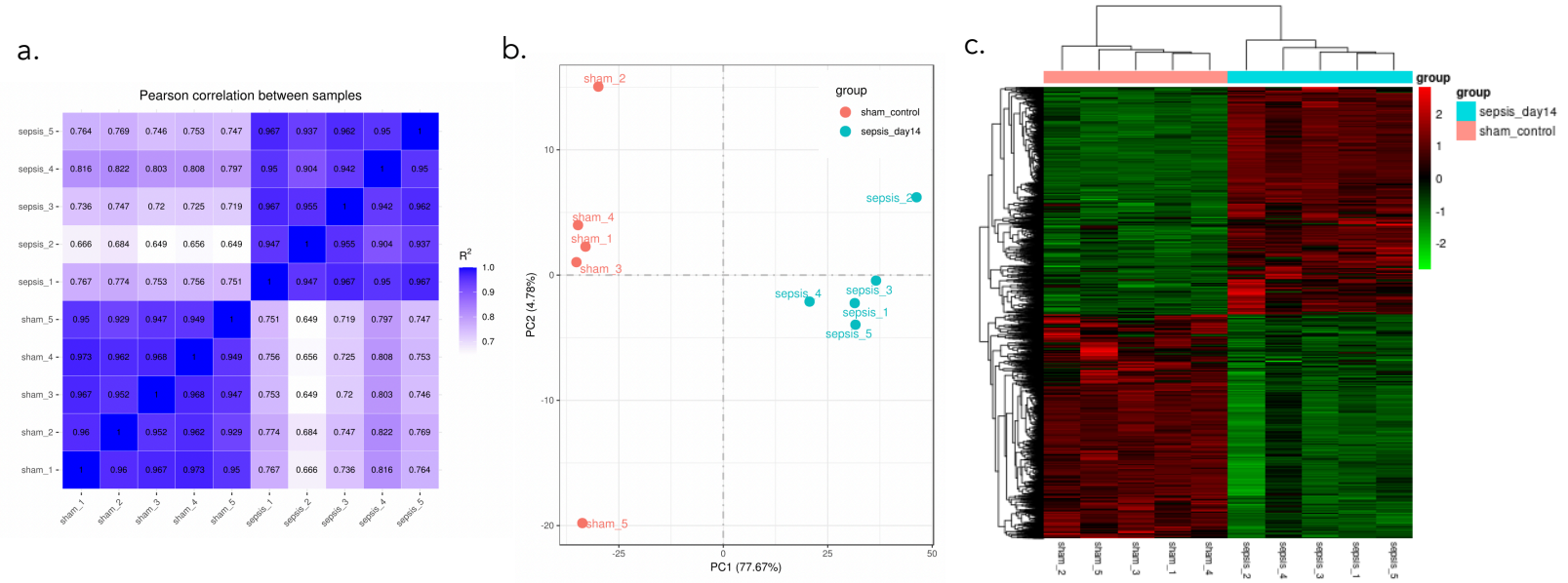

Figure 25. Correlation, Principal Component and Cluster analyses of RNA-sequencing data comparing the transcriptome of rpWAT from sham animals and at day 14 of sepsis recovery.

a. Inter-sample correlation heat map containing R^2 (square of Pearson correlation coefficient) for each sample. Values approaching 1 indicate strong correlation, here indicating consistency across biological replicates, and differences across sham and septic treatment groups.

b. Principal component analysis to demonstrate intergroup differences and intragroup sample duplication. The plot shows good intragroup duplication and significant intergroup separation.

c. Cluster analysis heatmap of differentially expressed gene clusters by gene sets with similar expression patterns. The map shows intragroup clustering and intergroup differential gene expression.

3.3.5.1 Comparison of sham adipocytes with adipocytes from animals recovering from sepsis shows increased inflammatory gene expression

The enrichment pathways, Gene Ontology (GO) and the Kyoto Encyclopaedia of Genes and Genomes (KEGG) allow differentially expressed genes to be grouped into functionally connected pathways. The pathways allow us to visualise altered tissue functions, the magnitude of which is indicated by the number of genes altered, whether they show increased or decreased expression and their statistical significance (padj).

The largest and most significant increases in gene expression in the GO enrichment pathways were 'Immune System Process' and 'Immune response'. KEGG enrichment echoed this with 'cytokine-cytokine receptor interaction' and 'haemopoeitic cell lineage' the pathways with most significantly increased expression.

Increased expression of genes related to immune cells and inflammation may indicate immune cell infiltration and/or increased expression in resident cells of adipose tissue. Quantification and deconvolution analysis (to see the contribution of each cell type) is unfortunately not possible without extensive costly work. Healthy adipose tissue contains various cell types including adipocytes, pre-adipocytes, T-cells, macrophages, neutrophils, plasma cells, mesothelial cells, endothelial cells, smooth muscle cells and mast cells.[147] Interpretation of bulk transcriptome data must recognise the limitations due to the lack of cell specificity.

Analysis of immune cell specific markers (which are more limited in rats than in humans and mice) showed both innate and adaptive immune cells already known to be present in adipose tissue. The gene expression changes may reflect alteration

of the proportions of cells, activation states or infiltration with new cells. Immune infiltration may be a result of adipose tissue browning, a systemic response to sepsis recovery, or a direct immune infiltration due to proximity to the peritoneum. Adipocyte markers were broadly reduced, supporting an immune infiltrate rather than a phenotypic switch by adipocytes. In keeping with enrichment pathways indicating inflammatory infiltrate, Il-6, TNFα, NFκB, IL-1ß and IFNγ were all significantly upregulated.

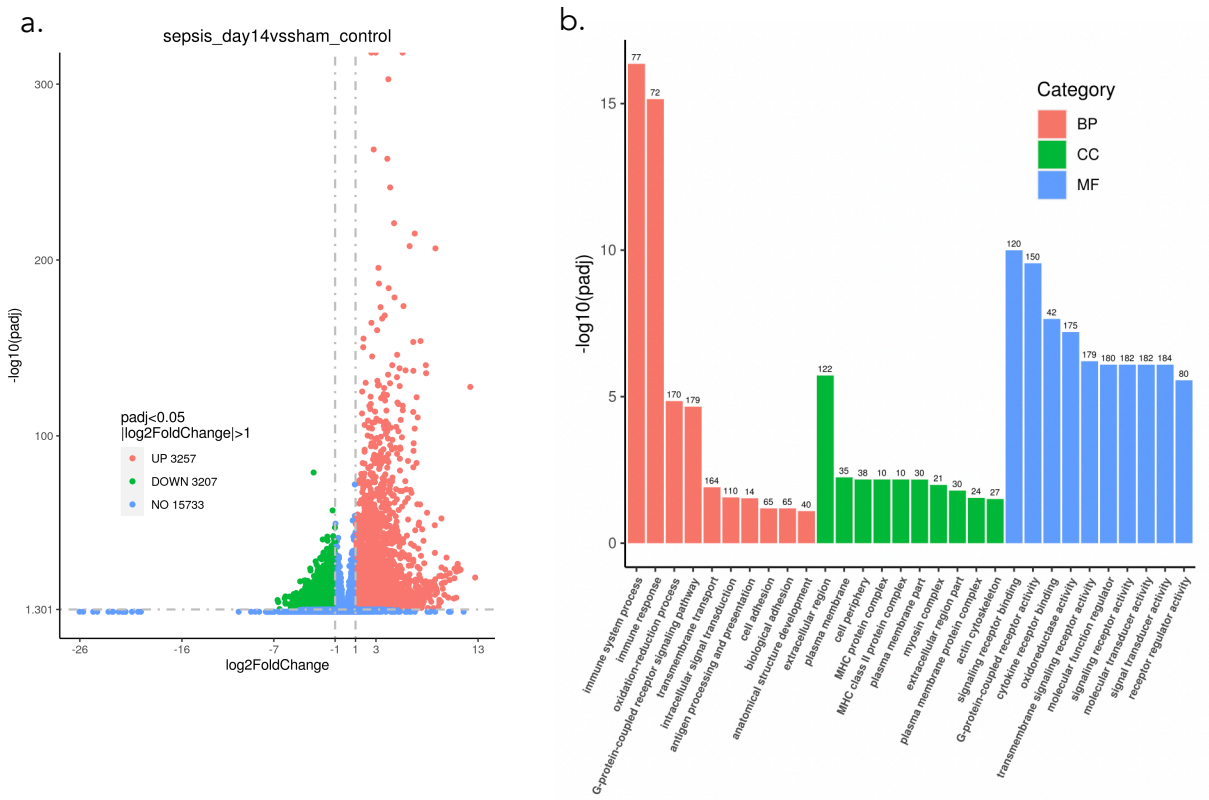

Figure 26. Differential gene expression plots.

Volcano plot of differentially expressed transcripts (log2 fold change >1, adjusted p-value <0.05) showing 3257 up regulated, 3207 down regulated and 15733 unchanged transcripts.

b. Gene Ontology Enrichment analysis plot of the 10 most significantly altered GO terms in the subclasses Biological Processes (BP), Cell Components (CC) and Molecular Functions (MF). The abscissa is the Gene Ontology Term, the ordinate is level of significance (-log10padjusted).

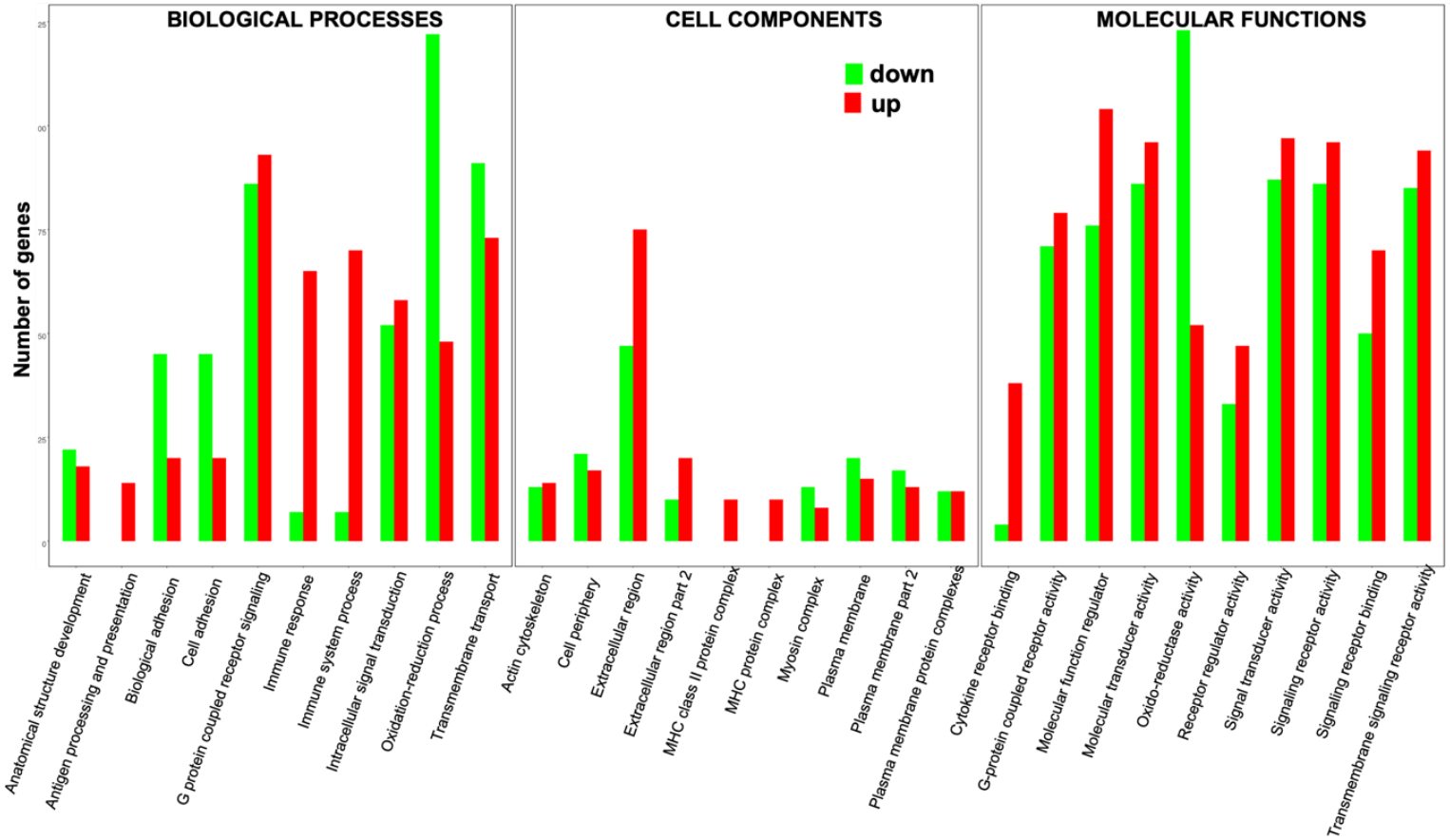

Figure 27. Differential gene expression plots.

Gene Ontological enrichment plot showing the number of up and down regulator transcripts within subclasses and terms. Of note immune response related terms are heavily upregulated, whilst mitochondrial related terms are largely down regulated.

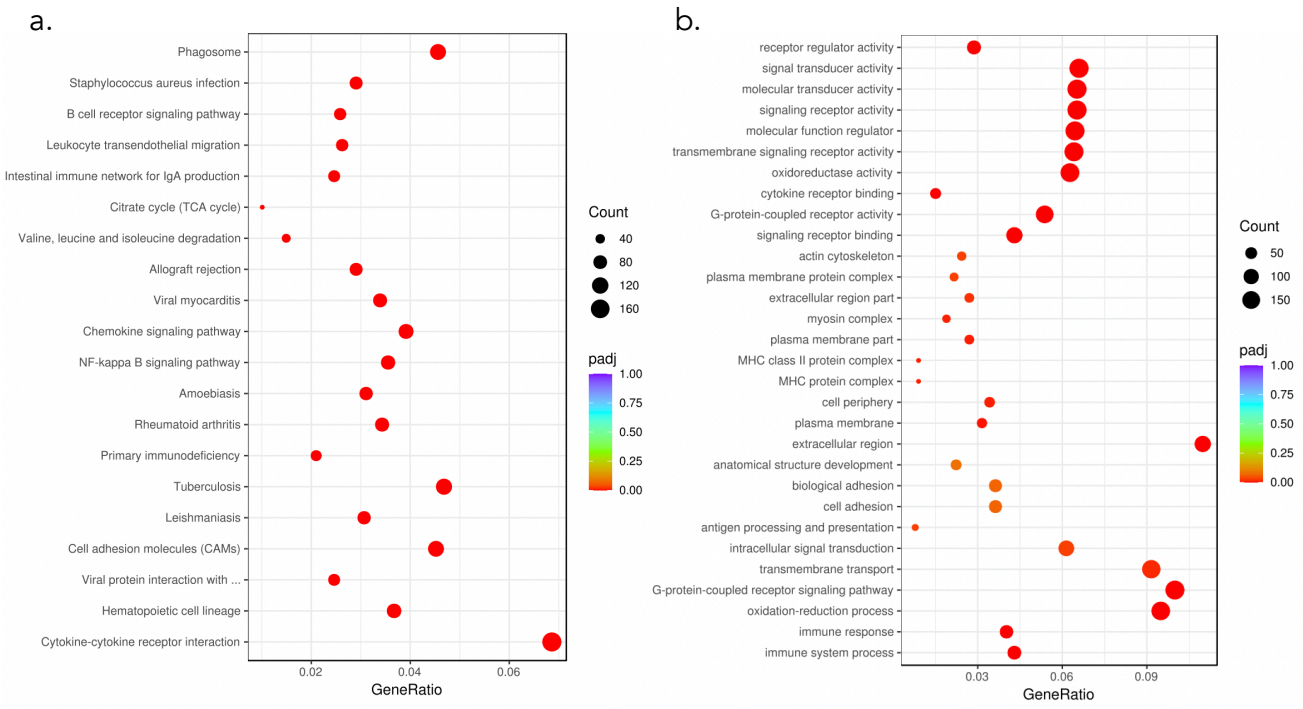

Figure 28. Enrichment analysis scatter plots.

a. Kyoto Encyclopaedia of Genes and Genomes enrichment analysis displaying the 20 most significant KEGG terms.

b. Gene Ontology enrichment analysis displaying the 30 most significant GO terms.

For both: the ordinate (y-axis label) is the enrichment term, the abscissa (x-axis) is the GeneRatio calculated as the ratio of the number of differential genes linked with the pathway to the total number of differential genes. Point size indicated the number of genes in the pathway. Point colour indicated level of significance (p-adjusted).

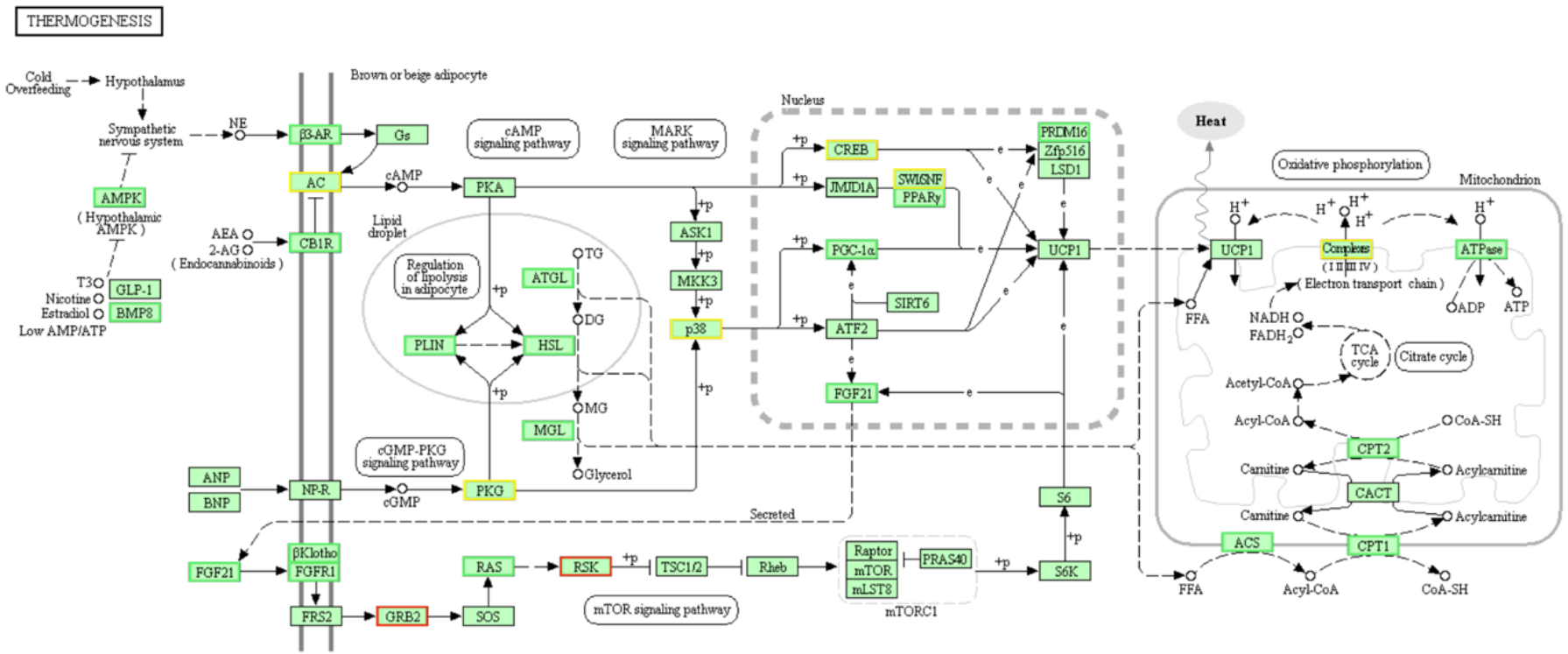

Figure 29. KEGG enrichment analysis pathway of genes related to thermogenesis.

Gene expression is indicated by the colour of the box: black – unchanged, red – up-regulated, green – down-regulated, yellow – both up and down regulation of associated genes. Thermogenesis pathway indicating predominantly down-regulated genes. UCP1 was unchanged. Figure generated as part of analysis package by NovoGene (Cambridge, UK).

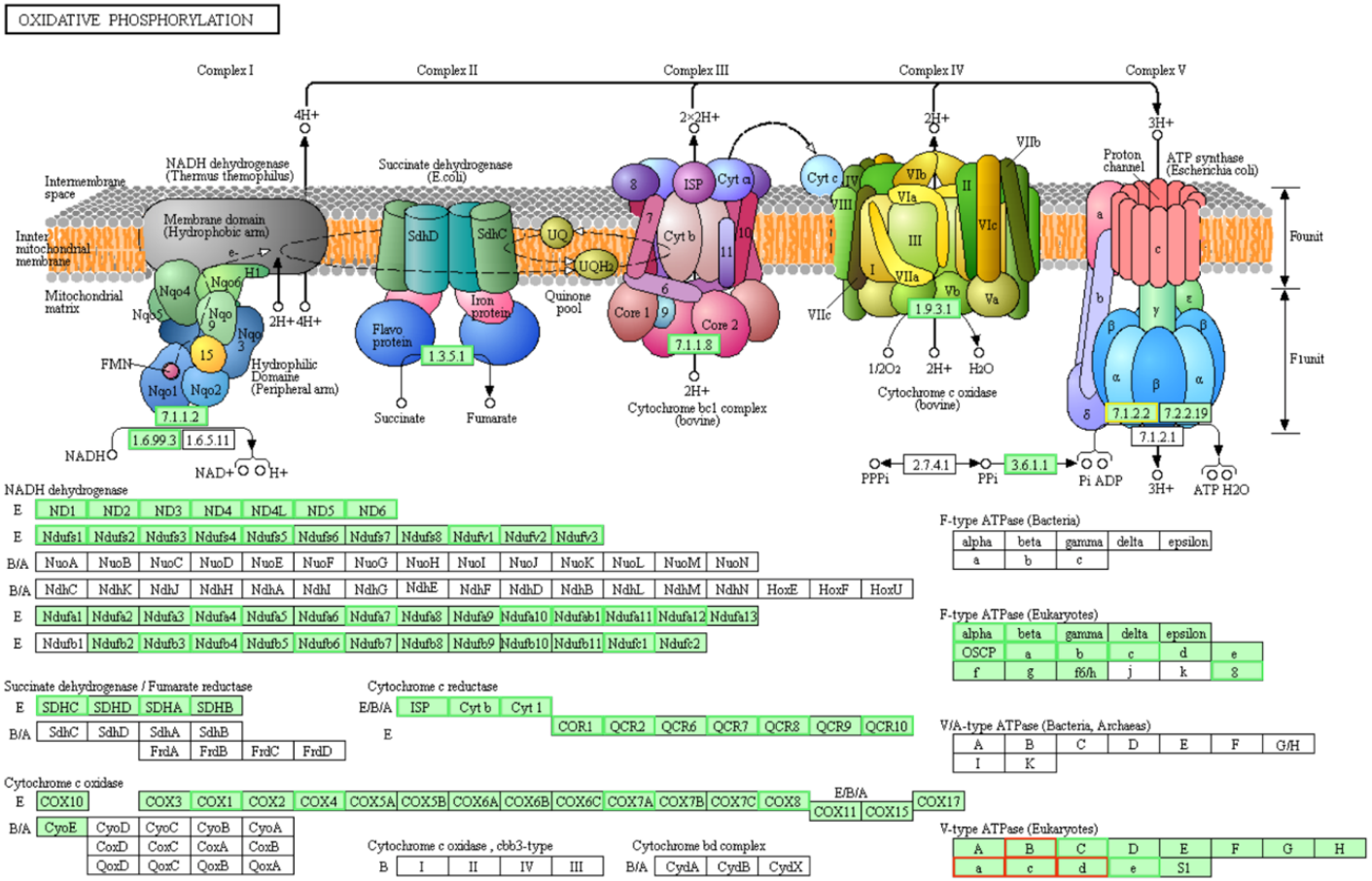

Figure 30. KEGG enrichment analysis pathway of genes related to oxidative phosphorylation.

Gene expression is indicated by the colour of the box: black – unchanged, red – up-regulated, green – down-regulated, yellow – both up and down regulation of associated genes. Oxidative phosphorylation pathways indicating predominant down regulation of mitochondrial oxidative phosphorylation apparatus. Figure generated as part of analysis package by NovoGene (Cambridge, UK).

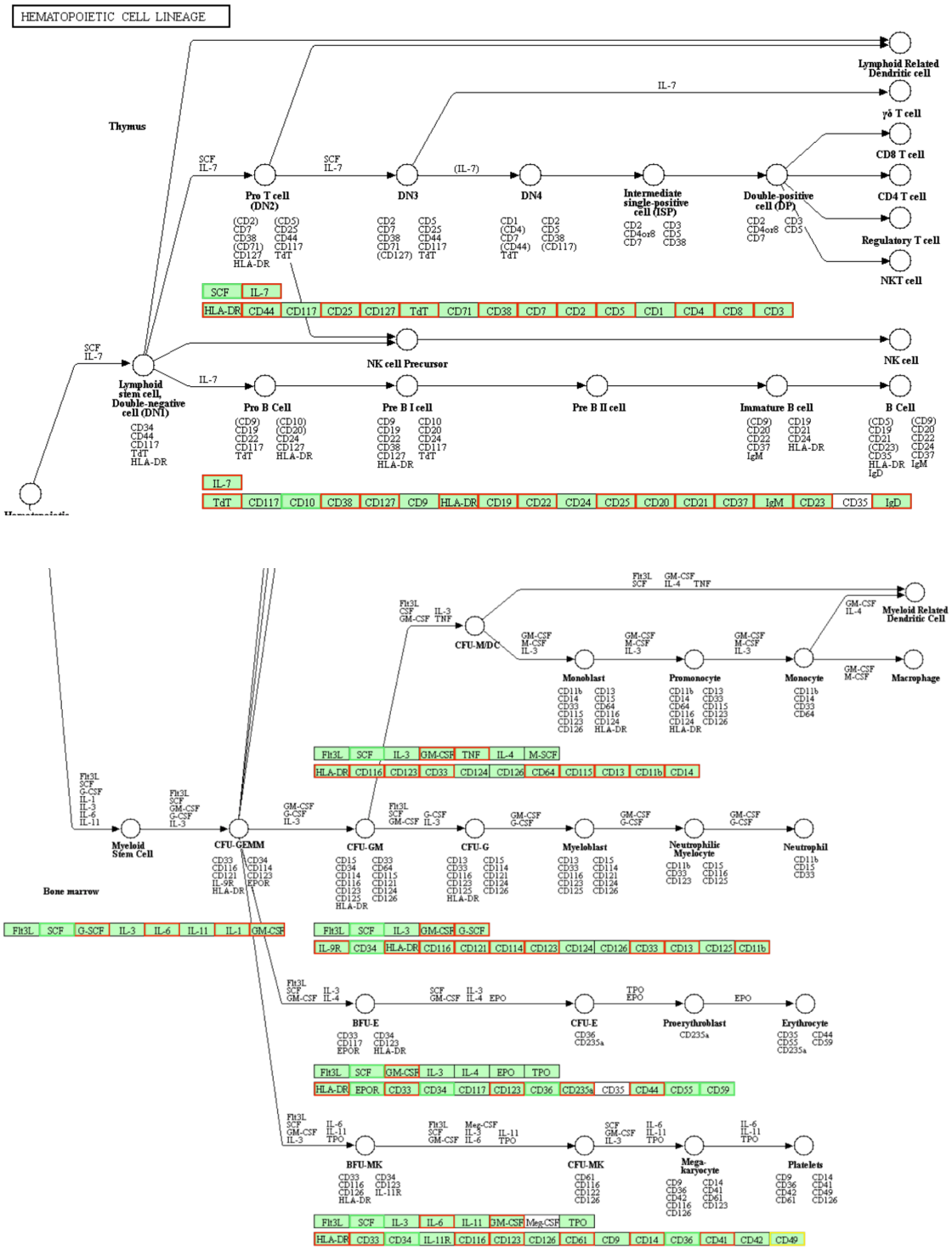

Figure 31. KEGG enrichment analysis pathways linking nodes of functionally associated genes.

Gene expression is indicated by the colour of the box: black – unchanged, red – up-regulated, green – down-regulated, yellow – both up and down regulation of associated genes.

Haematopoeitic cell lineage pathways indicating marked expression of pan-immune cell related genes, suggestive of marked immune infiltration of adipose tissue during sepsis recovery. Figure generated as part of analysis package by NovoGene (Cambridge, UK).

Classical markers of browning were interrogated. Of 23 markers identified in the literature (noting most are derived from the human and mouse literature) three were elevated, 4 were decreased and 16 unchanged. SERCA2, CD137 and CD40 were increased (defined as a change in expression and an adjusted p-value below 0.05. ß3-receptor, Aqp1, Car4 and Prdm16 were all decreased. Of note, UCP1, 2 and 3 gene expression was unchanged between sham and septic groups.

Processes associated with thermogenesis and browning were also interrogated. 10 markers of mitochondrial biogenesis were assessed, of which 8 were downregulated and 2 were unchanged. Transcription of genes intrinsic to lipolysis, adipose tissue specific lipase (atgl) and hormone sensitive lipase (hsl) were both downregulated. Taken together, rpWAT did not express a thermogenic program at day 14 of recovery from sepsis, compared to sham tissue, but did show marked inflammation.

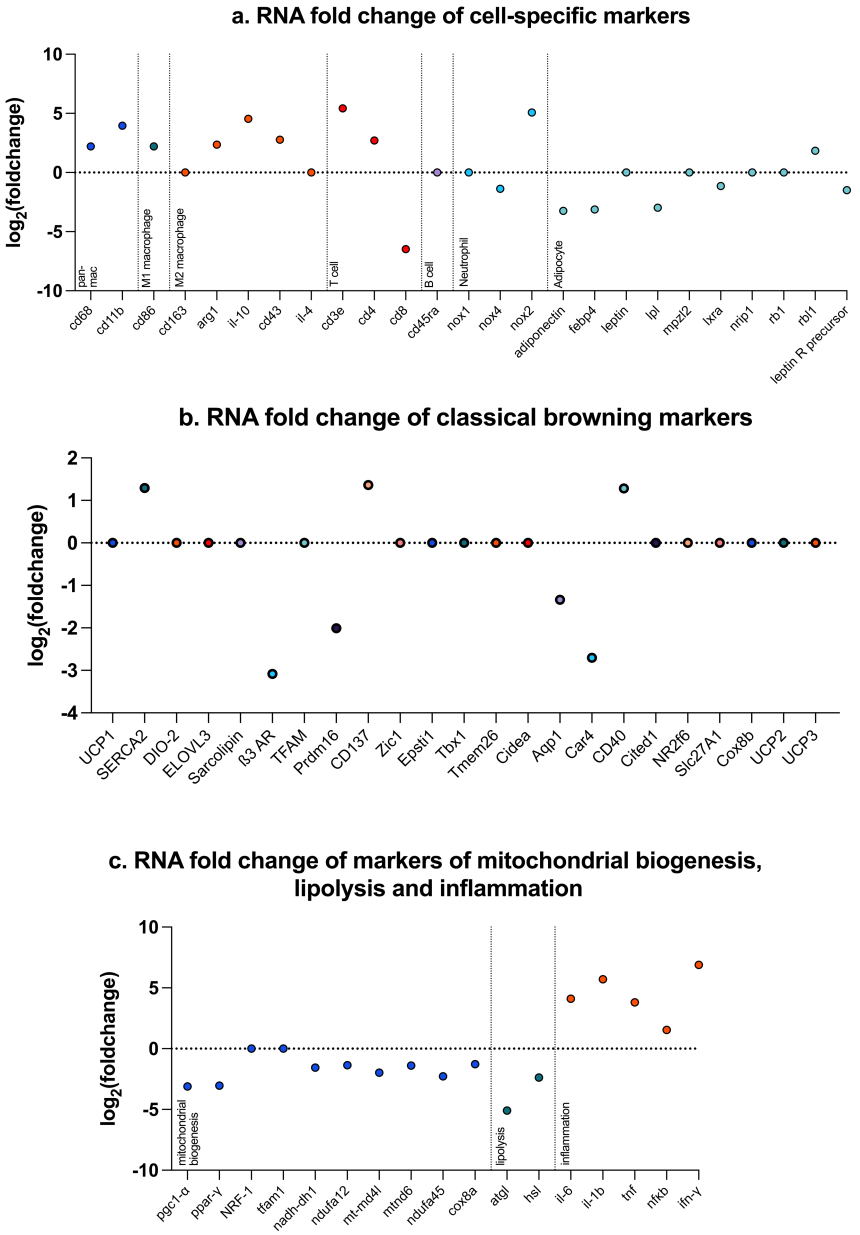

Figure 32. Transcript fold change in rpWAT at day 14 of sepsis recovery compared to rpWAT from sham animals.

a. RNA fold change of rat-specific cell markers supports immune cell infiltration or activation of neutrophils, macrophages, T-cells and B-cells, and reduced adipose tissue markers.

b. Classical browning markers showed an equivocal pattern with 3 genes upregulated, 4 down regulated and 16 unchanged. Of note, CD137 and Cd40 are immune-cell related and may therefore reflect immune infiltration rather than altered adipocyte phenotype.

c. The majority of mitochondrial biogenesis markers were downregulated. Two classical markers of lipolysis, adipose tissue specific lipase and hormone sensitive lipase, were both downregulated at day 14 of sepsis recovery. Markers of inflammation were upregulated.

3.3.5.2 Retroperitoneal adipose tissue from animals recovering from sepsis expresses thermogenic protein, SERCA2, but not UCP1

The canonical marker of adipose tissue browning is uncoupling protein 1 (UCP1). UCP1 expression is clearly demonstrated in brown adipose tissue as the positive control, but not in eWAT or rpWAT from sham animals or those recovering from sepsis. The absence of UCP1 marks the absence of classical browning.

In other UCP1 blots performed (not shown) bands appeared in sepsis recovery WAT but at approximately 5kDa smaller than BAT positive controls. This raised the possibility of post-translational protein modification. Therefore positive controls including BAT taken from animals receiving ß3-adrenergic stimulation or zymosan peritonitis were used to identify post-translational modification associated with altered conditions, but none was evident.

SERCA2 is a thermogenic mechanism constitutively expressed in human and rat skeletal muscle and is also present in beige and brown adipose tissue. RNA seq data indicated increased expression at day 14 of sepsis which was corroborated by increased protein expression at day 14 on Western blot. Relative protein expression was approximately four times higher in rpWAT taken at day 14 of sepsis recovery compared to sham ($p=0.016$).

The regulator of mitochondrial biogenesis, PGC1α, appeared to be upregulated at day 7 of recovery from sepsis although it failed to reach significance on densitometric analysis. RNA sequencing analysis found it was down regulated with a fold change of -3.1 at day 14 of sepsis recovery.

Complex 1 subunit NDUF9 was markedly raised at day 14 of sepsis recovery compared to both day 3 and sham in rpWAT. Conflictingly, Complex 1 subunits

were universally down-regulated or unchanged in RNA-seq profiling at the same timepoint.

Both UCP2 and mitochondrial transcription factor A (TFAM) were absent at the protein level at day 14 in rpWAT taken from animals recovering from sepsis.

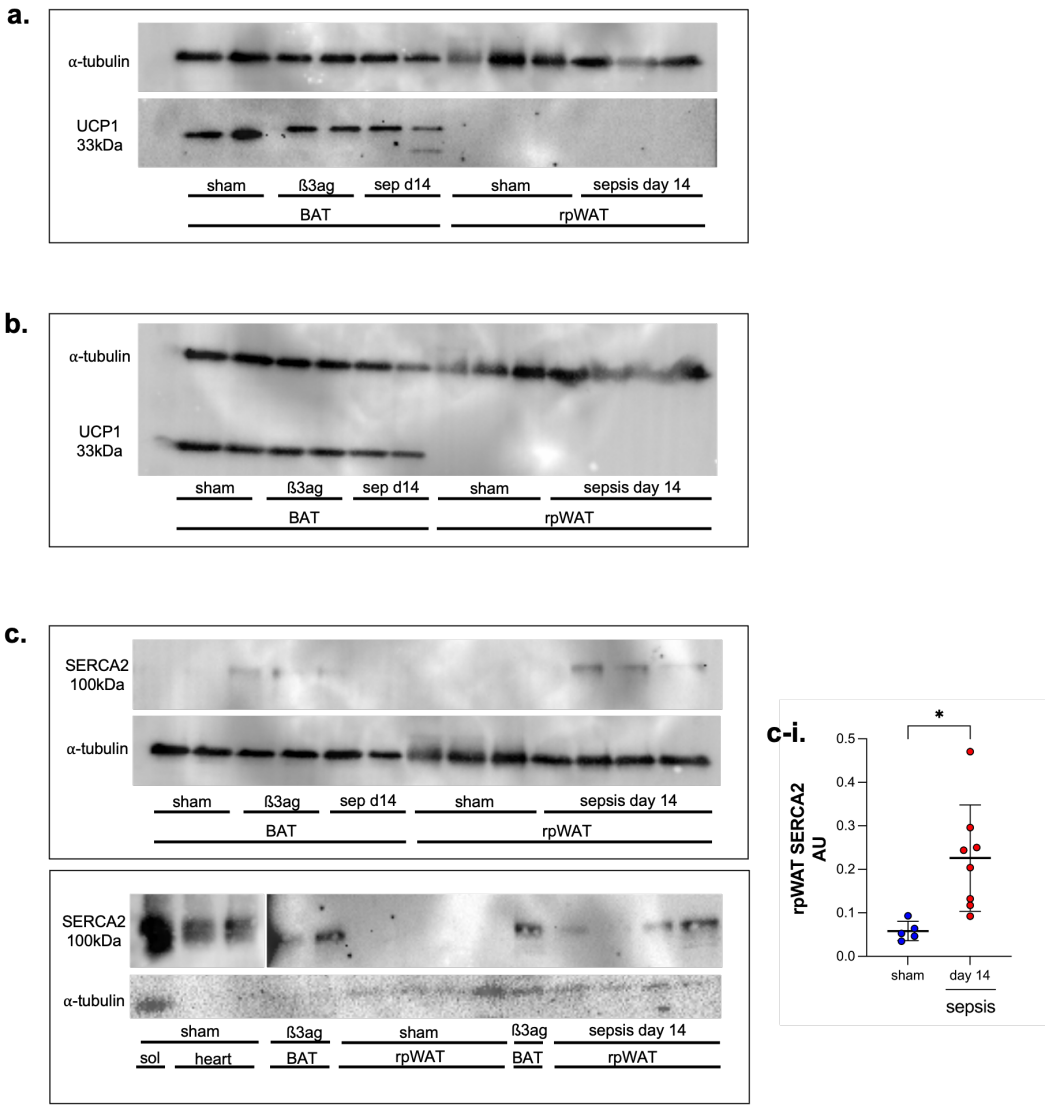

Figure 33. Western blots of thermogenesis-related proteins in rpWAT.

a. Western blot of BAT from sham and septic animals. BAT from animals stimulated with a ß3 agonist for 7 days was used use as a positive control to check for post-translational modification. Bands at 33kDa were present in BAT, but not rpWAT.

b. As a. but with an alternative primary UCP1 antibody.

c. Western blot of SERCA2 using sham soleus and sham heart as positive controls. BAT from animals stimulated with a ß3 agonist was also used as a positive control to look for induction of thermogenic mechanisms and post-tranlational modification. Clear bands were seen in positive controls and at day 14 of sepsis recovery, but not in sham rpWAT, indicating new expression in sepsis recovery tissue. Soleus and heart bands are shown from a shorter chemiluminescent exposure because the bands were too bright.

c-i. Ratiometric analysis showing SERCA2 expression is higher in rpWAT at day 14 of recovery from sepsis (p=0.012). Mean and SD. Unpaired t test.

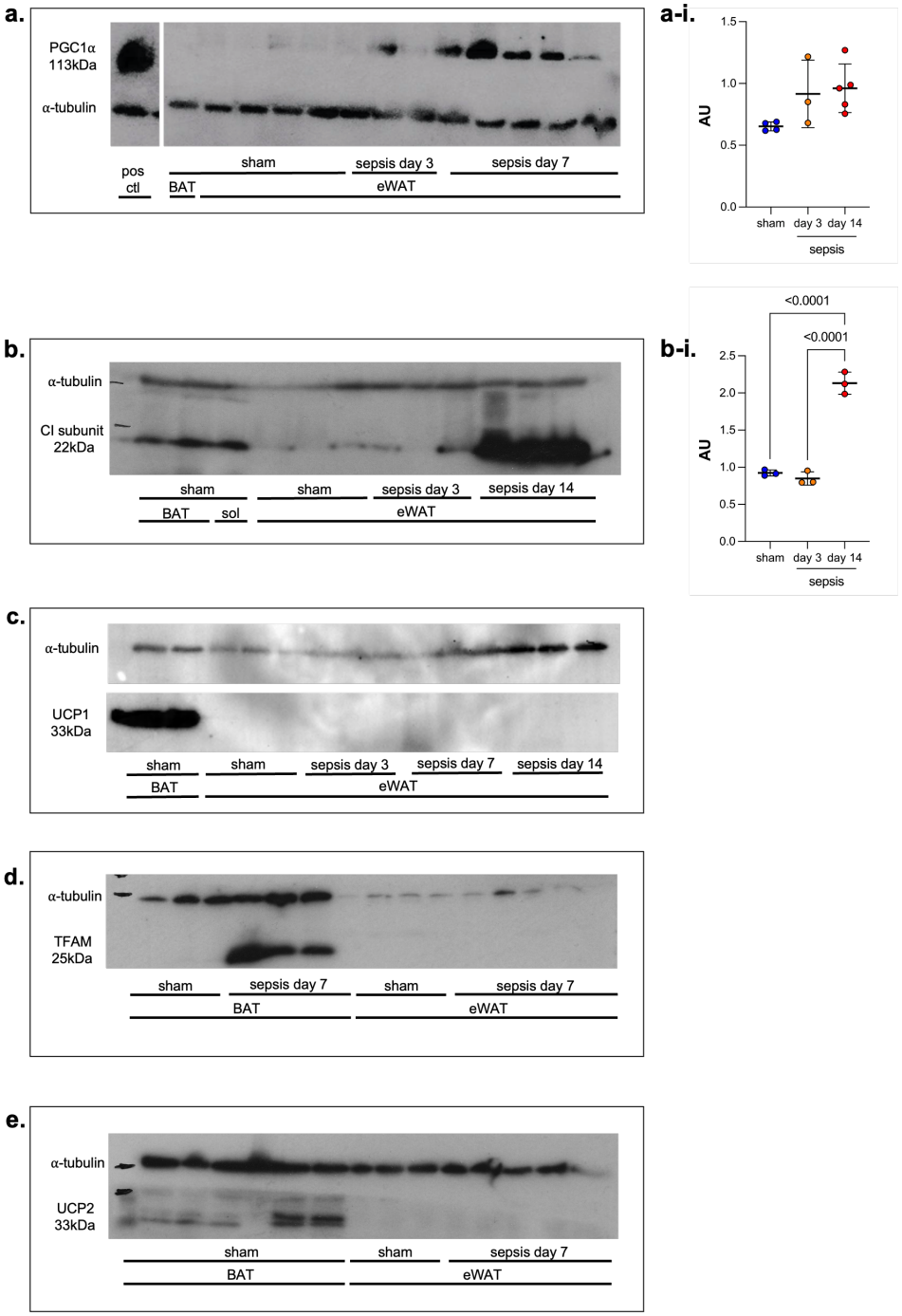

Figure 34. Western blots of proteins related to thermogenesis in eWAT.

a. Western blot of PGC1α expression in BAT and eWAT from sham animals and at days 3 and 7 of recovery from sepsis. Recombinant PGC1α was used as a positive control. Bands indicative of PGC1α were evident in eWAT from animals recovering from sepsis.

a-i. Ratiometric analysis of PGC1α expression was not significantly different between eWAT from sham and sepsis recovery animals.

b. Western blot of complex 1 subunit NDUF9 in BAT and soleus (positive controls) and eWAT from sham animals and at day 14 of recovery from sepsis. Strong bands indicated increased expression in complex 1 at day 14 of recovery from sepsis.

b-i. Complex 1 subunit NDUF9 expression was significantly higher in eWAT from day 14 of recovery from sepsis compared to sham eWAT.
c. Western blot of UCP1 in BAT and rpWAT from sham animals and at days 3, 7 and 14 of recovery from sepsis. UCP1 was not expressed during sepsis recovery.
d. Western blot of TFAM in BAT and eWAT from sham and day 7 of recovery from sepsis. Bands at the correct mass for TFAM were only seen in BAT from animals recovering from sepsis.
e. Western blot of UCP2 in BAT and eWAT from sham and day 7 of recovery from sepsis. No bands were seen in eWAT.

3.3.6 Chapter results summary

- Zymosan peritonitis causes an early hypometabolic phase from days 0-10 followed by a hypermetabolic phase at days 12-14.
- RER is reduced in the first week following the septic insult, indicating a switch to lipid metabolism and lipolysis.
- Oxygen consumption in eWAT from animals at day 3, 7 and 14 and rpWAT at day 14 of recovery from sepsis is higher than in tissue taken from sham animals, when normalised to mass.
- When normalised to protein content, oxygen consumption is not greater in WAT from sepsis recovery animals compared to sham animals, and has a lower maximal oxygen consumption rate.
- When normalised to mitochondrial density, oxygen consumption does not differ between rpWAT from sham or septic animals.
- When normalised to lipid droplet volume (used as a proxy for adipocyte size) and cell number, oxygen consumption in rpWAT from sham animals and those at day 14 of recovery from sepsis is statistically equivalent
- Serum lipase levels are increased at day 1 of sepsis, but circulating markers of lipolysis are otherwise unaltered during recovery from sepsis.
- RNA sequencing suggests there is marked inflammation of rpWAT at day 14 of recovery from sepsis. Markers of lipolysis, browning and thermogenic

activation are broadly unchanged or down regulated. SERCA2 gene expression is increased.

- UCP1 is not expressed in eWAT or rpWAT at day 14 of recovery from sepsis.
- SERCA2 protein expression is increased in rpWAT at day 14 of recovery from sepsis.

3.4 Discussion

The identification of browning as a maladaptive process driving cachexia and myopathy in burn-injury and cancer patients enabled therapeutic advances in care.[82,83] The similarity in pathophysiology of burn injury and sepsis and identification of browning in mouse models of sepsis warrants a thorough investigation in our model of sepsis.[102,106,148]

The canonical marker of browning of white adipose tissue/beige adipose tissue is the expression of UCP1, which was not present in this study. Beige adipose tissue demonstrates multiple other changes to enable thermogenesis: multi-loculation of lipid droplets, mitochondrial biogenesis and expression of UCP1-independent thermogenic pathways including futile substrate cycles, which must also be considered.[57]

Brown fat has been identified in humans using thermal imaging but direct visualisation of the temperature of eWAT using thermal imaging is a novel technique.[149] In this study no significant increase in eWAT temperature was seen, potentially because rapid temperature shifts due to anaesthesia and visceral exposure confounded results as heat loss may vary between animals and groups. eWAT is also felt to be more resistant to browning compared to other WAT deposits,

although UCP1 has been demonstrated in eWAT of mice recovering from sepsis.[102,106,150] rpWAT couldn't be visualised due to overlying bowel.

As explained in the introduction, oxygen consumption in human sepsis is most commonly raised in early and less severe sepsis and declines with increasing severity and then increases in the recovery phase in survivors.[62] In animal models of sepsis, mice develop a profoundly hypometabolic and hypothermic state whilst rats become hypometabolic but maintain their temperature if housed at or near thermoneutrality.[81] In this model, animals developed an initial hypometabolic phase followed by a hypermetabolic phase from day 12 onwards. The hypermetabolic phase is consistent with that seen in human sepsis, however the magnitude of the increase in metabolism was less than that reported in humans (60% increase in one study). Hypermetabolism is consistent with increased thermogenesis but could also be caused by increased activity of growth. Body mass gain was equivalent between groups at days 12-14 and although activity wasn't measured, appeared similar between sham and septic animals. Therefore the increased metabolism is likely due to another metabolic pathway which could include maladaptive thermogenesis.

Another vital aspect of browning is lipolysis.[94,151] In this study circulating lipase was elevated at day 1. Lipase catalyses the hydrolysis of triglycerides into glycerol and free fatty acids and is largely present in exocrine digestion and stored as granules in the pancreatic acinar cells. Elevation of lipase is not specific to lipolysis and can be elevated by inflammation generally, particularly that of the pancreas. Other markers of lipolysis, including glycerol and triglyceride levels were normal and not supportive of lipolysis at any timepoint. However the RER reduced in animals with sepsis indicating a switch to lipid metabolism which would require lipolysis. The RER had recovered to normal levels by day 14, indicating lipolysis was not perpetuated to a degree detectable by RER, again, not supportive of ongoing browning. Efforts to demonstrate hormone sensitive lipase and adipose tissue

specific lipase expression in WAT by Western blot could not be optimised due to poor antibody specificity, but mRNA levels were reduced for both. Overall, the trend towards smaller lipid droplet size and the fall in RER support the presence of lipolysis, at least in the early recovery phase.

High resolution respirometry was performed to directly measure oxygen consumption and indirectly measure heat production of adipose tissue. Initial experiments using eWAT showed increasing oxygen consumption per milligram of tissue with increasing recovery time. Experiments were then repeated using rpWAT due to concerns that the inflammatory milieu of ascites would infiltrate the eWAT as it lies in the peritoneal cavity and confound results and reports of eWAT resistance to browning. Normalisation to tissue protein content, mitochondrial density, lipid droplet volume (a proxy for adipocyte volume) and cell number largely abolished the increase, indicating the increased rate was potentially due to cell shrinkage and therefore a greater number of cells and mitochondria per milligram of tissue. Cell shrinkage is in-keeping with browning, but an equivalent metabolic rate is not. Immune cell infiltration may have additionally increased oxygen consumption in sepsis recovery tissue, hence the absence of a difference when normalised to cell number.

Frustratingly, efforts to measure leak respiration using oligomycin to block ATP synthase or GDP to block UCP1 could not be optimised in positive control tissue, BAT or in WAT.

Bulk RNA sequencing of rpWAT from sham animals and those at day 14 of recovery from sepsis was performed to try to identify a thermogenic gene expression signature. The primary findings evident on enrichment using GO and KEGG pathways were increases in markers across immune cell types including neutrophils,

M1 and M2 macrophages and B and T lymphocytes. In addition, adipocyte-specific markers were down regulated. The increase in immune cell related genomic material indicates either immune cell infiltration or inflammatory processes in resident adipose tissue cells, or both. The presence of immune-cell specific markers supports the genetic material coming from immune cells. This could be cautiously supported by the trend (albeit non-significant) towards greater numbers of nuclei in sepsis recovery rpWAT, although the nature of the cell cannot be determined using this technique.

The presence of greater numbers of immune cells in sepsis tissue compared to sham would render identifying a signal from adipocytes alone impossible. Immune cells have different cellular machinery and therefore transcriptomes compared to adipocytes, including less mitochondria, which could result in a dilution of mitochondrial and thermogenic gene expression in the transcriptome of septic tissues.[152] Resident adipose tissue cells are capable of expressing inflammatory signals themselves - single-cell transcriptome studies of inflamed pre-adipocytes in patients with cancer-associated cachexia showed a transition to a pro-inflammatory phenotype, and may represent inflammation of resident adipocytes in this study.[153]

Despite a lack of cell specificity for transcriptome data, adipose tissue inflammation and immune cell infiltration is consistent with browning and is seen extensively in other inflammatory conditions including cancer-associated cachexia and obesity.[153,154] In browning immune infiltration by predominantly M2 macrophages occurs.[92] Immune cells and not adipocytes have been shown to be the regulators of adipose tissue thermogenesis, with distinct populations in beige adipose tissue.[152] Indeed, macrophage depletion reduces cachexia in mouse models of cancer.[153]

The changes may not reflect a change in the types of immune cells present, but in their proportion and phenotype. A recent study using single cell RNA-sequencing showed on eWAT at 1 month after sepsis showed the same types of leukocytes but in altered proportions.[86] This may explain the transcriptomic switch towards an immune program without a significant increase in nuclei.

It is plausible the infiltrate resulted from proximity to the peritoneum also, which could only be answered by sampling of distant adipose tissue deposits. Attempts to use inguinal adipose tissue for this were unsuccessful due to shrinkage of the tissue resulting in very little for experimentation.

Regardless of the confounding effects of an immune infiltrate, bulk RNA-seq on adipose tissue is problematic because even in health it contains a huge variety of cells, many of which wouldn't directly express a thermogenic signature.[147] Future studies will require single-cell methods.

Taken together it is likely there is marked adipose tissue inflammation, a degree of infiltration and activation and phenotypic change of resident immune cells. Aspects of this could be consistent with browning processes, but overall the tissue did not demonstrate a thermogenic programme.

Nuclei and lipid droplet numbers were measured to try and quantify the immune cell infiltrate. Nuclei number represents all cells, the majority of which will be adipocytes, immune cells and cells of the vascular stromal fraction. Adipocyte number was approximated by the number of lipid droplets because most adipocytes contain one droplet. As mentioned in the introduction, browning causes multiloculation of lipid droplets resulting in multiple droplets per cell. If this had occurred it would falsely increase the number of adipocytes and falsely reduce

apparent fraction of non-adipocytes. However, on visualisation of lipid droplets multiloculation was not apparent, and small structures which could represent new droplets were excluded from the count. Accepting these caveats, there was a non-significant trend towards more nuclei in sepsis recovery tissue. This may reflect immune cell infiltration. Sampling error may also account for variable numbers of nuclei, although RNA-sequencing analysis showed good intragroup correlation between sepsis samples, suggesting the samples were similar in their cellular composition.

UCP1 is the canonical marker of browning but was unchanged at the mRNA level and absent at the protein level.[136] UCP1-independent thermogenic mechanisms are increasingly recognised in beige adipose tissue, including SERCA2 which was elevated at both the mRNA and protein level.[57] To my knowledge this is a novel finding in sepsis. Western blot samples were produced from bulk adipose tissue samples and must therefore also be interpreted as possibly containing an altered cell fraction and are only representative of a heterogeneous cell population. SERCA isoforms are expressed ubiquitously and are necessary for calcium homeostasis, but most prominently expressed in cardiac and skeletal muscle.[59] Expression in immune cells is reportedly low, suggesting increased expression at day 14 may be due to new expression in adipocytes.

No protein involved in thermogenesis can act independently. SERCA2 is an ATPase and therefore relies on oxidative-phosphorylation apparatus to generate a raised ATP/ADP ratio to drive calcium transport. The transcriptomic data show an almost uniform down regulation of thermogenic and bioenergetic machinery, which again is non-supportive of thermogenic activation. Elevation of PGC1α and complex 1 protein in eWAT at days 7 and 14, respectively, support metabolic activation, but

again, would be insufficient in supporting SERCA2, and as discussed later, activation of PGC1α did not result in increased mitochondrial density.

Timing is also an important limitation. RNA-sequencing and respirometry was performed exclusively at 14 days after septic insult in rpWAT. Browning may indeed occur later, or may have resolved by the time of sampling. However, the sepsis and burn injury literature support browning to occur at these time point, and myopathy is established, suggesting it is a reasonable timepoint to focus upon.

In order to overcome the implications of unclear contributions of immune cell fractions to experiments using bulk tissue, multiphoton microscopy was used to identify adipocytes directly and interrogate their mitochondrial function and metabolic state.

Chapter 4. Multiphoton microscopy of retroperitoneal white adipose tissue from sham animals and day 14 of recovery from sepsis

4.1 Background

Multiphoton microscopy (MPM) is a powerful technique that enables identification of specific cell types within tissues and interrogation of their bioenergetic machinery. In light of the highly heterogeneous nature of adipose tissue, complicated by inflammation as highlighted by the RNA-sequencing data, MPM was used to study adipocyte-specific phenotypic changes.

Advances in microscope hardware and fluorescent dyes have enabled detailed study of many cellular processes, the majority of which has been performed in cell culture models.[155] Cross-talk between tissues and cell populations at the local and systemic level is increasingly recognised as key to whole body metabolic control, particularly between immune cells, adipose tissue deposits and skeletal muscle.[87,88,156] For example, meteorin-like, a circulating hormone released by skeletal muscle after exercise and adipose tissue after cold exposure improves glucose sensitivity and induces thermogenic gene signatures in beige adipose tissue.[157] Studies of clonal cell lines or primary cell isolations often select for non-representative populations and do not reflect tissue cross-talk; whole organisms must be studied to appreciate the complex interplay between tissues.[158]

With this in mind, I developed in-vivo MPM of epididymal and inguinal white adipose tissue deposits using both topical and systemic dyes and pharmacological manipulation. This was performed in collaboration with Professor Matthew

Rodeheffer at Yale University. Unfortunately, in-vivo imaging became logistically and practically impossible to continue at UCL due to hardware issues.

Instead, MPM was performed on live explanted rpWAT imaged under physiological conditions. Use of explants allows for higher throughput, longer exposure to fluorescent dyes resulting in consistent staining, and imaging of rpWAT (otherwise impossible due to anatomical challenges) and therefore direct correlation with the respirometry, immunoblot and RNA-sequencing data. Its limitation is in its isolation from the circulation and other tissues, such as skeletal muscle.

MPM has been used to study myriad tissues and processes but, to the best of my knowledge, has not been used in the study of adipose tissue in sepsis. As thermogenesis is measured indirectly as oxygen consumption, and most of the oxygen consumed by the body is by mitochondria, metrics of mitochondrial function were used to investigate activation of thermogenesis during recovery from sepsis. These include mitochondrial membrane potential and the oxidation status of the NAD(P)H pool. MPM was also used to measure other features of browning including lipid droplet size, mitochondrial number and density and immune infiltration.

4.2 Methods background

Multiphoton microscopy is a form of fluorescence microscopy that utilises the phenomenon of photon absorption and emission in fluorescent molecules. It is similar in principle to traditional fluorescence microscopy which uses a single photon from a laser to excite a fluorophore, which then emits a photon of slightly lower energy. The emitted photon is captured by a detector and converted into data which can be analysed or visualised to represent properties of the fluorophore. MPM differs in that instead of relying on a single excitatory photon, it relies on two photons of half the energy (twice the wavelength) to excite the fluorophore near-simultaneously to deliver sufficient energy to excite a fluorophore and cause an emission that can be detected. As the excitatory photons are of lower energy they can penetrate deeper into tissue allowing for imaging depths up to the millimetre range, and are less toxic to tissues allowing imaging of live tissues.[159] This gives MPM its distinct advantages for imaging tissue.

Near-simultaneous excitation by two photons is achieved by pulsed laser of femtosecond frequency usually in the infra-red range. The probability of simultaneous excitation by two photons increases quadratically with photon intensity, resulting in very little excitation away from the focal area and a focal volume of approximately 1 femtolitre. By scanning the laser and photon excitation along x, y and z axes, 3 dimensional representations of tissues can be generated. Serial scanning through time adds a fourth dimension. The localisation of excitation and femto scale focal area removes the need for a pinhole to remove off-focus fluorescence, although most microscopes still have one available to optimise resolution.

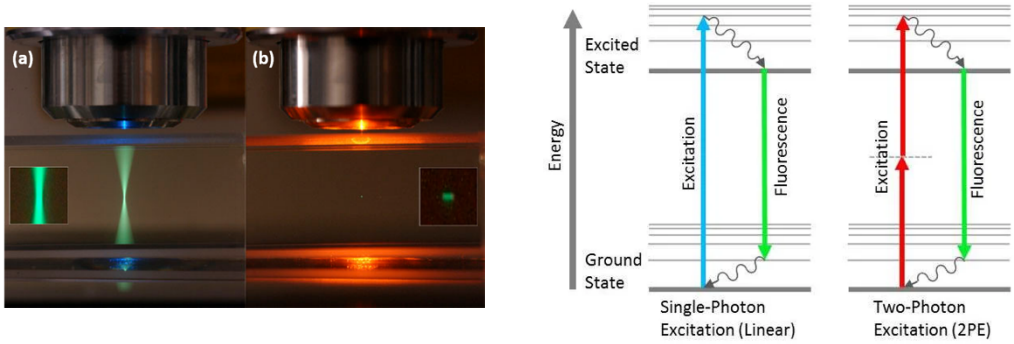

Figure 35. Demonstration of excitation volume and excitation and emission dynamics in single and two-photon microscopy.
Left: The excitation volumes of (a) single photon and (b) multiphoton microscopy. Small box inserts show the focal volume of respective imaging techniques, demonstrating the much smaller focal volume of multiphoton imaging and reduction of off-focus fluorescence. This results from the requirement for near-simultaneous excitation of fluorophores by 2 or more photons. Image courtesy of Dr Steven Ruzin, University of Berkeley.
Right: Jablonski diagram of single and two-photon excitation of an electron in a fluorophore resulting in emission of a photon on return to its ground state. The emitted photon is detected and used to generate an image and to derive properties of the fluorophore and associated processes and structures.

MPM does have disadvantages compared to single-photon confocal microscopy. The range of fluorophores and the excitation and emission spectra are less discrete, limiting imaging options and specificity. While off focus photobleaching is reduced, bleaching is much more pronounced in the excitation volume. Sample destruction can also occur due to the need for higher laser powers, which can result in boiling.

Imaging using three or more photons is possible, with accentuation of the principles, advantages and disadvantages discussed, and is encapsulated by the term 'multi-photon microscopy'.

A fluorophore is any molecule or compound that re-emits light after absorption. Fluorophores can be endogenous, known as autofluorescence, or added to samples as dyes and antibodies or expressed by the organism through genetic linking. Myriad fluorophores have been developed to either link to proteins or structures of interest or to alter fluorescence in response to altered environment. By altering

protein expression or environmental conditions, for example pharmacologically, subcellular processes can be interrogated in real time.[155]

4.2.1 Autofluorescence

The reduced pyridine nucleotide electron carriers NADH and NADPH are intrinsically fluorescent. When stimulated with a multiphoton laser at 720 nm, both molecules fluoresce with emission spectra of 435-485 nm and are indistinguishable. NADH drives ATP generation through glycolysis in the cytoplasm and oxidative phosphorylation via electron donation to complex I of the electron transport chain, while NADPH is predominantly involved in antioxidant defences. Their oxidised counterparts, NAD^+ and $NADP^+$ are not fluorescent. This phenomenon allows for label-free interrogation of the redox status of mitochondria.[160] In most cells the NAD^+/H pool is larger than the $NADP^+$/H pool.[161] However, the contribution of NADH and NADPH to autofluorescence is approximately equal because of redox states: the ratio of NADH/NAD^+ is typically kept low (oxidised) to allow for reduction by catabolic pathways e.g. the TCA cycle. By contrast, the NADPH/$NADP^+$ pool is maintained in a more reduced state to act as an electron donor for anabolic pathways.[160] Subsequently, the amounts of the fluorescent reduced forms are approximately equal. The two pools can be differentiated by fluorescence lifetime imaging, but this was not possible within the project timescale.[162] Direct comparison of autofluorescence between samples is not valid, therefore oxidising and reducing substances are used to establish a range and allow inferences about bioenergetics.

4.2.2 Measurement of mitochondrial membrane potential by TMRM

Tetramethylrhodamine methyl ester (TMRM) is a fluorophore used to measure mitochondrial membrane potential. TMRM is a lipophilic cation which accumulates

in the mitochondrial matrix in proportion with the $\Delta\psi_{mt}$, enabling measurement of the $\Delta\psi_{mt}$. At higher concentrations TMRM can quench itself, resulting in a falsely low signal and a paradoxical rise when mitochondria are depolarised. This phenomenon can be checked by depolarisation with a chemical uncoupler such as FCCP that would lead to a paradoxical rise in fluorescence.

4.2.3 Identification of lipid droplets and measurement of their volume by BODIPY

BODIPY is a fluorescent organoboron dye used to stain lipid droplets.[163] Browning causes lipolysis and shrinkage and multiloculation of lipid droplets and can be used to identify beige adipose tissue. As lipid droplets occupy the vast majority of the cytoplasm of white adipocytes, their volume is often used as a proxy for adipocyte volume.

4.2.4 Identification of nuclei in adipose tissue using Hoechst

Hoechst is a bis-benzimide dye used to stain DNA. Hoechst was chosen over other DNA dyes such as DAPI as it is less toxic and shows better tissue penetration, both important factors for live tissue staining. However, Hoechst is a tenacious dye with strong fluorescence at low concentrations and a wide emission spectrum, often resulting in emission bleed into other channels and sample contamination.

4.3 Methods and materials

4.3.1 Tissue preparation

Retroperitoneal WAT was dissected from sham and septic animals at day 14 after insult and immediately placed in ice cold biopsy preservation medium. Tissue was typically imaged within 30 minutes of dissection. Before imaging, tissue was

equilibrated to 37°C in physiological saline solution with HEPES buffer. The imaging stage was also heated to 37°C for the entirety of the protocol. rpWAT was gently dissected into approximately 2x2x1mm pieces for staining and imaging.

Table 7. Constituents of physiological saline solution.
All constituents were dissolved in deionised water, adjusted to pH 7.4 and then stored at -20°C.

Constituent	Final concentration (mM)
NaCl	118
KCl	4.7
$NaHCO_3$	10
$MgSO_4$	1.44
$KHPO_4$	1.2
CaCl	1.8
Glucose	5
Pyruvate	5
HEPES	10
pH	7.4

4.3.2 Fluorophores

For imaging protocols involving measurement of $\Delta\psi_{mt}$ or localisation of mitochondria, tissue was incubated in PSS with HEPES plus 50 nM TMRM for 20 minutes. The concentration and incubation time were determined by optimisation studies to ensure a consistent signal over time.

To examine adipose tissue architecture, rpWAT was incubated for 20 minutes in PSS with HEPES with 50 nM TMRM to identify mitochondria, 10 µM BODIPY to identify lipid droplets and 10 ng/ml Hoechst to stain nuclei.

4.3.3 Microscopy

All imaging was performed on a high-resolution upright Leica SP8 multiphoton microscope (Leica Microsystems, Wetzlar, Germany) with a titanium sapphire laser, an environmental chamber for accurate temperature control, 25x 0.95 NA water dipping objective and 2 internal and 2 external HyD photomultiplier detectors. Imaging conditions were controlled using Leica LAS-AF software.

4.3.3.1 Tissue mounting and perfusion

Tissue was immersed in PSS+HEPES at 37°C and placed in a 30 mm clear plastic dish (an inverted fluorodish lid) placed inside a 75 mm clear plastic dish to act as a perfusion gutter. Adipose tissue was anchored using a tissue net fashioned from a steel washer and nylon fishnet-tight material. To manipulate mitochondrial function tissue was perfused with PSS+HEPES at 37°C containing either 5mM sodium cyanide, 15μM oligomycin or 10μM FCCP by gentle aspiration of the existing buffer and slow addition of new buffer under direct live imaging to ensure stability of the tissue. The 25x water dipping objective was lowered directly into the imaging media over the tissue.

A representative area of adipocytes without vascular or connective tissue was identified using brightfield imaging and brought into maximal focus. Live multiphoton imaging was then used to focus the image and identify an appropriate stack avoiding vascular or connective tissue. Imaging to establish autofluorescence, mitochondrial membrane potential and adipose tissue architecture were performed as separate experiments on separate pieces of tissue from the same rpWAT sample. The following imaging conditions were optimised to ensure no over exposure of pixels during scanning when measuring AF and $\Delta\psi_{mt}$.

4.3.3.2 Imaging conditions

Table 8. Microscope settings for all imaging protocols.

	Autofluorescence	$\Delta\psi_{mt}$	rpWAT architecture
Size	1024x1024	1024x1024	1024x1024
Laser wavelength	720nm	800nm	800nm
Laser power	100%	10%	40%
Master gain	100%	50%	50%
Smart gain	500	150	500
Offset	50	50	50
Objective	25x 0.95 NA	25x 0.95 NA	25x 0.95 NA
Line averaging	4	2	2
Emission spectra	C1 - 435-485nm AF C2 – 550-610nm TMRM	550-610nm TMRM	C1 – 450-490nm Hoechst C2 – 490-530nm BODIPY C3 – 550-610nm TMRM
Pinhole	10 airy units	10 airy units	10 airy units
Digital zoom	3.27	1	1
Stack depth	100µm	100µm	100µm
Slice depth	5µm	5µm	5µm
Timelapse	3 minutes	3 minutes	1 stack
Temperature	37°C	37°C	37°C
Protocol imaging order	1. Baseline 2. 5mM CN 3. Washout 4. 10µM FCCP	1. Baseline 2. 15µM oligomycin 3. 10µM FCCP	Nil

4.3.3.3 Autofluorescence

The microscope was set up as displayed in Table 8. A baseline stack was taken of total autofluorescence. The tissue was then perfused with imaging media containing 5 mM cyanide to inhibit complex IV. Four further stacks were taken at 3 minute intervals. Tissue was then gently perfused with normal imaging medium to washout

cyanide and then perfused with media containing 10 μM FCCP and 5 further stacks taken at 3 minute intervals. This method establishes baseline fluorescence and then maximal and minimal fluorescence, reflecting maximally reduced and oxidised NAD(P)H pools, respectively. A range between minimal and maximal fluorescence is then established which can be used to normalise baseline fluorescence.[164] TMRM fluorescence was imaged simultaneously to allow co-localization of autofluorescence with mitochondria.

4.3.3.4 $\Delta\psi_{mt}$

A baseline stack was taken after which the tissue was perfused with imaging medium containing 15μM oligomycin. Four further stacks were then taken at 3 minute intervals. Medium containing 10 μM FCCP was added and five further stacks taken at 3 minute intervals.

4.3.3.5 Adipose tissue architecture

A single stack was taken encompassing the depth of at least one whole adipocyte, typically 100 μm deep.

4.3.4 Image Analysis

4.3.4.1 Autofluorescence

Analysis was performed in Fiji (Image J v2.3.0/1.53q). Stacks were split into single channels to separate autofluorescence and TMRM signal. Each stack was made into a 2D image as a SumSlices Z project. Any vascular tissue visualised in the field was digitally removed by free hand selection. Using the TMRM image, regions of interest were drawn around mitochondria. These regions of interest were then

superimposed onto the autofluorescence images and thresholded using the Otsu algorithm. Raw Interval Density (RiD) was then measured to represent the area of positive pixels and their cumulative fluorescence. This was repeated for all stacks using the same region of interest.

The peak fluorescence after addition of cyanide and the nadir of fluorescence after addition of FCCP was used to establish a range (0-1). Baseline fluorescence was then normalised to this range (as a value between 0 and 1).

4.3.4.2 $\Delta\psi_{mt}$

As above, stacks were transformed into 2D images as a SumSlices Z project. If vascular tissue was present it was removed by freehand selection. Images were then thresholded using the Otsu algorithm and Raw Interval Density used as the measure of mitochondrial membrane potential. Changes in $\Delta\psi_{mt}$ after additions of oligomycin were taken to reflect the proportion of $\Delta\psi_{mt}$ coupled to phosphorylation. FCCP was added to ensure the TMRM signal was mitochondrial and the signal was not quenched due to excessive TMRM accumulation (indicated by a reduction in signal).

4.3.4.3 Adipose tissue architecture

Mitochondrial density was measured using baseline stacks from $\Delta\psi_{mt}$ imaging experiments. Stacks were converted into 2D images as a SumSlices Z Project and thresholded using the Otsu algorithm. Individual adipocytes were then isolated using a region of interest and positive pixels taken to represent mitochondria. Density was then calculated as the proportion of positive pixels in the total adipocyte area. Total number of mitochondria and mitochondrial density per cell were then derived.

Lipid droplet volume was measured using the surface wizard function of Imaris Software (Zurich, Switzerland). The green channel was isolated and objects capable of containing a 35μm^3 sphere were selected. Surfaces were then generated for each lipid droplet and the threshold set to remove as many surfaces formed due to artefact and debris as possible. Each droplet was checked to ensure separation from adjacent droplets. Those that were conjoined were separated using the 'cut' function and the volumes of the droplets recorded. The same process was performed as a batch for all images.

Nuclear number was also measured using the surface wizard of Imaris software. The blue channel was isolated and objects capable of containing a 5 μm^3 sphere selected. Surfaces were generated and the threshold altered to ensure only nuclei (which are easily recognisable) were included in the analysis and artefact removed. The total number of nuclei per image was recorded.

4.4 Results

4.4.1 Adipose Tissue Architecture

4.4.1.1 Lipid droplet volume

Mean lipid droplet volume in rpWAT taken at day 14 after sepsis was 105000 μm^3 compared to 157000 μm^3 in sham rpWAT. Despite the trend, droplet volume was not normally distributed in either group and there was no significant difference between groups on non-parametric testing (p=0.15). The mean volume from each sample also did not differ between groups (p=0.12).

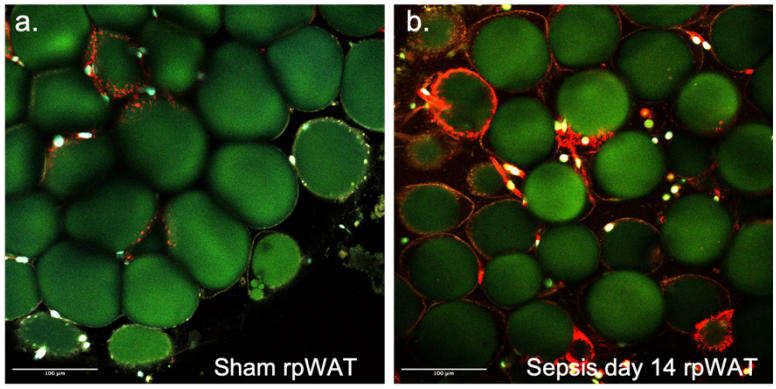

Figure 36. Representative images of retroperitoneal adipose tissue from sham and day 14 of sepsis recovery.
a. Representative image of sham rpWAT explant tissue architecture. Lipid droplets are depicted in green, mitochondria in red and nuclei in white. Scale bar is 100μm.
b. Representative image of rpWAT at day 14 of recovery from sepsis. Structures are depicted in the same colours used in sham tissue. Scale bar is 100μm.

4.4.1.2 Nuclei number

The mean number of nuclei per stack (443 x 443 x 100 μm) was 432 in septic tissue compared to 250 in sham (p=0.025). When nuclei were normalised to lipid droplet

number, used as a proxy count of the number of adipocytes (assuming 1 lipid droplet per adipocyte), there was no significant difference between the number of nuclei per adipocyte in sham and septic tissue, indicating that the increased cell density is due to adipocyte shrinkage, rather than infiltration.

4.4.1.3 Mitochondrial density

Mitochondrial density was significantly higher in rpWAT from animals at day 14 after septic insult compared to sham ($p<0.0001$). When normalised to the number of adipocytes (counted as number of lipid droplets) there was no significant difference in the number of mitochondria per cell/lipid droplet.

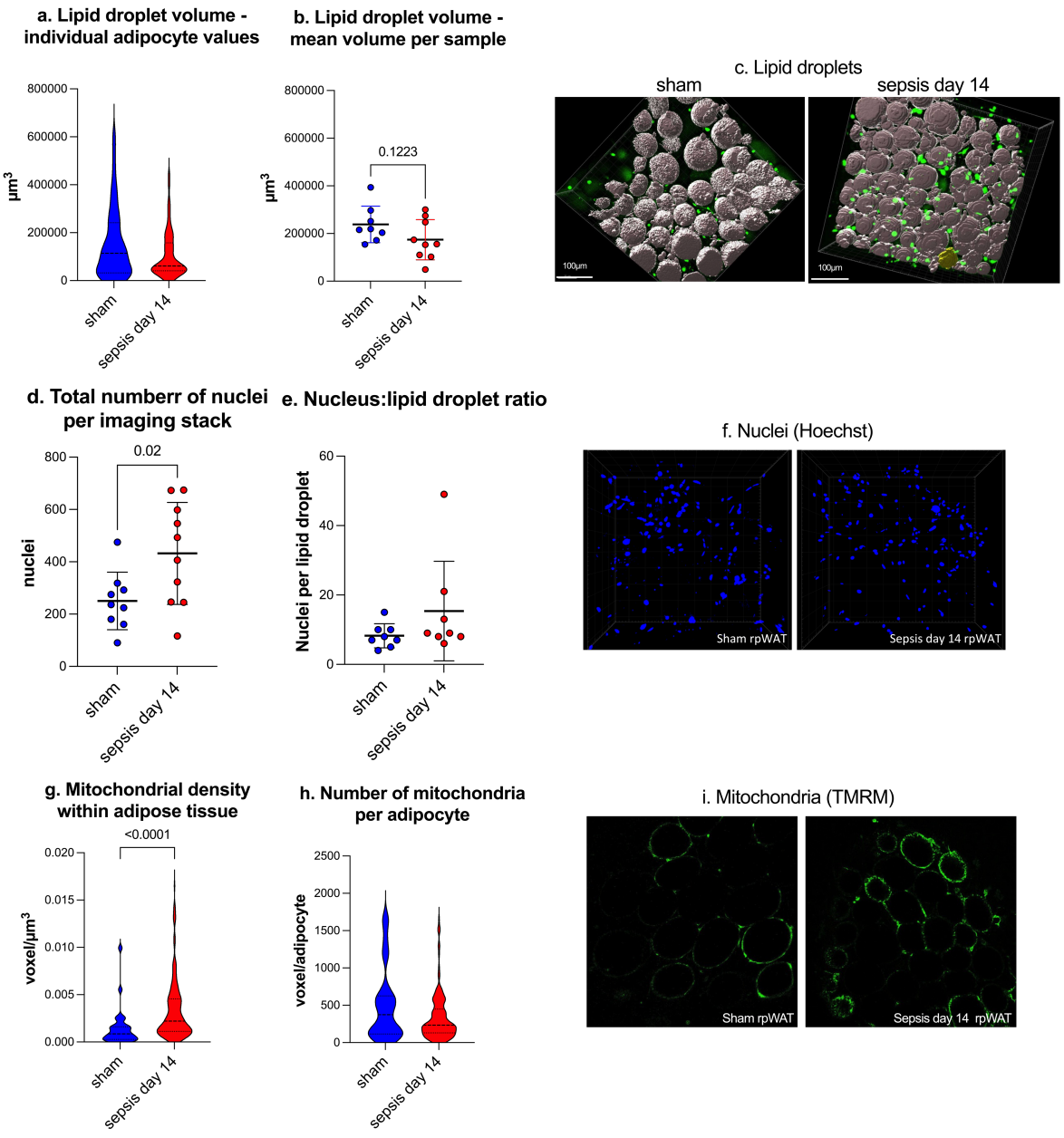

Figure 37. Adipose tissue architecture – lipid droplet volume, mitochondrial density and number of nuclei.

a. Violin plot of individual lipid droplet volumes in rpWAT from sham and at day 14 of sepsis recovery. No significant difference was seen between groups (Mann-Whitney).

b. Scatter plot of the mean lipid droplet volume per sample from sham and day 14 of sepsis recovery. No significant difference between groups (unpaired Student's t-test).

c. Representative images generated in Imaris to identify and calculate lipid droplet volumes.

d. Total number of nuclei per imaging stack in rpWAT sham and day 14 of sepsis recovery. Nuclei were significantly more numerous in rpWAT during sepsis recovery.
e. Nuclear number normalised to lipid droplet number. Lipid droplet number was used as a proxy for adipocyte number as the vast majority of adipocytes contain a single droplet. There was no significant difference between groups.
f. Representative images generated in Imaris to identify and calculate the number of nuclei.
g. Violin plot of mitochondrial density within rpWAT from sham and day 14 of sepsis recovery. Mitochondrial density was significantly higher ($p<0.001$) in rpWAT at day 14 of sepsis recovery (Mann-Whitney).
h. Number of mitochondria per adipocyte. There was no significant difference in the total number of mitochondria per adipocyte between sham and Day 14 sepsis recovery tissue (Mann-Whitney).
i. Representative images of rpWAT stained with TMRM demonstrating the peri-lipid droplet distribution of mitochondria within adipocytes.

4.4.1.4 NAD(P)H autofluorescence in rpWAT from sham and sepsis recovery animals

NAD(P)H fluorescence was measured at baseline and after complex IV inhibition to establish a maximally reduced pool (peak fluorescence), and after FCCP to establish a maximally oxidised pool (fluorescence nadir). The mean dynamic range, relative to the baseline measurement, was 0.59 in sham rpWAT and 1.27 in sepsis recovery rpWAT; this was not significantly different ($p=0.1$).

The NAD(P)H pool at baseline was more oxidised in rpWAT from sepsis recovery animals compared to sham (0.29 vs 0.67 of dynamic range, $p=0.03$).

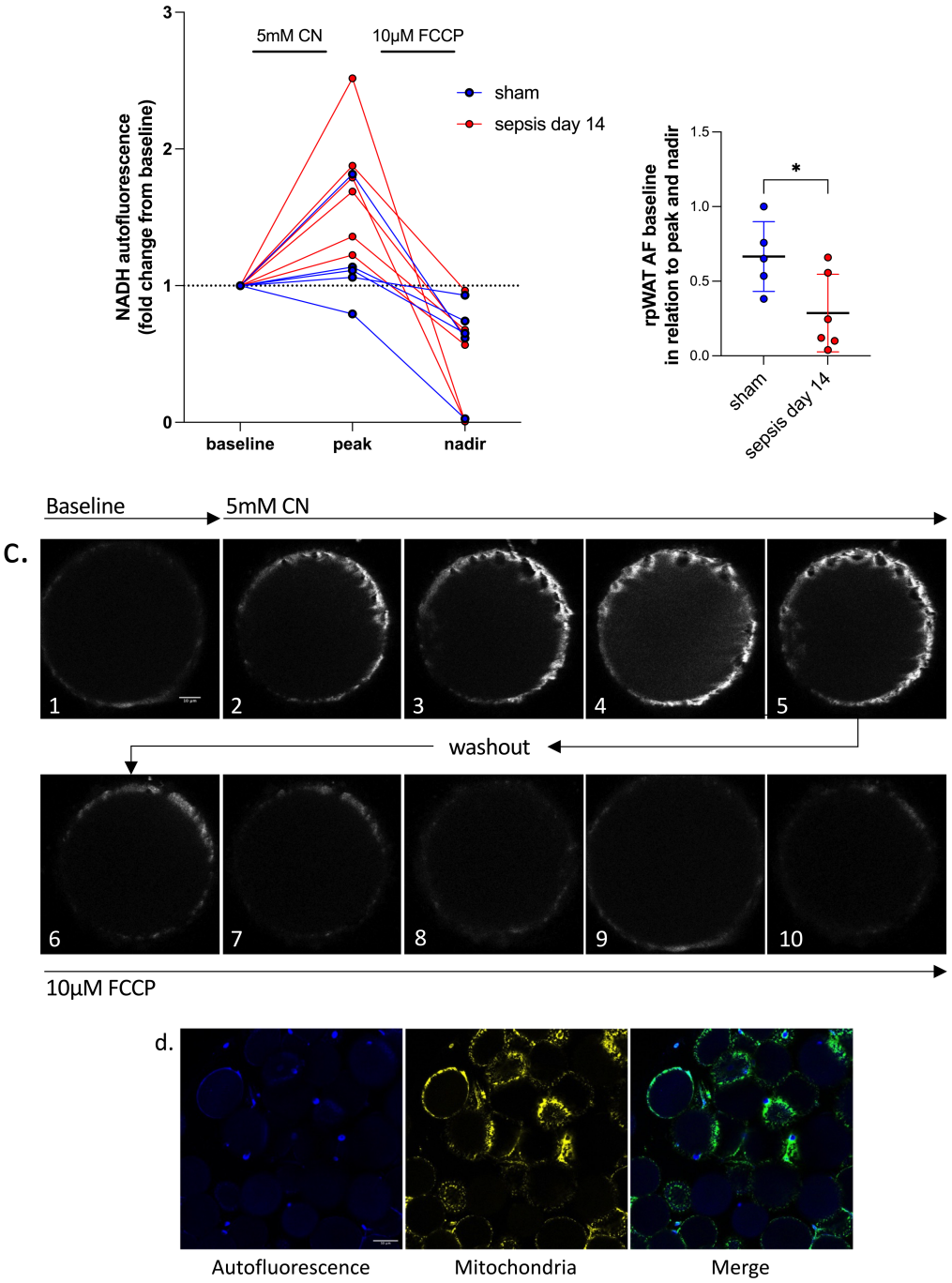

Figure 38. Data and representative multiphoton microscopy images of autofluorescence in rpWAT from sham and day 14 of recovery from sepsis.

a. NAD(P)H autofluorescence at baseline, peak after blockade of complex IV using sodium cyanide, and nadir after chemical depolarisation using FCCP. Values shown as fold change from baseline.

b. NAD(P)H pool in rpWAT from sham and day 14 of recovery from sepsis. Values are calculated as the ratio of the baseline to the range from peak to nadir. The NAD(P)H pool was significantly lower in rpWAT from day 14 of recovery (Student's t-test).

c. Representative image of autofluorescence in one adipocyte at baseline, increasing after maximal reduction of the pool by addition of sodium cyanide and then maximal oxidation of the pool following addition of FCCP.
d. Representative images of adipocytes demonstrating co-localization of autofluorescence (left), mitochondria stained with TMRM (middle) and both channels merged. Note the presence of nuclear staining in the autofluorescence image due to contamination with Hoechst. Nuclear fluorescence was subtracted from quantitative analysis.

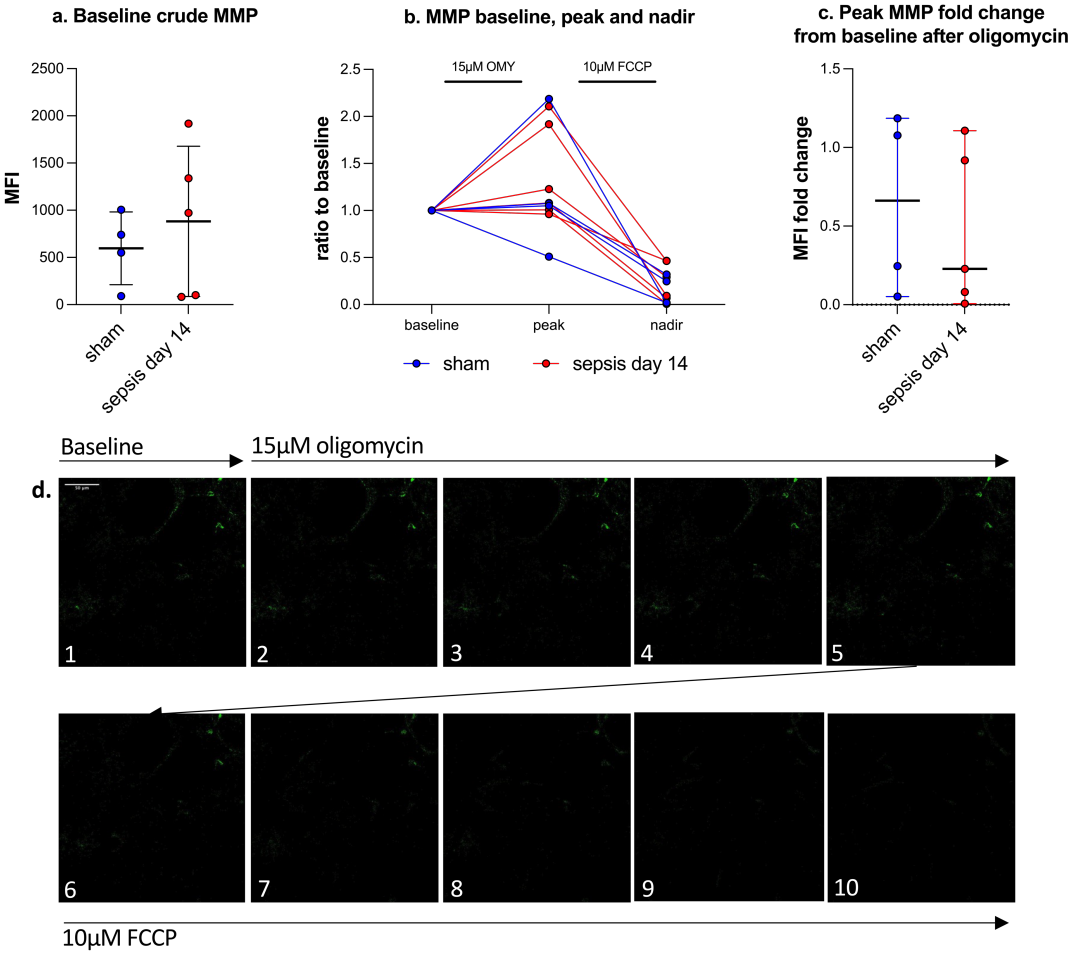

Figure 39. Mitochondrial membrane potential data and representative multiphoton microscopy images of rpWAT from sham and day 14 of sepsis recovery.
a. $\Delta\psi$mt measured by TMRM fluorescence in rpWAT from sham and sepsis recovery animals measured as mean fluorescence intensity of TMRM at baseline.
b. Dynamic measurement of $\Delta\psi$mt measured by TMRM fluorescence in rpWAT at baseline, after inhibition of ATP synthase using oligomycin (omy) and after dissipation of the $\Delta\psi$mt using FCCP.
c. $\Delta\psi$mt fold change measured by TMRM fluorescence following addition of oligomycin. No significant difference was seen between rpWAT from sham and sepsis recovery groups.

d. Representative images of TMRM fluorescence indicating $\Delta\psi$mt in rpWAT at baseline and after addition of oligomycin and FCCP. Images are dim to avoid over-exposure and saturation of fluorescence detection.

4.4.1.5 Static and dynamic $\Delta\psi_{mt}$ measurement in rpWAT from sham and sepsis recovery animals

Baseline $\Delta\psi_{mt}$ did not differ between sham and sepsis recovery groups (Figure 39a). Following the addition of oligomycin to inhibit ATP synthase, the increase in $\Delta\psi_{mt}$ also did not differ between groups, indicting equivalent oxidative phosphorylation coupling.

4.4.2 Results summary

- Lipid droplet volume did not differ significantly between sham and sepsis recovery groups, but trended towards smaller volumes in sepsis recovery rpWAT. This does not support the presence of browning.
- Mitochondrial density was higher in rpWAT from sepsis recovery animals, but the number of mitochondria per adipocyte was not increased. This does not support the presence of browning.
- More nuclei were present per imaging field in rpWAT from sepsis recovery animals, but was not increased when normalised to the number of lipid droplets. This does not support significant infiltration of rpWAT.
- The NAD(P)H pool was more oxidised in rpWAT from sepsis recovery animals compared to sham. This suggests increased metabolic activity in rpWAT from animals at day 14 of recovery from sepsis, compared to control.
- $\Delta\psi_{mt}$ did not differ between sham and sepsis groups at baseline or following inhibition of ATP synthase

4.5 Discussion

The hallmarks of beige adipose tissue indicate its thermogenic intension: expression of UCP1 aka 'thermogenin', expression of UCP-1-independent thermogenic pathways, multi-locular lipid droplets and increased mitochondrial biogenesis and density.[82,165] The studies above aimed to identify morphological and bioenergetic changes consistent with browning of rpWAT in the recovery phase of an experimental model of sepsis in rats. These studies did not demonstrate classical browning.

A cardinal marker of browning is reduced adipocyte volume due to shrinkage of lipid droplets.[166] Shrinkage is caused by lipolysis of triglycerides stored in lipid droplets to provide substate for beta-oxidation.[167] Studies of adipocyte and lipid droplet size in sepsis are inconsistent: murine models of sepsis induced by caecal ligation and puncture found reduced size and multi-loculation of lipid droplets and reduced adipocyte size overall.[106,168] Conversely, many studies in humans report an increase in fat mass, but these are confounded by concomitant lipid-rich parenteral nutrition.

Most studies measure lipid droplet size from immunohistochemistry slides. However, many methods of fixation use solvents that interfere with lipid structure. Despite efforts to circumvent this, when this technique was used, adipocytes frequently 'collapsed', rendering volume measurement unreliable. In this study, MPM imaging was used instead as tissue structure is unaltered and imaging can be performed without a cover slip which can also alter morphology.

The median lipid droplet volume was smaller in rpWAT from animals recovering from sepsis, but did not reach significance compared to sham using non-parametric analysis. The finding is perhaps surprising as fat mass is visibly reduced, and total

animal fat mass was reduced in the same model.[126] The absence of a difference may result from sampling error or result from the singular timepoint as adipocytes may have begun to expand again by this point. Further studies of different timepoints would be needed to reconcile this.

Equivalence of lipid droplet size does not support the presence of browning. This is corroborated by the lack of elevated circulating markers of lipolysis and down-regulation of hormone sensitive lipase and adipose triglyceride lipase mRNA levels at day 14 of sepsis recovery. Multi-loculation of lipid droplets, another hallmark of browning, was also absent. This was evident on visual inspection of lipid droplet architecture and a similar size between sham and sepsis recovery groups. Despite this, the reduction in RER seen on whole body respirometry clearly demonstrates lipolysis, which is known to occur in severe stress states such as sepsis. However, it is important to note that lipolysis and the shrinkage of adipocytes and lipid droplets are not specific to browning.

While lipid droplets may not be statistically significantly different between groups, the median value used for later normalisation of other processes (respiration rates, mitochondrial density, nuclear density) is different and therefore impacts other measurements.

The number of nuclei was used to measure the number of cells to quantify immune infiltration indicated by the RNA sequencing data and for normalisation of other studies including oxygen consumption. The number of nuclei was increased per microscopy field, but when adjusted for the volume of lipid droplets, the number of nuclei was equivalent between sham and septic rpWAT. Thus, MPM did not reveal evidence of a significant increase in the number of cells consistent with immune infiltration. This may result from sampling differences between tissue used for RNA-

seq and MPM studies, however all other conditions were consistent, supporting the validity of the finding. Notably, nuclear staining does not differentiate between types of immune cell, so while numbers may be equivalent, the infiltrate may contain different proportions of cells, as reported in single cell RNA sequencing studies of adipose tissue in sepsis.[86]

The same effect was seen for mitochondrial density. Density increased per microscopic field as more adipocytes were visualised per field. However, when normalised for the reduced lipid droplet volume, the number of mitochondria per adipocyte was equivalent between groups. This does not support the presence of browning which involves increased mitochondrial biogenesis.

The increased cell and mitochondrial number per imaging field indicates that more mitochondria will have been present in the tissue used for respirometry. This explains why differences in OCR between groups are lost when normalised to cell and mitochondrial number, as seen in Chapter 3.

The finding that the NAD(P)H pool was more oxidised in rpWAT from day 14 of sepsis recovery could support an increased metabolic rate in this group. However, this is a crude measurement that may reflect individual or combined factors. A reduction in the NADH pool may result from increased electron donation into complex I as a result of increased oxidation. This would be consistent with the increased oxygen consumption seen during respirometry. However, it is not clear if the proton gradient generated is then coupled to phosphorylation for downstream processes (including ATP-dependent thermogenesis), uncoupled and dissipated as heat, or results in increased superoxide production. No uncoupling proteins were found in rpWAT from sepsis recovery animals, however the increase in SERCA2 levels, an ATP-dependent thermogenic pathway, could explain the oxidised state.

Similarly, oxygen species were not measured. A rise in ROS could also produce similar findings and, in turn, result in a smaller reduced NAD(P)H pool and therefore reduced autofluorescence. The true meaning of a reduced NADH pool can also only be interpreted in the context of measurement of TCA cycle flux and substrates required for NADH production, as a reduction may be due to decreased synthesis and not just increased use. The finding could support increased metabolism, however quantification of $FADH_2$ or NADPH by fluorescence lifetime imaging is required for more specific understanding.

Isolated and dynamic measurements of $\Delta\psi_{mt}$ between groups revealed no differences in crude $\Delta\psi_{mt}$ or the proportion of $\Delta\psi_{mt}$ contributing to phosphorylation. The data displayed wide variability between samples raising questions about validity and comparability. On addition of oligomycin to inhibit ATP synthase the impact was highly variable ranging from minimal to a doubling of $\Delta\psi_{mt}$ in both groups. Most studies reports a more modest increase in $\Delta\psi_{mt}$ of 20-30% following addition of oligomycin, indicating this may be spurious. Regardless, no differences were seen between the groups indicating an equivalent coupling efficiency and the absence of increased uncoupled thermogenesis.

4.5.1 Conclusion

Retroperitoneal adipose tissue at day 14 of recovery from zymosan peritonitis does not develop classical browning. It does however show a more oxidised NAD(P)H pool in the context of increased SERCA2 expression, consistent with increased calcium cycling within adipocytes in this model of sepsis-induced cachexia.

Chapter 5. Discussion

Sepsis remains a significant cause of mortality and continues to impact the physical and psychological health and quality of life of survivors.[169] The foremost issues in the recovery phase are cachexia and muscle weakness. These impair recovery and are associated with increased long-term mortality. No specific treatment exists to reverse these complications. Minimisation of risk factors while still in acute care is often challenging and involves multiple risk-benefit analyses that are often difficult for the treating clinician to appreciate. This study attempts to identify a cause of sepsis-induced myopathy in order to identify novel therapeutic targets.

Zymosan peritonitis administered to rats is an appropriate model against which comparison can be drawn to human sepsis and recovery. While a sterile insult, zymosan is an agonist of many pattern recognition receptors activated in infectious sepsis and caused a severe inflammatory syndrome that is far more prolonged than a bacterial peritonitis insult. The rats had a two-week mortality rate of 17%; this is of a similar order to human sepsis and demonstrates the presence of organ failure which is required for the diagnosis of sepsis.[10] As a model for studying the recovery phase of sepsis, the animals developed hypermetabolism and displayed both cachexia and a critical illness myopathy consistent with that seen in humans.[27]

5.1 Classical browning is not present at 14 days after zymosan peritonitis

My primary hypothesis was that thermogenic mechanisms are expressed in adipose tissue in the recovery phase of sepsis due to browning. Classical markers of browning were not found in this model. The canonical marker of browning is expression of UCP1 protein in white adipose tissue deposits. After exhaustive efforts

to optimise immunoblot methods, UCP1 could not be demonstrated in either eWAT or rpWAT at 14 days after sepsis. Other classical markers of browning, including increased mitochondrial density and multiloculation of lipid droplets, were also absent.[82] Expression of a thermogenic program requires a field change in the transcriptome and this too was comprehensively absent at day 14 post-sepsis. Thermogenic, oxidative and mitochondrial machinery pathways were near-ubiquitously downregulated. The findings may reflect the absence of a thermogenic program, or may result from the time samples were taken. Browning is known to reverse in the absence of stimulation.[97] However, UCP1 and other thermogenic mechanisms were absent at earlier timepoints, arguing against the presence of browning before or at 14 days. While browning may occur after 14 days, as seen in burn injury where UCP1 expression increases to 30 days, hypermetabolism, cachexia and myopathy were all present at 14 days.[83] Accordingly, browning cannot be implicated as causative of the hypermetabolism and cachexia demonstrated in this model.

Whole organism respirometry of days 0-14 after septic insult showed a hypometabolic acute phase (decrease in VO_2) and a hypermetabolic phase (increase in VO_2) at days 11-14. Prolongation of the study to understand the trajectory of the hypermetabolic phase is an important future direction. While rat sepsis does not mimic human sepsis in the initial phase as it becomes hypometabolic rather than hyper-metabolic (or inappropriately normo-metabolic compared to health), the presence of hypermetabolism in the recovery phase does reflect the human recovery profile.

To my knowledge, this is the first study to measure functional markers of browning in WAT in sepsis using respirometry. In keeping with the literature, initial respirometry studies were normalised to tissue mass.[170] Per milligram of tissue, both

eWAT and rpWAT were hypermetabolic during sepsis recovery. However, when the impact of adipocyte shrinkage was controlled for, by measurements of lipid droplet size, protein content and number of mitochondria, the increase in metabolic rate was abolished. The same was the case when the impact of immune cell infiltration was accounted for by normalisation to the number of nuclei. These data conflict with a hypermetabolic phenotype in eWAT and/or rpWAT during the recovery phase, and also support an absence of browning. This finding was corroborated by direct visualisation of adipose tissue thermogenesis using thermal imaging, which did not demonstrate increased heat production in animals recovering from sepsis.

5.2 During recovery from sepsis rpWAT shows altered metabolism and expresses mediator of calcium cycling, SERCA2

Despite the absence of classical browning, alterations in whole-body and adipose tissue metabolism were identified. Activation of lipolysis was evident by the fall in respiratory exchange ratio seen in in the first week post-insult and the trend towards reduced lipid droplet size (albeit non-significant) during recovery from sepsis. Lipolysis is an intrinsic aspect of browning, but also occurs independently to release free fatty acids in times of stress; this phenomenon is well described in sepsis and inflammation.[94]

Two findings demonstrated novel insights into adipose tissue metabolism in the recovery phase of sepsis – the increased expression of SERCA2 and oxidation of the NAD(P)H pool at day 14 after the septic insult.

Explanted rpWAT demonstrated a more oxidised NAD(P)H pool at day 14 of recovery from sepsis, compared to sham rpWAT. The NAD(P)H pool consists of the NAD^+/H and $NADP^+$/H pools that are indistinguishable without imaging by FLIM.

Oxidation (and reduction in autofluorescence) can represent increased oxidation of NADH due to increased respiration, increased oxidation of NADPH by oxidising species, or reduced production of either. With the current data it is not possible to discern which processes are responsible. While tempting to conclude it is due to increased ATP-dependent thermogenesis through SERCA2, this is less likely as the expression of mRNA of other related proteins in the calcium cycling pathway were down-regulated and there was no increase in rpWAT oxygen consumption to indicate increased thermogenesis. Oxidation of the pool may therefore represent increased oxidative stress which is also well recognised in inflammatory states.[171] Further study is necessary to understand the role of adipose tissue inflammation and oxidative stress in sepsis.

SERCA2 is a recognised component of ATP-dependent thermogenic mechanisms in brown and beige adipose tissue. Demonstration of SERCA2 expression in adipose tissue in the recovery phase of sepsis is – to my knowledge - novel.

5.3 Expression of SERCA2 in adipose tissue in the recovery phase of sepsis

Both mRNA and protein expression of SERCA2 were elevated at day 14 of sepsis recovery. SERCA2 is a highly conserved protein involved in calcium transport and maintenance of endoplasmic reticulum calcium gradients, as well as thermogenic mechanisms.[59] Its role is best described in the sarcoplasmic reticulum of skeletal and cardiac muscle but is expressed across other cell types within the endoplasmic reticulum, including white adipose tissue. As discussed in the introduction chapter, SERCA-mediated calcium cycling is used for non-shivering thermogenesis in skeletal muscle and BAT in mammals to maintain body temperature, and is reported in beige adipocytes in mice exposed to cold stress.[172] To my knowledge, this is the

first study to describe increased SERCA2 expression in adipose tissue in a model of sepsis.

The predominant isoform reported in beige adipose tissue is SERCA2, as found in this study. The primary role of SERCA2 in humans is in regulating cardiac and skeletal muscle contractility; its role in thermogenesis in humans remains to be established, but is intrinsic to facultative thermogenesis in mouse models.[59] Mutations of SERCA2 are extremely rare. Homozygous missense deletions of SERCA2 in humans results in a keratinising skin disease, but cardiac function remains normal. Deletion of both copies is universally fatal across species.[173,174]

SERCA2-mediated cycling generates heat through two mechanisms. The first is a simple calcium cycle where it transports calcium directly back into the ER following release through the ryanodine receptor and IP3 calcium channel. This requires ATP hydrolysis and therefore releases heat. The second process involves 'regulins' such as sarcolipin that uncouple hydrolysis of ATP from calcium transport. This results in increased cytosolic calcium which can modulate cellular function, including increasing mitochondrial calcium flux and oxidative phosphorylation.[58] Identification of regulins and microscopy of intracellular calcium flux could further identify whether one or both mechanisms are activated. Alterations in intracellular calcium flux may have non-thermogenic implications. Calcium is involved in myriad cellular functions including insulin resistance and hyperglycaemia which also occurs in sepsis. SERCA-mediated calcium cycling is also implicated in immunity and endoreticular stress. These dictate cell fate and may signal a role for adipose tissue behaviour in sepsis. Future studies to delineate the role of calcium in adipose tissue are warranted.[59,173]

The presence of SERCA2 in rpWAT of rats at day 14 of recovery from sepsis is intriguing. It may represent a UCP1-independent thermogenic mechanism

expressed in adipose tissue. However, there were no other indicators of thermogenesis to support this, and most other genes in the SERCA2 thermogenic pathway were down-regulated. It may also result from immune cell infiltration, although immune cell SERCA expression is low, and there was no evidence of increased cell numbers in septic tissue compared to control. Further studies are required to ascertain its cellular origin in the adipose tissue studied and its role in adipose tissue in the recovery phase of sepsis.

Importantly, the above results must be interpreted as representing bulk tissue. Adipose tissue consists of multiple cell types that change in proportion and behaviour during sepsis.[86] The transcriptomic data clearly showed a broad increase in genes related to inflammation. This may represent immune infiltration, activation and proliferation of resident immune cells or adipocyte immune expression. Comparison between different adipose tissue cell populations and activation states means that only tentative conclusions can be drawn about specific processes, such as thermogenesis, as heterogeneity between cell types has not been accounted for. While specific adipocyte phenotype changes are obscured by cell heterogeneity, it is clear that adipose tissue as a whole does not take on a gross thermogenic phenotype, at least in this model.

5.4 Thermogenic activation of white adipose tissue in zymosan peritonitis is unlikely to explain myopathy

The second aspect of my hypothesis was that hypermetabolism induced by browning drives skeletal muscle wasting to release substrates for further hypermetabolism. In patients with burn injury, hypermetabolism is profound and long lasting.[6] In this model, hypermetabolism was evident from days 12-14 and may persist for longer. Expression of SERCA2 was only three times that of sham rpWAT,

and multiple orders below that of skeletal muscle controls. Furthermore, there was no evidence of thermogenesis in WAT at the times studied, therefore the hypermetabolism must be generated from elsewhere. In addition, the transcriptomic data indicate little supportive machinery to drive high metabolic rates. In a study of mice exposed to prolonged cold stress (4-6 weeks at 4°C) inguinal WAT showed intensive classical browning. [136] However it remained less thermogenic than BAT from normally housed animals, indicating very marked thermogenic activation would need to occur to drive hypermetabolism.

If indeed the hypermetabolic phase demonstrated at days 11-14 in animals recovering from sepsis is due to thermogenesis, it may be driven by existing non-shivering thermogenic machinery in existing thermogenic organs – BAT and skeletal muscle. The study of these tissues and their thermogenic properties would make an interesting focus for future studies.

5.5 Why might browning be present in burn injury and cancer-associated cachexia, but not sepsis?

Browning has been demonstrated in patients with burn injury and cancer-associated cachexia, which are in part similar but do differ from sepsis. Studies of burn injury include patients and animals with 30-60% total body surface area burns, a much more severe and prolonged stress than that seen in sepsis.[98] Sepsis is also a frequent complication of burn injury and may contribute to further browning.[148] Importantly, thermostatic control is lost following burn injury due to loss of skin, hair and fluid which may lead to prolonged cold stress which is a classic driver of browning. Although patients were reported to be cared for in a thermoneutral environment (33°C) in the seminal studies, it is plausible the heat loss caused a persistent adrenergic stress, driving browning.[83]

Cancer-associated cachexia is often studied in those with advanced and pre-terminal disease, indicating a protracted illness, large tumour burden and persistent inflammatory state.[82]

Sepsis on the other hand, including the model studied, is more heterogeneous and may not be as severe or prolonged as burn injury or cancer-associated cachexia. It may be the case that animals with a severe enough insult to drive browning do not survive the acute phase. Browning may require a more protracted and severe insult than is possible to recover from if driven by sepsis.

5.6 Factors in human sepsis which may influence the presence of browning

The management of humans with sepsis is complex, heterogeneous and involves many factors that influence both metabolism, adipose tissue and myopathy.[175] The use of catecholamines to manage cardiovascular failure is foremost. Noradrenaline and adrenaline are frequently used to manage hypotension in humans with sepsis, and both have been shown to induce browning of white adipose tissue in animal models.[89] Humans frequently receive one or more supra-physiological doses of intravenous catecholamines (up to 1 μg/kg/min or even higher); this will induce lipolysis, alter immune cell function and elevate metabolism.[176] It is plausible that the addition of high doses of catecholamines in humans drives browning, which is not seen in the animal model studied.

Patients also frequently receive medications known to exacerbate critical illness myopathy, including neuromuscular blocking drugs (rocuronium, atracurium) and corticosteroids (dexamethasone, hydrocortisone). These were not used in the model and may cause a more severe recovery phenotype than that driven by sepsis alone.

As management of sepsis improves (or iatrogenic harm decreases), more patients survive the acute phase of illness. However, sepsis is followed by a profound immunoparesis resulting in repeated bouts of infections and sepsis. These serve to worsen critical illness myopathy and delay the recovery phase.[177] Again, this was not reflected in this model which used a single insult.

5.7 Cachexia as a multi-system disease

Cachexia is increasingly recognised as a multi-system disorder.[32] In the absence of browning, it may still be responsible in large part for the post-sepsis syndrome of bio-psycho-social morbidity, as it affects almost all body systems.

Cachexia is associated with many diseases beyond sepsis, but is best understood in patients with cancer in whom it occurs in up to 80% of patients, and is the cause of death in 20-25%.[31] The cancer literature indicates multiple roles for adipose tissue in the pathology of cachexia independent of thermogenesis. In patients with pancreatic cancer, loss of adipose tissue alone correlates with poor survival.[178] Lipolysis itself has been shown to be the instigator of muscle breakdown – in mice injected with colon or lung cancer, knockout of lipases prevented muscle loss.[100] Excessive oxidation of free fatty acids in muscle is an early propagator of muscle breakdown, indicating a chronology of adipose and muscle wasting.[32] This is reflected in the early drop in respiratory quotient (indicating lipolysis) and myopathy seen in this study.

Patients with cachexia frequently die of cardiac and respiratory failure; heart weight is found to be reduced in patients with cachexia.[32] Cardiomyopathy occurs in much the same way as a skeletal myopathy, with protein ubiquitination and disordered

autophagy.[32] Endocrine and metabolic dysfunction are characterised by insulin resistance and hepatic steatosis while gastro-intestinal barrier dysfunction leads to anorexia and endotoxaemia.[31] Cachexia and cancer are strongly associated with depression and anxiety, which may also result from ongoing immunometabolic disturbances as well as being circumstantial.[31,32]

Recent studies have identified Growth/Differentiation Factor 15 (GDF15) as a circulating mediator of cachexia and potential therapeutic target in a large study of patients with lung cancer.[179] Interestingly, *gdf15* mRNA was elevated 3 fold in rpWAT in this study.

As with cancer, cachexia in survivors of sepsis should be studied and understood as a multi-system disease which contributes to all aspects of the post-intensive care syndrome, further supporting the need for increased understanding. The production of circulating factors associated with cachexia, such as GDF15, requires further investigation in survivors of sepsis.

5.8 Limitations of the study

While the model is appropriate, limitations of the study must be recognised which preclude firm conclusions and extrapolation of results to humans.

The model reflects human sepsis recovery in many aspects but not in others. The insult was not a true infection and the study period did not extend as long as in human survivors. As discussed, other aspects of human sepsis that may impact upon adipose tissue and browning but were not reflected in the model include the use of catecholamines, multimorbidity and multiple and prolonged septic episodes that will significantly increase the stress response.

The rats were healthy and did not suffer from co-morbid conditions that are directly related to adipose tissue and metabolism, such as obesity, metabolic syndrome and type 2 diabetes. Most humans with sepsis are adults who have stopped growing however the model utilised healthy rats of juvenile adult age that are still growing. This has implications for metabolic rate, measurement of body mass and the development of cachexia. Rats typically do not stop growing until 8-9 months, but purchasing of rats at this age would be prohibitively expensive.

As discussed in section 5.1, the metabolic response of rodents to sepsis differs to humans. Rodents develop a hypometabolic phase, whilst humans become either hypermetabolic or 'abnormally normometabolic' due to tissue dysoxia in the most severe cases.[62,64] This is a marked limitation recognised in the use of animal models for the study of inflammation and sepsis. Extensive work by our group has demonstrated rats show a metabolic picture more similar to human sepsis than mice, however, this limitation must be recognised when interpreting and extrapolating data to humans.[81]

Most humans with sepsis are older and often have an element of sarcopenia. This provides a worse baseline state upon which critical illness myopathy and cachexia will develop.[27] This was not the case in healthy rats of juvenile adult age, which may result in a different phenotype of myopathy.[180]

Only male Wistar rats were utilised in this study. Sex-related differences impact upon metabolism and are known to influence adipose tissue type and distribution as well as affecting sepsis outcomes, at least before the menopause.[180,181]

Sham control animals were not pair-fed to control for the reduced food intake of septic animals. The changes seen in septic animals could be in part due to starvation. This limitation is mitigated by the reality that feeding is often absent in acute human illness, and early parenteral nutrition exacerbates critical illness myopathy.[30]

This study highlighted the marked influence of inflammation and likely immune infiltration in adipose tissue in sepsis. One patient group profoundly affected by sepsis are immunosuppressed patients, particularly those with haematological malignancies who are frequently pancytopenic.[13] This study is not generalisable to this important group of patients.

Measures of muscle function were not possible due to changes in Home Office rules on animal testing, meaning no practicable functional strength or fatiguability were performed.

5.9 Conclusions

- Zymosan peritonitis causes hypermetabolism, cachexia and myopathy akin to that seen in human survivors of sepsis

- Classical browning of white adipose tissue was not present in rats recovering from experimental sepsis up to 14 days

- SERCA2 expression is increased in rpWAT at 14 days after a sepsis insult, and may alter metabolism in the recovery phase of sepsis.

- In this model, myopathy and cachexia occur in the absence of adipose tissue browning.

5.10 Future directions

Further work on the drivers of critical illness- and sepsis-induced myopathy are warranted in order to identify novel treatments. The increasing size and age of the population, combined with improved care will result in more survivors of sepsis. Improving their long term physical health with improve their quality of life and psychological health.

Further studies are warranted to elucidate the role of SERCA in adipose tissue in sepsis:

- Adipose tissue isolation and single-cell transcriptomics and proteomics to find the cellular source of SERCA2 in adipose tissue.
- Identification of 'regulins' to understand if SERCA2 ATP hydrolysis is coupled or uncoupled to calcium transport.
- Multiphoton microscopy using calcium probes to measure cytosolic calcium fluxes.

- Single cell transcriptomics, proteomics and lipidomics to understand the metabolic and immune phenotype of adipose tissue in sepsis and account for cellular heterogeneity.

- Development of animal models which encompass both sexes, aged animals, multimorbidity (including immunosuppression), therapies received by humans (catecholamines in particular) and multiple septic insults.

- In light of the finding that thermogenic mechanisms are unlikely to drive cachexia in this model of sepsis, study of other forms of adipose-skeletal muscle interaction is warranted. Multiple adipokines, batokines (from BAT) and myokines have been found to influence myopathic processes in stress states, which need to be studied in sepsis.[88]

Ultimately, studies must be performed in patients once important mechanisms have been established in animal models, to confirm their importance and their potential as therapeutic targets.

Reference List

1. Singer, M. *et al.* The Third International Consensus Definitions for Sepsis and Septic Shock (Sepsis-3). *JAMA* **315**, 801–10 (2016).
2. Fazzini, B. *et al.* Physical and psychological impairment in survivors of acute respiratory distress syndrome: a systematic review and meta-analysis. *Br J Anaesth* **129**, 801–814 (2022).
3. Margaret S. Herridge, M. D. M. P. H. *et al.* One-Year Outcomes in Survivors of the Acute Respiratory Distress Syndrome Margaret. *New England Journal of Medicine* **348**, 683–693 (2003).
4. Patsouris, D. *et al.* Burn Induces Browning of the Subcutaneous White Adipose Tissue in Mice and Humans. *Cell Rep* **13**, 1538–1544 (2015).
5. Porter, C. *et al.* Uncoupled skeletal muscle mitochondria contribute to hypermetabolism in severely burned adults. *Am J Physiol Endocrinol Metab* **307**, 462–467 (2014).
6. Porter, C. *et al.* The metabolic stress response to burn trauma: current understanding and therapies. *The Lancet* **388**, 1417–1426 (2016).
7. Rumbus, Z. *et al.* Fever Is Associated with Reduced , Hypothermia with Increased Mortality in Septic Patients : A Meta-Analysis of Clinical Trials. 1–15 (2017) doi:10.1371/journal.pone.0170152.
8. Parillo, J. E. & Kumar, A. *Historical aspects of critical illness and critical care medicine*. (Saunders, 2009).
9. Tidswell, R., Inada-Kim, M. & Singer, M. Sepsis: the importance of an accurate final diagnosis. *Lancet Respir Med* **2016**, 1–2 (2020).
10. Shankar-Hari, M., Harrison, D. A., Rubenfeld, G. D. & Rowan, K. Epidemiology of sepsis and septic shock in critical care units: Comparison between sepsis-2 and sepsis-3 populations using a national critical care database. *Br J Anaesth* **119**, 626–636 (2017).

11. Stanzani, G., Tidswell, R. & Singer, M. Do critical care patients hibernate? Theoretical support for less is more. *Intensive Care Med* **46**, 495–497 (2020).
12. Singer, M., Inada-Kim, M. & Shankar-Hari, M. Sepsis hysteria: excess hype and unrealistic expectations. *The Lancet* **394**, 1513–1514 (2019).
13. Tidswell, R. & Singer, M. Sepsis - Thoughtful management for the non-expert. *Clinical Medicine, Journal of the Royal College of Physicians of London* **18**, (2018).
14. Kaukonen, K. M., Bailey, M., Suzuki, S., Pilcher, D. & Bellomo, R. Mortality related to severe sepsis and septic shock among critically ill patients in Australia and New Zealand, 2000-2012. *JAMA* **311**, 1308–1316 (2014).
15. Shankar-Hari, M., Harrison, D. A. & Rowan, K. M. Differences in Impact of Definitional Elements on Mortality Precludes International Comparisons of Sepsis Epidemiology-A Cohort Study Illustrating the Need for Standardized Reporting. *Crit Care Med* **44**, 2223–2230 (2016).
16. Shubin, N. J., Monaghan, F. & Ayala, A. Anti- Inflammatory Mechanisms of Sepsis. **17**, 108–124 (2011).
17. Singer, M. & Brealey, D. Mitochondrial dysfunction in sepsis. *Biochem Soc Symp* **66**, 149–166 (1999).
18. Brealey, D. *et al.* Association between mitochondrial dysfunction and severity and outcome of septic shock. *Lancet* (2002) doi:10.1016/S0140-6736(02)09459-X.
19. Hotchkiss, R. S. *et al.* Apoptotic cell death in patients with sepsis, shock, and multiple organ dysfunction. *Crit Care Med* **27**, 1230–51 (1999).
20. Singer, M. The role of mitochondrial dysfunction in sepsis-induced multi-organ failure. *Virulence* **5**, 66–72 (2014).
21. Carré, J. E. *et al.* Survival in critical illness is associated with early activation of mitochondrial biogenesis. *Am J Respir Crit Care Med* **182**, 745–751 (2010).

22. Vanhorebeek, I., Latronico, N. & Van den Berghe, G. ICU-acquired weakness. *Intensive Care Med* **46**, 637–653 (2020).
23. Jukka Takala, M.D., Ph. D. *et al.* Increased Mortality Associated with Growth Hormone Treatment in Critically Ill Adults. *New England Journal of Medicine* 785–792 (1999).
24. Preau, S. *et al.* Protein recycling and limb muscle recovery after critical illness in slow- and fast-twitch limb muscle. *Am J Physiol Regul Integr Comp Physiol* **316**, R584–R593 (2019).
25. Puthucheary, Z. A. *et al.* Metabolic phenotype of skeletal muscle in early critical illness. *Thorax* **73**, 926–935 (2018).
26. Dos Santos, C. *et al.* Mechanisms of chronic muscle wasting and dysfunction after an intensive care unit stay: A pilot study. *Am J Respir Crit Care Med* **194**, 821–830 (2016).
27. Lad, H. *et al.* Intensive care unit-acquired weakness: Not just another muscle atrophying condition. *Int J Mol Sci* **21**, 1–30 (2020).
28. Wollersheim, T. *et al.* Dynamics of myosin degradation in intensive care unit-acquired weakness during severe critical illness. *Intensive Care Med* **40**, 528–539 (2014).
29. Bierbrauer, J. *et al.* Early type II fiber atrophy in intensive care unit patients with nonexcitable muscle membrane. *Crit Care Med* **40**, 647–650 (2012).
30. Hermans, G. *et al.* Effect of tolerating macronutrient deficit on the development of intensive-care unit acquired weakness: A subanalysis of the EPaNIC trial. *Lancet Respir Med* **1**, 621–629 (2013).
31. Porporato, P. Understanding cachexia as a cancer metabolism syndrome. *Oncogenesis* **5**, (2016).
32. Ferrara, M., Samaden, M., Ruggieri, E. & Vénéreau, E. Cancer cachexia as a multiorgan failure: Reconstruction of the crime scene. *Front Cell Dev Biol* **10**, 1–17 (2022).

33. Small, P. M., Täuber, M. G., Hackbarth, C. J. & Sande, M. A. Influence of body temperature on bacterial growth rates in experimental pneumococcal meningitis in rabbits. *Infect Immun* **52**, 484–7 (1986).
34. Mackowiak, P. A., Chervenak, F. A. & Grünebaum, A. Defining Fever. *Open Forum Infect Dis* **8**, (2021).
35. Rhodes, A. *et al.* Surviving Sepsis Campaign: International Guidelines for Management of Sepsis and Septic Shock: 2016. *Intensive Care Med* **43**, 304–377 (2017).
36. Drewry, A. M. *et al.* Antipyretic Therapy in Critically Ill Septic Patients: A Systematic Review and Meta-analysis. *Crit Care Med* **45**, 806–813 (2017).
37. Egi, M. *et al.* The Japanese Clinical Practice Guidelines for Management of Sepsis and Septic Shock 2020 (J-SSCG 2020). *J Intensive Care* **9**, 1–144 (2021).
38. Drewry, Anne M. Mohr, Nicholas. Ablordeeppey, Enyo. Hotchkiss, R. Therapeutic Hyperthermia Is Associated With Improved Survival in Afebrile Critically Ill Patients With Sepsis: A Pilot Randomized Trial. (2022) doi:10.1097/CCM.0000000000005470.
39. Itenov, T. S. *et al.* Induced hypothermia in patients with septic shock and respiratory failure (CASS): a randomised, controlled, open-label trial. *Lancet Respir Med* **6**, 183–192 (2018).
40. Mourvillier, B. *et al.* Induced Hypothermia in Severe Bacterial Meningitis. *JAMA* **310**, 2174 (2013).
41. Rohm, M., Zeigerer, A., Machado, J. & Herzig, S. Energy metabolism in cachexia. *EMBO Rep* **20**, 1–13 (2019).
42. Porporato, P. Understanding cachexia as a cancer metabolism syndrome. *Oncogenesis* **5**, (2016).
43. Hamada, Y. & Hayashi, N. Chewing increases postprandial diet-induced thermogenesis. *Sci Rep* **11**, 1–7 (2021).

44. Rolfe, D. F. & Brown, G. C. Cellular energy utilization and molecular origin of standard metabolic rate in mammals. *Physiol Rev* **77**, (1997).
45. Cannon, B. & Nedergaard, J. Brown Adipose Tissue: Function and Physiological Significance. *Physiol Rev* **84**, 277–359 (2004).
46. Silva, J. E. Thermogenic mechanisms and their hormonal regulation. *Physiol Rev* **86**, 435–464 (2006).
47. Maloney, S. K., Fuller, A., Mitchell, D., Gordon, C. & Michael Overton, J. Translating animal model research: Does it matter that our rodents are cold? *Physiology* **29**, 413–420 (2014).
48. Bal, N. C. *et al.* Sarcolipin is a newly identified regulator of muscle-based thermogenesis in mammals. *Nat Med* (2012) doi:10.1038/nm.2897.
49. Jastroch, M., Divakaruni, A. S., Mookerjee, S., Treberg, J. R. & Brand, M. D. Mitochondrial proton and electron leaks. *Essays Biochem* **47**, 53–67 (2010).
50. Pohl, E. E., Rupprecht, A., Macher, G. & Hilse, K. E. Important trends in UCP3 investigation. *Front Physiol* **10**, 1–16 (2019).
51. GOLOZOUBOVA, V. *et al.* Only UCP1 can mediate adaptive nonshivering thermogenesis in the cold. *The FASEB Journal* **15**, 2048–2050 (2001).
52. Mills, E. M., Banks, M. L., Sprague, J. E. & Finkel, T. Pharmacology: Uncoupling the agony from ecstasy. *Nature* (2003) doi:10.1038/426403a.
53. Jezek, P., Garlid, K. D. & Jabu, M. Mitochondrial Uncoupling Proteins : Subtle Regulators of Cellular Redox Signaling. **29**, (2018).
54. Parker, N., Crichton, P. G., Vidal-Puig, A. J. & Brand, M. D. Uncoupling protein-1 (UCP1) contributes to the basal proton conductance of brown adipose tissue mitochondria. *J Bioenerg Biomembr* **41**, 335–342 (2009).
55. Cypess, A. M. *et al.* Identification and Importance of Brown Adipose Tissue in Adult Humans. *New England Journal of Medicine* **360**, 1509–1517 (2009).
56. Leitner, B. P. *et al.* Mapping of human brown adipose tissue in lean and obese young men. *Proc Natl Acad Sci U S A* **114**, 8649–8654 (2017).

57. Roesler, A. UCP1-independent thermogenesis. 709–725 (2020).
58. Pant, M., Bal, N. C. & Periasamy, M. Sarcolipin: A Key Thermogenic and Metabolic Regulator in Skeletal Muscle. *Trends in Endocrinology and Metabolism* Preprint at https://doi.org/10.1016/j.tem.2016.08.006 (2016).
59. Periasamy, M. *et al.* Role of SERCA Pump in Muscle Thermogenesis and Metabolism. *Compr Physiol* **7**, 879–890 (2017).
60. Trenker, M., Malli, R., Fertschai, I., Levak-Frank, S. & Graier, W. F. Uncoupling proteins 2 and 3 are fundamental for mitochondrial Ca2+ uniport. *Nat Cell Biol* **9**, 445–452 (2007).
61. Wu, C. *et al.* Hypermetabolism in the Initial Phase of Intensive Care Is Related to a Poor Outcome in Severe Sepsis Patients. *Ann Nutr Metab* **66**, 188–95 (2015).
62. Kreymann, G. *et al.* Oxygen consumption and resting metabolic rate in sepsis, sepsis syndrome, and septic shock. *Critical care medicine* vol. 21 1012–1019 Preprint at https://doi.org/10.1097/00003246-199307000-00015 (1993).
63. Zauner, C., Schuster, B. I., Schneeweiss, B., Lennon, E. & Seidner, D. Similar metabolic responses to standardized total parenteral nutrition of septic and nonseptic critically III patients. *Nutrition in Clinical Practice* **17**, 43–44 (2002).
64. Coss-Bu, J. A. *et al.* Resting energy expenditure and nitrogen balance in critically ill pediatric patients on mechanical ventilation. *Nutrition* **14**, 649–652 (1998).
65. Uehara, M., Plank, L. D. & Hill, G. L. Components of energy expenditure in patients with severe sepsis and major trauma: a basis for clinical care. *Crit Care Med* **27**, 1295–302. (1999).
66. Henning, D. J. *et al.* The Absence of Fever Is Associated With Higher Mortality and Decreased Antibiotic and IV Fluid Administration in Emergency Department Patients With Suspected Septic Shock. *Crit Care Med* **45**, e575–e582 (2017).

67. Sundén-Cullberg, J. *et al.* Fever in the Emergency Department Predicts Survival of Patients With Severe Sepsis and Septic Shock Admitted to the ICU*. *Crit Care Med* **45**, 591–599 (2017).

68. Mackowiak, P. A., Marling-Cason, M. & Cohen, R. L. Effects of temperature on antimicrobial susceptibility of bacteria. *J Infect Dis* **145**, 550–3 (1982).

69. Ozveri, E. S. *et al.* The effect of hyperthermic preconditioning on the immune system in rat peritonitis. *Intensive Care Med* **25**, 1155–9 (1999).

70. Tardo-Dino, P. E. *et al.* The effect of a physiological increase in temperature on mitochondrial fatty acid oxidation in rat myofibers. *J Appl Physiol* **127**, 312–319 (2019).

71. Kluger, M., Ringler, D. & Anver, M. Fever and survival. *Science (1979)* **188**, (1975).

72. Roth, J. & Blatteis, C. M. Mechanisms of fever production and lysis: Lessons from experimental LPS fever. *Compr Physiol* **4**, 1563–1604 (2014).

73. Blatteis, C. M. Effect of propranolol on endotoxin induced pyrogenesis in newborn and adult guinea pigs. *J Appl Physiol* **40**, 35–39 (1976).

74. Okamatsu-Ogura, Y., Kitao, N., Kimura, K. & Saito, M. Brown fat UCP1 is not involved in the febrile and thermogenic responses to IL-1β in mice. *Am J Physiol Endocrinol Metab* **292**, 1135–1139 (2007).

75. Arulkumaran, N. *et al.* Renal tubular cell mitochondrial dysfunction occurs despite preserved renal oxygen delivery in experimental septic acute kidney injury. *Crit Care Med* **46**, e318–e325 (2018).

76. Moon, J. S. *et al.* UCP2-induced fatty acid synthase promotes NLRP3 inflammasome activation during sepsis. *Journal of Clinical Investigation* **125**, 665–680 (2015).

77. Schrauwen, P. & Hesselink, M. UCP2 and UCP3 in muscle controlling body metabolism. *Journal of Experimental Biology* **205**, 2275–2285 (2002).

78. Peng, W. *et al.* UCP2 silencing aggravates mitochondrial dysfunction in astrocytes under septic conditions. *Mol Med Rep* **20**, 4459–4466 (2019).
79. Riley, C. L. *et al.* The complementary and divergent roles of uncoupling proteins 1 and 3 in thermoregulation. *Journal of Physiology* **594**, 7455–7464 (2016).
80. Zolfaghari, P. S. *et al.* Skeletal muscle dysfunction is associated with derangements in mitochondrial bioenergetics (but not UCP3) in a rodent model of sepsis. *Am J Physiol Endocrinol Metab* **308**, E713-25 (2015).
81. Zolfaghari, P. S., Pinto, B. B., Dyson, A. & Singer, M. The metabolic phenotype of rodent sepsis: cause for concern? *Intensive Care Med Exp* **1**, (2013).
82. Petruzzelli, M. *et al.* A switch from white to brown fat increases energy expenditure in cancer-associated cachexia. *Cell Metab* **20**, 433–447 (2014).
83. Sidossis, L. S. *et al.* Browning of Subcutaneous White Adipose Tissue in Humans after Severe Adrenergic Stress. *Cell Metab* **22**, 219–227 (2015).
84. Zwick, R. K., Guerrero-Juarez, C. F., Horsley, V. & Plikus, M. V. Anatomical, Physiological, and Functional Diversity of Adipose Tissue. *Cell Metab* **27**, 68–83 (2018).
85. Pellegrinelli, V. *et al.* Dysregulation of macrophage PEPD in obesity determines adipose tissue fibro-inflammation and insulin resistance. *Nat Metab* **4**, 476–494 (2022).
86. Cho, D. S., Schmitt, R. E., Dasgupta, A., Ducharme, A. M. & Doles, J. D. Single-cell deconstruction of post-sepsis skeletal muscle and adipose tissue microenvironments. *J Cachexia Sarcopenia Muscle* **11**, 1351–1363 (2020).
87. Kong, X. *et al.* Brown Adipose Tissue Controls Skeletal Muscle Function via the Secretion of Myostatin. *Cell Metab* **28**, 631-643.e3 (2018).
88. Kong, X. *et al.* IRF4 is a key thermogenic transcriptional partner of PGC-1**α**. *Cell* **158**, 69–83 (2014).

89. Li, C. *et al.* Obesity protects against sepsis-induced and norepinephrine-induced white adipose tissue browning. *Am J Physiol Endocrinol Metab* **321**, E433–E442 (2021).

90. Kajimura, S., Spiegelman, B. M. & Seale, P. Brown and beige fat: Physiological roles beyond heat- generation. doi:10.1016/j.cmet.2015.09.007.

91. Wu, J. *et al.* Beige adipocytes are a distinct type of thermogenic fat cell in mouse and human. *Cell* **150**, 366–376 (2012).

92. Nguyen, K. D. *et al.* Alternatively activated macrophages produce catecholamines to sustain adaptive thermogenesis. *Nature* **480**, 104–108 (2011).

93. Cardwell, R. J., Birkhahn, R. H., Crist, K. A., Lee, E. M. & Thomford, N. R. Palmitate and stearate kinetics in the rat during sepsis and trauma. *Journal of Surgical Research* **50**, 51–56 (1991).

94. Abdullahi, A. & Jeschke, M. G. White Adipose Tissue Browning: A Double-edged Sword. (2016) doi:10.1016/j.tem.2016.06.006.

95. Xiu, F., Diao, L., Qi, P., Catapano, M. & Jeschke, M. G. Palmitate differentially regulates the polarization of differentiating and differentiated macrophages. *Immunology* **147**, 82–96 (2016).

96. Bartelt, A. & Heeren, J. Adipose tissue browning and metabolic health. *Nat Rev Endocrinol* **10**, 24–36 (2014).

97. Altshuler-Keylin, S. *et al.* Beige Adipocyte Maintenance Is Regulated by Autophagy-Induced Mitochondrial Clearance. *Cell Metab* **24**, 402–419 (2016).

98. Herndon, D. N. *et al.* Long-term propranolol use in severely burned pediatric patients: A randomized controlled study. *Ann Surg* **256**, 402–411 (2012).

99. Abdullahi, A. *et al.* IL-6 SIGNAL FROM THE BONE MARROW IS REQUIRED FOR THE BROWNING OF WHITE ADIPOSE TISSUE POST BURN INJURY. doi:10.1097/SHK.0000000000000749.

100. Das, S. K. *et al.* Adipose triglyceride lipase contributes to cancer-associated cachexia. *Science (1979)* **333**, 233–238 (2011).
101. Goossens, C. *et al.* Adipose tissue protects against sepsis-induced muscle weakness in mice: From lipolysis to ketones. *Crit Care* **23**, 1–17 (2019).
102. Crowell, K. T., Soybel, D. I. & Lang, C. H. Inability to replete white adipose tissue during recovery phase of sepsis is associated with increased autophagy, apoptosis, and proteasome activity.
103. Ayalon, I. *et al.* Sepsis Induces Adipose Tissue Browning in Nonobese Mice But Not in Obese Mice. *SHOCK* **50**, 557–564 (2018).
104. Goossens, C., vander Perre, S., van den Berghe, G. & Langouche, L. Proliferation and differentiation of adipose tissue in prolonged lean and obese critically ill patients. *Intensive Care Med Exp* **5**, (2017).
105. Casaer, M. P. *et al.* Impact of early parenteral nutrition on muscle and adipose tissue compartments during critical Illness. *Crit Care Med* **41**, 2298–2309 (2013).
106. Ayalon, I. *et al.* SEPSIS INDUCES ADIPOSE TISSUE BROWNING IN NONOBESE MICE BUT NOT IN OBESE MICE. **50**, 557–564 (2018).
107. Langouche, L. *et al.* Critical illness induces alternative activation of M2 macrophages in adipose tissue. *Crit Care* **15**, (2011).
108. Marques, M. B. & Langouche, L. Endocrine, metabolic, and morphologic alterations of adipose tissue during critical illness. *Crit Care Med* **41**, 317–325 (2013).
109. Langouche, L. *et al.* Alterations in adipose tissue during critical illness: an adaptive and protective response? *Crit Care* **14**, P591 (2010).
110. Arulkumaran, N., Saeed, S. & Singer, M. Renal inflammation in a rodent model of sepsis and recovery. in *European society of Intensive Care Medicine* (2013).

111. Marques, M. B. & Langouche, L. Endocrine, metabolic, and morphologic alterations of adipose tissue during critical illness. *Crit Care Med* **41**, 317–325 (2013).

112. Ebihara, T. *et al.* Adipocytokine Profile Reveals Resistin Forming a Prognostic-Related Cytokine Network in the Acute Phase of Sepsis. *Shock* **56**, 718–726 (2021).

113. Glass, C. K. & Olefsky, J. M. Inflammation and lipid signaling in the etiology of insulin resistance. *Cell Metab* **15**, 635–645 (2012).

114. Leuwer, M. *et al.* Endotoxaemia leads to major increases in inflammatory adipokine gene expression in white adipose tissue of mice. *Pflugers Arch* **457**, 731–741 (2009).

115. Sell, H., Dietze-Schroeder, D., Kaiser, U. & Eckel, J. Monocyte chemotactic protein-1 is a potential player in the negative cross-talk between adipose tissue and skeletal muscle. *Endocrinology* **147**, 2458–2467 (2006).

116. Olefsky, J. M. & Glass, C. K. *Macrophages, inflammation, and insulin resistance*. *Annual Review of Physiology* vol. 72 (2009).

117. Pepper, D. J. *et al.* Increased body mass index and adjusted mortality in ICU patients with sepsis or septic shock: a systematic review and meta-analysis. (2014) doi:10.1186/s13054-016-1360-z.

118. Wang, S. *et al.* The role of increased body mass index in outcomes of sepsis: A systematic review and meta-analysis. *BMC Anesthesiol* **17**, 1–11 (2017).

119. Goossens, C. *et al.* Premorbid obesity, but not nutrition, prevents critical illness-induced muscle wasting and weakness. *J Cachexia Sarcopenia Muscle* **8**, 89–101 (2017).

120. Lee, J. G. H. *et al.* Survival benefit of a low ratio of visceral to subcutaneous adipose tissue depends on LDL clearance versus production in sepsis. *Crit Care* **22**, 1–9 (2018).

121. Awata, W. M. C. *et al.* Perivascular adipose tissue contributes to lethal sepsis-induced vasoplegia in rats. *Eur J Pharmacol* **863**, 172706 (2019).

122. Jolley, S. E. & Hough, C. L. The authors reply. *Crit Care Med* **45**, e330–e331 (2017).

123. Karampela, I., Christodoulatos, G. S. & Dalamaga, M. The Role of Adipose Tissue and Adipokines in Sepsis: Inflammatory and Metabolic Considerations, and the Obesity Paradox. *Curr Obes Rep* **8**, 434–457 (2019).

124. Jocken, J. W. E. *et al.* Effect of beta-adrenergic stimulation on whole-body and abdominal subcutaneous adipose tissue lipolysis in lean and obese men. *Diabetologia* **51**, 320–327 (2008).

125. Rooyackers, O. E., Saris, W. H. M., Soeters, P. B. & Wagenmakers, A. J. M. Prolonged changes in protein and amino acid metabolism after zymosan treatment in rats. *Clin Sci* **87**, 619–626 (1994).

126. Hill, N. E. *et al.* Detailed characterization of a long-term rodent model of critical illness and recovery. *Crit Care Med* **43**, e84–e96 (2015).

127. Volman, T. J. H., Hendriks, T. & Goris, R. J. A. Zymosan-induced generalized inflammation: Experimental studies into mechanisms leading to multiple organ dysfunction syndrome. *Shock* **23**, 291–297 (2005).

128. Sato, M. *et al.* Direct Binding of Toll-Like Receptor 2 to Zymosan, and Zymosan-Induced NF-κB Activation and TNF-α Secretion Are Down-Regulated by Lung Collectin Surfactant Protein A. *The Journal of Immunology* **171**, (2003).

129. Kelly, B. A. & Carchman, R. A. The relationship between lysosomal enzyme release and protein phosphorylation in human monocytes stimulated by phorbol esters and opsonized zymosan. *Journal of Biological Chemistry* **262**, (1987).

130. Nauseef, W. M., Root, R. K., Malech, H. L. & Newman, S. L. Inhibition of zymosan activation of human neutrophil oxidative metabolism by a mouse monoclonal antibody. *Blood* **62**, (1983).

131. Humes, J. L. *et al.* Evidence for two sources of arachidonic acid for oxidative metabolism by mouse peritoneal macrophages. *Journal of Biological Chemistry* **257**, (1982).

132. Pillemer, L. & Ecker, E. E. ANTICOMPLEMENTARY FACTOR IN FRESH YEAST. *Journal of Biological Chemistry* **137**, (1941).

133. Mainous, M. R., Tso, P., Berg, R. D. & Deitch, E. A. Studies of the Route, Magnitude, and Time Course of Bacterial Translocation in a Model of Systemic Inflammation. *Archives of Surgery* **126**, (1991).

134. Reitman, M. L. Of mice and men – environmental temperature, body temperature, and treatment of obesity. *FEBS Lett* **592**, 2098–2107 (2018).

135. Rudaya, A. Y., Steiner, A. A., Robbins, J. R., Dragic, A. S. & Romanovsky, A. A. Thermoregulatory responses to lipopolysaccharide in the mouse: Dependence on the dose and ambient temperature. *Am J Physiol Regul Integr Comp Physiol* **289**, 1244–1252 (2005).

136. Shabalina, I. G. *et al.* UCP1 in Brite/Beige Adipose Tissue Mitochondria Is Functionally Thermogenic. *Cell Rep* **5**, 1196–1203 (2013).

137. Huet, O. *et al.* Induced mild hypothermia reduces mortality during acute inflammation in rats. *Acta Anaesthesiol Scand* **51**, 1211–1216 (2007).

138. Thomas-Rüddel, D. O. *et al.* Fever and hypothermia represent two populations of sepsis patients and are associated with outside temperature. *Crit Care* **25**, 1–10 (2021).

139. Ganeshan, K. *et al.* Energetic Trade-Offs and Hypometabolic States Promote Disease Tolerance. *Cell* **177**, 399-413.e12 (2019).

140. Rudiger, A. & Singer, M. Mechanisms of sepsis-induced cardiac dysfunction. *Crit Care Med* **35**, 1599–1608 (2007).

141. Dyson, A., Rudiger, A. & Singer, M. Temporal changes in tissue cardiorespiratory function during faecal peritonitis. *Intensive Care Med* **37**, 1192–1200 (2011).

142. Minnaard, R., Schrauwen, P., Schaart, G. & Hesselink, M. K. C. UCP3 in muscle wasting, a role in modulating lipotoxicity? *FEBS Lett* **580**, 5172–5176 (2006).

143. Zhang, X. *et al.* MAPKs/AP-1, not NF-**κ**B, is responsible for MCP-1 production in TNF-**α**-activated adipocytes. *Adipocyte* **11**, 477–486 (2022).

144. Gnaiger, E. *Mitochondrial Pathways and Respiratory Control An Introduction to OXPHOS Analysis*. *Mitochondrial Physiology Network* (2014).

145. Romeiro, N. C., Ferreira, C. M. & Oliveira, M. F. Assessment of mitochondrial physiology of murine white adipose tissue by mechanical permeabilization and lipid depletion. *Anal Biochem* **611**, (2020).

146. Weidlich, D. *et al.* Lipid droplet–size mapping in human adipose tissue using a clinical 3T system. *Magn Reson Med* **86**, 1256–1270 (2021).

147. Norreen-Thorsen, M. *et al.* A human adipose tissue cell-type transcriptome atlas. *Cell Rep* **40**, (2022).

148. Murton, A. *et al.* Sepsis Increases Muscle Proteolysis in Severely Burned Adults, but Does not Impact Whole-Body Lipid or Carbohydrate Kinetics. *Shock* **52**, 353–361 (2019).

149. Law, J. *et al.* Thermal imaging is a noninvasive alternative to PET/CT for measurement of brown adipose tissue activity in humans. *Journal of Nuclear Medicine* **59**, 516–522 (2018).

150. Wu, J. *et al.* Beige adipocytes are a distinct type of thermogenic fat cell in mouse and human. *Cell* **150**, 366–376 (2012).

151. Abdullahi, A. *et al.* Browning of white adipose tissue after a burn injury promotes hepatic steatosis and dysfunction. doi:10.1038/s41419-019-2103-2.

152. Qi, Y. & Hui, X. H. The Single-Cell Revelation of Thermogenic Adipose Tissue. *Mol Cells* **45**, 673–684 (2022).
153. Han, J. *et al.* Single-cell sequencing unveils key contributions of immune cell populations in cancer-associated adipose wasting. *Cell Discov* **8**, (2022).
154. Hildreth, A. D. *et al.* Single-cell sequencing of human white adipose tissue identifies new cell states in health and obesity. *Nat Immunol* **22**, 639–653 (2021).
155. Masedunskas, A. *et al.* Intravital microscopy: A practical guide on imaging intracellular structures in live animals. *Bioarchitecture* **2**, 143–157 (2012).
156. Boström, P. *et al.* A PGC1-**α**-dependent myokine that drives brown-fat-like development of white fat and thermogenesis. *Nature* **481**, 463–468 (2012).
157. Rao, R. R. *et al.* Meteorin-like is a hormone that regulates immune-adipose interactions to increase beige fat thermogenesis. *Cell* **157**, 1279–1291 (2014).
158. Specht, H. *et al.* Single-cell proteomic and transcriptomic analysis of macrophage heterogeneity using SCoPE2. *Genome Biol* **22**, 1–27 (2021).
159. David R. Miller, Jeremy W. Jarretta, A. M. H. and A. K. D. Deep Tissue Imaging with Multiphoton Fluorescence Microscopy. *Physiol Behav* **176**, 139–148 (2018).
160. Blacker, T. S. & Duchen, M. R. Investigating mitochondrial redox state using NADH and NADPH autofluorescence. *Free Radic Biol Med* **100**, 53–65 (2016).
161. Blacker, T. S. *et al.* Separating NADH and NADPH fluorescence in live cells and tissues using FLIM. *Nat Commun* **5**, (2014).
162. Blacker, T., Berecz, T., Duchen, M. & Szabadkai, G. Assessment of Cellular Redox State Using NAD(P)H Fluorescence Intensity and Lifetime. *Bio Protoc* **7**, 1–15 (2017).
163. Qiu, B. & Simon, M. BODIPY 493/503 Staining of Neutral Lipid Droplets for Microscopy and Quantification by Flow Cytometry. *Bio Protoc* **6**, 1–6 (2016).

164. Duchen, M. R., Surin, A. & Jacobson, J. Imaging mitochondrial function in intact cells. *Methods Enzymol* **361**, 353–389 (2003).

165. Saraf, M. K. *et al.* Morphological changes in subcutaneous white adipose tissue after severe burn injury. *Journal of Burn Care and Research* **37**, e96–e103 (2016).

166. Chen, L., Jin, Y., Wu, J. & Ren, Z. Lipid Droplets: A Cellular Organelle Vital for Thermogenesis. *Int J Biol Sci* **18**, 6176–6188 (2022).

167. Han, J., Meng, Q., Shen, L. & Wu, G. Interleukin-6 induces fat loss in cancer cachexia by promoting white adipose tissue lipolysis and browning. *Lipids Health Dis* **17**, 14 (2018).

168. Marques, M. B. *et al.* Critical illness induces nutrient-independent adipogenesis and accumulation of alternatively activated tissue macrophages. *Crit Care* **17**, (2013).

169. Latronico, N. & Bolton, C. F. Critical illness polyneuropathy and myopathy: A major cause of muscle weakness and paralysis. *Lancet Neurol* **10**, 931–941 (2011).

170. Porter, C. *et al.* Human and Mouse Brown Adipose Tissue Mitochondria Have Comparable UCP1 Function. *Cell Metab* **24**, 246–255 (2016).

171. Martínez-Fernández, L. *et al.* Inflammation and oxidative stress in adipose tissue: Nutritional regulation. *Obesity: Oxidative Stress and Dietary Antioxidants* 63–92 (2018) doi:10.1016/B978-0-12-812504-5.00004-0.

172. Horino, M., Ikeda, K. & Yamada, T. The Role of Thermogenic Fat Tissue in Energy Consumption. 3166–3179 (2022).

173. Periasamy, M. & Kalyanasundaram, A. SERCA pump isoforms: Their role in calcium transport and disease. *Muscle Nerve* **35**, 430–442 (2007).

174. Guarnieri, A. R., Benson, T. W. & Tranter, M. Calcium Cycling as a Mediator of Thermogenic Metabolism in Adipose Tissue. *Mol Pharmacol* **102**, 51–59 (2022).

175. Tidswell, R. & Singer, M. Sepsis – thoughtful management for the non-expert. 62–68 (2018).
176. Corrigan, J. J., Fonseca, M. T., Flatow, E. A., Lewis, K. & Steiner, A. A. Hypometabolism and hypothermia in the rat model of endotoxic shock: Independence of circulatory hypoxia. *Journal of Physiology* **592**, 3901–3916 (2014).
177. Shankar-Hari, M., Rubenfeld, G. D., Ferrando-Vivas, P., Harrison, D. A. & Rowan, K. Development, Validation, and Clinical Utility Assessment of a Prognostic Score for 1-Year Unplanned Rehospitalization or Death of Adult Sepsis Survivors. *JAMA Netw Open* **3**, e2013580 (2020).
178. Yu, S. Y., Luan, Y., Dong, R., Abazarikia, A. & Kim, S. Y. Adipose Tissue Wasting as a Determinant of Pancreatic Cancer-Related Cachexia. *Cancers (Basel)* **14**, 1–12 (2022).
179. Al-Sawaf, O. *et al. Body composition and lung cancer-associated cachexia in TRACERx. Nature Medicine* vol. 29 (2023).
180. Kondo, Y., Miyazato, A., Okamoto, K. & Tanaka, H. Impact of Sex Differences on Mortality in Patients With Sepsis After Trauma: A Nationwide Cohort Study. *Front Immunol* **12**, 1–6 (2021).
181. Janssen, I., Heymsfield, S. B., Wang, Z. M. & Ross, R. Skeletal muscle mass and distribution in 468 men and women aged 18-88 yr. *J Appl Physiol* **89**, 81–88 (2000).